



UNIVERSIDADE FEDERAL DO CEARÁ
CENTRO DE TECNOLOGIA
DEPARTAMENTO DE ENGENHARIA DE TELEINFORMÁTICA
PROGRAMA DE PÓS-GRADUAÇÃO EM ENGENHARIA DE TELEINFORMÁTICA

OTACÍLIO BEZERRA LEITE NETO

OPTIMAL CONTROL AND ESTIMATION OF ACTIVATED SLUDGE PLANTS

FORTALEZA – CE
2021

OTACÍLIO BEZERRA LEITE NETO

OPTIMAL CONTROL AND ESTIMATION OF ACTIVATED SLUDGE PLANTS

Dissertação de Mestrado apresentada ao Programa de Pós-Graduação em Engenharia de Teleinformática, do Departamento de Engenharia de Teleinformática da Universidade Federal do Ceará, como requisito parcial para obtenção do Título de Mestre em Engenharia de Teleinformática. Área de concentração: Reconhecimento de Padrões e Sistemas Dinâmicos.

Orientador: Prof. Dr. Francesco Corona.

Co-Orientador: Profa. Dra. Michela Mulas.

Dados Internacionais de Catalogação na Publicação
Universidade Federal do Ceará
Biblioteca Universitária

Gerada automaticamente pelo módulo Catalog, mediante os dados fornecidos pelo(a) autor(a)

- L554o Leite Neto, Otacílio Bezerra.
Optimal control and estimation of activated sludge plants / Otacílio Bezerra Leite Neto. – 2021.
116 f. : il. color.
- Dissertação (mestrado) – Universidade Federal do Ceará, Centro de Tecnologia, Programa de Pós-Graduação em Engenharia de Teleinformática, Fortaleza, 2021.
Orientação: Prof. Dr. Francesco Corona.
Coorientação: Profa. Dra. Michela Mulas.
1. Processo de lodo ativado. 2. Reúso de água. 3. Propriedades dinâmicas. 4. Controle de modelo preditivo. 5. Estimação de horizonte móvel. I. Título.

CDD 621.38

OTACÍLIO BEZERRA LEITE NETO

OPTIMAL CONTROL AND ESTIMATION OF ACTIVATED SLUDGE PLANTS

Dissertação de Mestrado apresentada ao Programa de Pós-Graduação em Engenharia de Teleinformática, do Departamento de Engenharia de Teleinformática da Universidade Federal do Ceará, como requisito parcial para obtenção do Título de Mestre em Engenharia de Teleinformática. Área de concentração: Reconhecimento de Padrões e Sistemas Dinâmicos.

Aprovada em: ___/___/_____.

BANCA EXAMINADORA

Prof. Dr. Francesco Corona (Orientador)
Universidade Federal do Ceará (UFC)

Profa. Dra. Michela Mulas (Coorientador)
Universidade Federal do Ceará (UFC)

Prof. Dr. Benoît Chachuat
Imperial College London

AGRADECIMENTOS

Aos meus pais, Tereza Diana e Otacílio Filho, pela vida, pelo incentivo à educação, por confiarem em meus objetivos, e, sobretudo, pelo amor que me dão, e aos meus irmãos Camilla Menezes e Matheus Menezes, pelo companheirismo.

Aos meus orientadores, prof. Francesco Corona e profa. Michela Mulas, pelos ensinamentos, pelas valiosas discussões, pela amizade, e por todas as oportunidades que me confiaram.

À minha amada Mariana Sátiro, por todo o amor, carinho e companhia, e por sempre cuidar de mim e apoiar meus projetos de vida. Que o nosso futuro juntos seja feliz e sublime.

A todos meus colegas do Departamento de Teleinformática e do Departamento de Computação da Universidade Federal do Ceará, cuja amizade levarei para o resto da vida. Em especial, aos amigos do Programa de Educação Tutorial do Departamento de Computação.

A todos os professores e pesquisadores que, durante essa jornada, me presentearam com conhecimento, reflexões e oportunidades de me aprofundar na vida acadêmica.

À minha madrinha Socorro Menezes – a Tia Cocoli –, por todo o amor e as lições que me deu durante sua vida. Espero continuar a trazê-la orgulho.

Aos colegas e co-autores do projeto Control4Reuse: Jérôme Harmand, Erik Dahlquist, Farouk Aichouche, Eva Nordlander, Heidi Marais, Antoine Haddon e Eva Thorin.

O presente trabalho foi realizado com apoio da Coordenação de Aperfeiçoamento de Pessoal de Nível Superior Brasil (CAPES) - Código de Financiamento 001.

“Let no one ignorant of geometry enter here.”

entrance to Plato’s Academy

RESUMO

O tratamento de águas residuais está enfrentando desafios sem precedentes devido a requisitos de efluentes mais rígidos, minimização de custos, reutilização sustentável de água, nutrientes e outros recursos, bem como expectativas crescentes do público em atingir altos padrões de serviço. Devido à sua ampla difusão, os processos de lodo ativado desempenham um papel fundamental no tratamento biológico de águas residuais e sua operação ótima tem um grande impacto tecnológico e social. A disciplina de teoria do controle oferece a estrutura matemática para direcionar os sistemas de tratamento de águas residuais a um estado desejado. Controle de modelo preditivo (MPC) e estimação de horizonte móvel (MHE) têm sido as tecnologias escolhidas para muitas aplicações industriais, incluindo estações de tratamento. Neste trabalho, as propriedades dinâmicas e a operação ótima de plantas de lodo ativado são investigadas. Para a primeira tarefa, o sistema dinâmico que consiste em 145 variáveis de estado, 13 controles, 14 distúrbios e 15 saídas, é mapeado em redes complexas nas quais as propriedades de controlabilidade e observabilidade de estado são estudadas, tanto do ponto estrutural quanto do ponto de vista clássico. Para a segunda tarefa, estratégias de controle ótimo e estimativa ótima são projetadas para operar uma planta de lodo ativado tanto para operações de tratamento de águas residuais quanto para reúso. No reúso de águas residuais, um controlador preditivo de *zero-offset* é projetado para operar a planta quando ela for requisitada a produzir água de qualidade sob medida para ser usada na fertirrigação de safra agrícola. Os problemas ótimos de controle e estimativa são resolvidos através do método de transcrição direta, que consiste em converter os problemas em programas não-lineares e, em seguida, resolvê-los numericamente. De acordo com nossos resultados, as plantas de lodo ativado são controláveis apenas no sentido estrutural, sendo incontroláveis no sentido convencional e inobserváveis tanto no sentido estrutural quanto convencional. Sendo estáveis sob a operação convencional, esses processos ainda são estabilizáveis e detectáveis, apesar de seu controle e observação serem qualificados como tarefas de alta exigência. Apresentamos e discutimos os resultados da simulação de um controlador preditivo capaz de melhorar o desempenho da planta de tratamento sob diferentes regimes de afluentes. Em seguida, mostramos e discutimos os resultados para um controlador de *zero-offset* que é capaz de seguir uma trajetória de referência sob condições de afluentes constante, embora seja apenas parcialmente capaz de seguir esses pontos de referência sob afluentes dinâmicos. Finalmente, resultados são apresentados para os controladores de modelo preditivos de saída baseados em medições parciais, ruidosas, do estado interno da planta.

Palavras-chave: Processo de lodo ativado. Propriedades dinâmicas. Redes complexas. Controle de modelo preditivo. Controle ótimo. Estimação de horizonte móvel. Estimação ótima. Reúso de água.

ABSTRACT

Wastewater treatment is facing unprecedented challenges due to stricter effluent requirements, costs minimisation, sustainable reuse of water, nutrients, and other resources, as well as increasing expectations in the public to attain high service standards. Due to their wide diffusion, activated sludge processes play a key role in the biological treatment of wastewater and their efficient operation has a large technological and societal impact. The discipline of control theory offers the mathematical framework for steering wastewater treatment systems toward a desired state. Model predictive control (MPC) and moving horizon estimation (MHE) have been the chosen technologies for many industrial applications, including treatment plants. In this work, the dynamical properties and optimal operation of activated sludge plants are investigated. For the first task, the dynamical system consisting of 145 state variables, 13 controls, 14 disturbances, and 15 outputs, is mapped onto complex networks in which full-state controllability and observability properties are studied, from both a structural and a classical point of view. For the second task, optimal control and estimation strategies are designed for operating an activated sludge plant for both wastewater treatment and reuse operations. In wastewater reuse, a zero-offset predictive controller is designed to operate the plant when it is required to produce water of tailored quality to be used for agricultural crop fertigation. The optimal control and estimation problems are solved through the direct transcription method consisting of converting the problems into nonlinear programs, then solving them numerically. According to our results, activated sludge plants are only controllable in a structural sense, being uncontrollable in the conventional sense and unobservable both in the structural and conventional sense. Being stable under the conventional operation, these processes are still stabilizable and detectable, despite their control and observation being qualified as high-demanding tasks. We present and discuss the simulation results for a predictive controller that is capable to improve the performance of the plant for wastewater treatment under different influent regimes. Then, we show and discuss the results for a zero-offset controller that is capable to track a reference trajectory under constant influent conditions, albeit being only partially capable to track these set-points under dynamic influent. Finally, results are presented for the output model predictive controllers based on partial, noisy, measurements of the plant's internal state.

Keywords: Activated sludge process. Dynamical properties. Complex networks. Model predictive control. Optimal control. Moving horizon estimation. Optimal estimation. Water reuse.

LIST OF FIGURES

Figure 1 – Biological wastewater treatment: process layout, highlighting the activated sludge plant. The first two bio-reactors comprise the anoxic section, while the last three comprise the aerobic section.	5
Figure 2 – Activated sludge plant: process variables and their relative locations in the plant layout.	6
Figure 3 – Dry weather scenario, $t \in [0, 7]$: Time-series for influent flow-rate (Q_{IN}), and influent nitrogen and organic concentrations (X_{SS}^{IN} , S_{NH}^{IN} , BOD_5^{IN} , COD^{IN} , and N_{TOT}^{IN}), over a 1-week period.	10
Figure 4 – A table beside a figure	10
Figure 5 – Reuse control: Control hierarchy of the crop-treatment system. A fertigation plan for optimal crop growth is generated by the crop system, then imported as reference for the treatment plant.	11
Figure 6 – Reuse control: Nitrogen reference trajectories generated by the crop system for one growing season (140 days). Each scenario differs with respect to the initial soil nitrogen content being assumed.	12
Figure 7 – Network $\mathcal{G} = (\mathcal{V}, \mathcal{E})$ (left panel) associated to structured system (A, B, C) (right panels). State vertices $x_i \in \mathcal{V}_A$ are in black, input vertices $u_k \in \mathcal{V}_B$ are in blue, and output vertices $y_k \in \mathcal{V}_C$ are in red. State-state edges $(x_i, x_j) \in \mathcal{E}_A$, input-state edges $(u_k, x_j) \in \mathcal{E}_B$, and state-output edges $(x_i, y_k) \in \mathcal{E}_C$ are dyed to match the corresponding entries in (A, B, C) . To reduce clutter, state self-loops are omitted.	39
Figure 8 – Network $\mathcal{G}_{SS} = (\mathcal{V}_{SS}, \mathcal{E}_{SS})$ (left) associated to linearisation (A^{SS}, B^{SS}, C^{SS}) (right). State vertices $x_i \in \mathcal{V}_{A^{SS}}$ and state-state edges $(x_i, x_j) \in \mathcal{E}_{A^{SS}}$ are in black, input vertices $u_k \in \mathcal{V}_{B^{SS}}$ and input-state edges $(u_k, x_j) \in \mathcal{E}_{B^{SS}}$ are in blue, and output vertices $y_k \in \mathcal{V}_{C^{SS}}$ and state-output edges $(x_i, y_k) \in \mathcal{E}_{C^{SS}}$ are in red. State self-loops have been omitted.	41
Figure 9 – Spectrum $\sigma(A^{SS})$: Eigenvalues $\lambda_i \in \sigma(A^{SS})$, left, and associated eigenvectors $v_i(\lambda_i)$, right. The grid in the complex plane displays lines corresponding to constant damping factors (diagonal lines) and natural frequencies (vertical lines, in rad/days) for the associated system modes.	41
Figure 10 – Time evolution of the normalised system modes $\frac{t^k e^{\lambda_i t}}{\max_t t^k e^{\lambda_i t}}$ ($k = 0, \dots, \mu(\lambda_i) - 1$) for the real eigenvalues (top plots) and complex conjugated pairs of eigenvalues (bottom plots) from the spectrum $\sigma(A^{SS}) = \{\lambda_i, v_i(\lambda_i)\}_{i=1}^{N_x}$. The curves are grouped based on each mode's time constant $\tau_i = 1/\text{Re}[\lambda_i]$	42
Figure 11 – Pair (A^{SS}, B^{SS}) : Eigenvectors $v_i(\lambda_i)$ for $\lambda_i \in \sigma(A^{SS})$ with $\text{rank}([\lambda_i I - A^{SS} \ B^{SS}]) < N_x$	43

Figure 12 – Pair (A^{SS}, C^{SS}) : Eigenvectors $v_i(\lambda_i)$ for $\lambda_i \in \sigma(A^{SS})$ with $\text{rank}([\lambda_i I - A^{SS} \ C^{SS^T}]^T) < N_x$	43
Figure 13 – System (A^{SS}, B^{SS}, C^{SS}) : Average controllability centrality $C_C(n_x)$, top, and average observability centrality $C_o(n_x)$, bottom, associated to each state variable.	45
Figure 14 – System (A_{co}, B_{co}, C_{co}) : Cumulative sum $\Lambda(N)$ for the eigenvalues of the infinite-horizon controllability Gramian $W_c(\infty)$, top, and observability Gramian $W_o(\infty)$, bottom.	46
Figure 15 – Open-loop simulation: Effluent-based output variables corresponding to nitrogen components, top panels, and organic matter, bottom panels. Shaded areas denote the values above the quality limits.	48
Figure 16 – Open-loop simulation, $t \in [7, 14]$: Estimation of the effluent-based output variables.	49
Figure 17 – Open-loop, $t \in [7, 14]$: Estimates (black) and true values (grey) for influent flow-rate Q_{IN} and concentrations $x^{A(IN)}$. Concentrations $X_{BA}^{IN} = X_P^{IN} = S_O^{IN} = S_{NO}^{IN} = 0$ and $S_{ALK}^{IN} = 7$ are omitted.	50
Figure 18 – Open-loop, $t \in [7, 14]$: Estimates (black) and true values (grey) for the chemical concentrations in the first reactor, $x^{A(1)}$. As $S_O^{A(1)} \approx 0$, this variable is omitted.	50
Figure 19 – Treatment, MPC: Regulation of the effluent-based output variables.	52
Figure 20 – Treatment control, MPC: Influent flow-rate Q_{IN} , flow-rates (Q_A, Q_R, Q_W) , oxygen transfer coefficients $K_{La}^{(1\rightsquigarrow 5)}$, and extra carbon flow-rates $Q_{EC}^{(1\rightsquigarrow 5)}$, left panels, together with nitrogen forms $S_{NH}^{A(1\rightsquigarrow 5)}$ and $S_{NO}^{A(1\rightsquigarrow 5)}$, soluble oxygen $S_O^{A(1\rightsquigarrow 5)}$, and total suspended solids $X_{SS}^{S(1\rightsquigarrow 10)}$, right panels.	53
Figure 21 – Treatment, MPC: Effluent quality index (EQI) under open-loop and closed-loop operation.	53
Figure 22 – Treatment, Output-MPC: Estimation and regulation of the effluent-based output variables.	54
Figure 23 – Treatment, Output-MPC: Effluent quality index (EQI) under closed-loop operations.	55
Figure 24 – Reuse, MPC: Reference tracking of effluent total nitrogen, $N_{TOT}^{S(10)}$	57
Figure 25 – Reuse, MPC: Influent flow-rate Q_{IN} , flow-rates (Q_A, Q_R, Q_W) , oxygen transfer coefficients $K_{La}^{(1\rightsquigarrow 5)}$, and extra carbon flow-rates $Q_{EC}^{(1\rightsquigarrow 5)}$, left panels, together with nitrogen forms $S_{NH}^{A(1\rightsquigarrow 5)}$ and $S_{NO}^{A(1\rightsquigarrow 5)}$, soluble oxygen $S_O^{A(1\rightsquigarrow 5)}$, and total suspended solids $X_{SS}^{S(1\rightsquigarrow 10)}$, right panels.	58
Figure 26 – Comparison, Output-MPC: Estimation and tracking of effluent total nitrogen, $N_{TOT}^{S(10)}$	59
Figure 27 – Case I, MPC: Reference tracking of effluent total nitrogen, $N_{TOT}^{S(10)}$	60

Figure 28 – Case I, $t \in [49, 112]$: Influent flow-rate Q_{IN} , flow-rates (Q_A, Q_R, Q_W) , oxygen transfer coefficients $K_L a^{(1 \rightsquigarrow 5)}$, and extra carbon flow-rates $Q_{EC}^{(1 \rightsquigarrow 5)}$, left panels, together with nitrogen forms $S_{NH}^{A(1 \rightsquigarrow 5)}$ and $S_{NO}^{A(1 \rightsquigarrow 5)}$, soluble oxygen $S_O^{A(1 \rightsquigarrow 5)}$, and total suspended solids $X_{SS}^{S(1 \rightsquigarrow 10)}$, right panels.	61
Figure 29 – Case II, MPC: Reference tracking of effluent total nitrogen, $N_{TOT}^{S(10)}$	62
Figure 30 – Case II, $t \in [49, 112]$: Influent flow-rate Q_{IN} , flow-rates (Q_A, Q_R, Q_W) , oxygen transfer coefficients $K_L a^{(1 \rightsquigarrow 5)}$, and extra carbon flow-rates $Q_{EC}^{(1 \rightsquigarrow 5)}$, left panels, together with nitrogen forms $S_{NH}^{A(1 \rightsquigarrow 5)}$ and $S_{NO}^{A(1 \rightsquigarrow 5)}$, soluble oxygen $S_O^{A(1 \rightsquigarrow 5)}$, and total suspended solids $X_{SS}^{S(1 \rightsquigarrow 10)}$, right panels.	63
Figure 31 – Comparison, $t \in [49, 112]$: Nitrogen removal shown by the difference between influent N_{TOT}^{IN} and effluent N_{TOT}^{IN} total nitrogen for the predictive control in Case I (left) and Case II (right).	64
Figure 32 – Comparison, Output-MPC: Estimation and tracking of effluent total nitrogen, $N_{TOT}^{S(10)}$	66
Figure 33 – Crop model: Nitrogen concentrations of irrigation water, F_N , for optimal crop growth.	86

LIST OF TABLES

Table 1 –	Activated sludge plant: Process variables by location ($'A(r)'$, in the r -th biological reactor with $r = 1, \dots, 5$, or $'IN'$ in the influent wastewater; $'S(l)'$ in the l -th layer of the settler with $l = 1, \dots, 10$) and type ($'D'$, disturbance; $'S'$, state variable; $'M'$ measurement; and $'C'$, control).	8
Table 2 –	Influent time-series: Flow-weighted average influent conditions for each disturbance scenario.	9
Table 3 –	Treatment control: Quality limits and steady-state references for the effluent-based outputs (left), and diagram of the regulation control task (right).	10
Table 4 –	System (A_{co}, B_{co}, C_{co}) : Energy-related metrics.	46
Table 5 –	Activated sludge plant: controllable inputs for the default open-loop operation.	48
Table 6 –	MHE: Output, disturbance and state estimation accuracies ($J_{NMSE}(y, \hat{y})$, $J_{NMSE}(w, \hat{w})$, and $J_{NMSE}(x, \hat{x})$, respectively), under the different disturbance regimes.	51
Table 7 –	Results: Control performances in terms of effluent quality index (EQI, kg PU d^{-1}), number of quality limit crossings and percentage of time in violation ($\#Crossings$ and $\%Violation$, respectively, for $S_{NH}^{S(10)}$ and $N_{TOT}^{S(10)}$), operation cost index (OCI), and energy costs (PE, AE and CAE).	55
Table 8 –	Results: Tracking accuracy in terms of normalised mean squared errors (NMSE), together with operation cost index (OCI) and energy costs (PE, AE and CAE).	59
Table 9 –	Results: Tracking accuracy, $J_{NMSE}(\tilde{y}, \tilde{y}^{sp})$, with respect to each reference trajectories.	65
Table 10 –	Results: Energy costs (PE, AE, and CAE) and operational cost indices (OCI, in kWh d^{-1}).	65
Table 11 –	Results: Tracking accuracy in terms of normalised mean squared errors (NMSE), together with operation cost index (OCI) and energy costs (PE, AE and CAE).	67
Table 12 –	Benchmark Model No. 1: Model constant parameters.	82
Table 13 –	Benchmark Model No. 1: Steady-state point $SS := (x^{SS}, u^{SS}, w^{SS}, y^{SS})$	83
Table 14 –	Crop system: State and input variables.	84
Table 15 –	Crop system: Model constant parameters.	85

CONTENTS

1	INTRODUCTION	1
1.1	Related publications	3
1.2	Thesis organization	3
1.3	Activated sludge plants	4
1.3.1	<i>Benchmark state-space model description</i>	5
1.3.2	<i>Influent wastewater data description</i>	7
1.3.3	<i>Process operation and control objectives</i>	10
2	THEORETICAL PRELIMINARIES	13
2.1	Dynamical models properties	13
2.1.1	<i>Stability</i>	14
2.1.2	<i>Controllability and observability</i>	15
2.1.3	<i>Reduced-order models and stabilisability</i>	19
2.2	Model predictive control	21
2.2.1	<i>Discretise-then-optimise and the direct method</i>	22
2.2.2	<i>Receding-horizon control</i>	24
2.2.3	<i>Zero-offset affine quadratic regulator</i>	27
2.3	Moving horizon estimation	29
2.3.1	<i>Inference problem and MAP estimation</i>	30
2.3.2	<i>Moving horizon estimation strategy</i>	33
2.4	Output model predictive control	36
2.4.1	<i>Output affine quadratic regulator (Output-AQR)</i>	37
3	RESULTS AND DISCUSSIONS	39
3.1	Analysis of activated sludge plant models	39
3.1.1	<i>Structural controllability and observability analysis</i>	39
3.1.2	<i>Stability, controllability and observability analysis</i>	40
3.2	Wastewater treatment: regulation	47
3.2.1	<i>Open-loop: simulation and state-estimation</i>	48
3.2.2	<i>Model predictive control for conventional treatment</i>	51
3.3	Wastewater reuse: set-point tracking	56
3.3.1	<i>Case study: toy effluent reference trajectory</i>	56
3.3.2	<i>Case study: supply nitrogen for optimal crop growth</i>	59
4	CONCLUSION	69
	REFERENCES	71
	APPENDIX A – MODEL EQUATIONS AND PARAMETERS	78
	APPENDIX B – OMITTED PROOFS AND DEFINITIONS	86

1 INTRODUCTION

Wastewater treatment is facing unprecedented challenges due to stricter effluent requirements, costs minimisation, as well as the need for sustainable management addressing the implications of climate change, rising populations, and the increasing public expectations for high service standards. Besides conventional treatment, wastewater reuse is one of the practices which has proven itself inherently circular and useful in satisfying the supply of water of varying quality for industrial, urban and agricultural activities. Because of their wide diffusion, activated sludge processes play a key role in the biological treatment of wastewater and their efficient operation and control has a large technological and societal impact.

Many control strategies for activated sludge plants have been proposed in the industrial and academic literature. More than forty years ago the first specialised conference on Instrumentation, Control and Automation of Water and Wastewater systems was founded with the firm goal of encouraging the application of automation techniques to wastewater treatment plants. Pioneering works, as Olsson, Eklund, et al. (1973) and Olsson and Andrews (1978), inspired numerous researchers and practitioners to approach this specific field. Extensive reviews of the various control systems can be found in Olsson, Nielsen, et al. (2005), Olsson, Carlsson, et al. (2014) and, specifically for aeration systems, in Åmand et al. (2013). While many control strategies for operating wastewater treatment plants have been proposed, their use for water reclamation is an active research area with important challenges for the health of the public and the environment (AIT MOUHEB et al., 2018; THWAITES et al., 2018; RICART; RICO, 2019). Important research efforts have been possible thank to a number of support tools providing simulation protocols for real-world activated sludge processes. The Benchmark Simulation Model no. 1 (BSM1, Gernaey et al. (2014)), specifically, offers a simulation protocol and a general platform for analysing common activated sludge processes subjected to typical municipal wastewater influent.

Control theory offers the mathematical framework for steering the wastewater treatment systems toward a desired state. Model predictive control (MPC) has been the chosen technology for many industrial applications (FORBES et al., 2015). A number of wastewater treatment applications were presented and different MPC configurations and algorithms were tested using as platform the BSM1 in its original configuration or with *ad-hoc* modifications. Rosen et al. (2002) investigated different model-based alternatives on a reduced BSM1 system for high ammonia peaks control. On the same attempt, Alex et al. (2002) developed a MPC using a parsimonious deterministic model for the prediction of the effluent ammonia concentration. A linear quadratic dynamic matrix control is applied to maintain the effluent quality within regulation-specified limits by Corriou and Pons (2004). Stare et al. (2007), Holenda et al. (2008), Shen et al. (2008) and Ostace et al. (2011) compared and tested different MPC configurations. The BSM1 has been used for testing a nonlinear multi-objective model-predictive control scheme (HAN et al., 2014). Sotomayor and Garcia (2002) and Ekman (2008) investigated different predictive control

approaches on distinct activated sludge process. Francisco et al. (2015) selected the controlled variables for a non-linear MPC structure through a self-optimising procedure. Zeng and Liu (2015), Zhang and Liu (2019) and Moliner-Heredia et al. (2019) tackled the problem by using economic MPC.

The availability of BSMs has stimulated the design of several modelling and control solutions, yet too little has been done to study this model and its measurements from a system analytical perspective. To the best of our knowledge, still too few works discuss, for example, state estimation and observability of BSMs. Arnold and Dietze (2001) explores the use of moving horizon estimation (MHE) based on real data from a BSM-like treatment plant. Busch et al. (2013) considers the BSM with an ideal splitter and investigates both extended Kalman filters (EKF) and MHE based on an optimal set of measurement variables. Similarly, Zeng, Liu, et al. (2016) proposes a distributed EKF strategy for the plant considering an ideal splitter, and also provides a brief discussion about each subsystem observability properties. Further studies on centralized and distributed estimation are done by Yin and Liu (2018), Yin, Decardi-Nelson, et al. (2018) and Yin and Liu (2019), considering an unrealistic large set of measurement variables.

In this work, we analyse the dynamical properties of activated sludge plants and study their optimal operation for both wastewater treatment and water reuse applications. For the latter, we investigate the feasibility of operating the treatment plant to produce reusable water of tailored quality for crop irrigation. In both cases, we focus on the predictive control and estimation of activated sludge plants as described by the Benchmark Simulation Model no. 1 (BSM1). We consider the default proposed model, without simplifications or changes to the original layout.

To study the dynamical properties of the plants, we mapped the dynamical system consisting of 145 state variables, 13 controls, 14 disturbances and 15 outputs onto complex networks in which we studied full-state controllability and observability properties of the model from a structural and a classical point of view. As we are primarily interested in determining whether the plant is controllable and observable under all feasible linearisations, we studied the structural controllability and observability of the model (LIN, 1974; REINSCHKE, 1988; LIU et al., 2011, 2013). Assuming a linearisation commonly used in the literature, the classical controllability and observability properties of the plant are verified using Popov-Belevitch-Hautus tests (HAUTUS, 1970). Finally, we complement the analysis by evaluating energy-based metrics that quantify the control and observation efforts needed to operate this class of wastewater treatment plants (MÜLLER; WEBER, 1972; PASQUALETTI et al., 2014; SUMMERS et al., 2016).

Once the properties of the dynamical models are understood, we approach the control and estimation problems using, respectively, model predictive control (MPC, Borrelli et al. (2017) and Rawlings, Mayne, et al. (2020)) and moving horizon estimation (MHE, Rao et al. (2003) and Rawlings and Bakshi (2006)). We consider a zero-offset control strategy based on successive linear approximations of the process dynamics along the reference trajectories (KEVICZKY;

BALAS, 2006; FALCONE et al., 2007; GROS et al., 2020). By coupling MHE with MPC, we also consider the output model predictive control (Output MPC) in which knowledge about the process state is not assumed. All discussed optimal control and estimation problems are tackled by the direct method consisting on their transcriptions to standard nonlinear programs (NLP, Boyd and Vandenberghe (2004)) to be solved using efficient numerical methods (BETTS, 2010). For the activated sludge plant, a simple regulation control objective is proposed for the conventional wastewater treatment task, whereas zero-offset reference tracking is considered for the water reuse application. The latter is formulated as the task of operating the treatment plant to produce effluent nitrogen according to an optimal fertigation plan for crop growth. The plant is simulated under typical influent conditions and the controller performances are evaluated in terms of pre-defined effluent quality metrics, tracking accuracy and operational costs.

1.1 Related publications

During the development of this work, the following scientific contributions have been published:

- NETO, O. B. L.; MULAS, M.; CORONA, F. On the controllability of activated sludge plants. In: 2020 EUROPEAN CONTROL CONFERENCE (ECC). **Proceedings of the 2020 European Control Conference**. IEEE, 2020. p. 581–586. DOI: 10.23919/ECC51009.2020.9143863
- NETO, O. B. L.; MULAS, M.; CORONA, F. On the observability of activated sludge plants. **IFAC-PapersOnLine**, v. 53, n. 2, p. 16802–16807, 2020. 21th IFAC World Congress. DOI: 10.1016/j.ifacol.2020.12.1151
- NETO, O. B. L.; HADDON, A.; AICHOUCHE, F.; HARMAND, J.; MULAS, M.; CORONA, F. Predictive control of activated sludge plants to supply nitrogen for optimal crop growth. In: 11TH IFAC SYMPOSIUM ON ADVANCED CONTROL OF CHEMICAL PROCESSES. **Proceedings of the 11th IFAC Symposium on Advanced Control of Chemical Processes**. IFAC, 2021. (to appear)

1.2 Thesis organization

This document is organized into four parts, each comprised of a number of sections.

- I. The remainder of Chapter 1, Section 1.3, presents the activated sludge plant used as a representation of biological wastewater treatment plants, then overviews its control objectives.
- II. Chapter 2 presents the theoretical background of this work. Section 2.1 reviews the notions of stability, controllability and observability of dynamical systems and presents weaker

properties based on canonical decompositions. Section 2.2 overviews the model predictive control strategy and its realisation for zero-offset control problems. Section 2.3 introduces the moving horizon estimation strategy for reconstructing the internal state of a system based on a set of noisy measurements. Finally, Section 2.4 proposes an output predictive control strategy by combining model predictive control and moving horizon estimation.

III. Chapter 3 presents the experimental results of this work. Section 3.1 discusses our results on the full-state stability, controllability and observability of activated sludge plants. Section 3.2 presents the simulation results obtained by the predictive control of the activated sludge plant for conventional treatment. Finally, Section 3.3 presents the simulation results for the zero-offset predictive controllers operating the treatment plant when the process is requested to produce effluent nitrogen according to a trajectory reference.

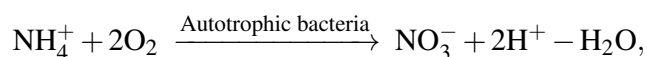
IV. Chapter 4 presents the concluding remarks and bibliography used for this work.

Furthermore, Appendix 4 presents the explicit differential equations and constant parameters defining the dynamical models discussed in this work. A selection of omitted definitions and proofs are provided in Appendix 4, for the sake of completeness.

1.3 Activated sludge plants

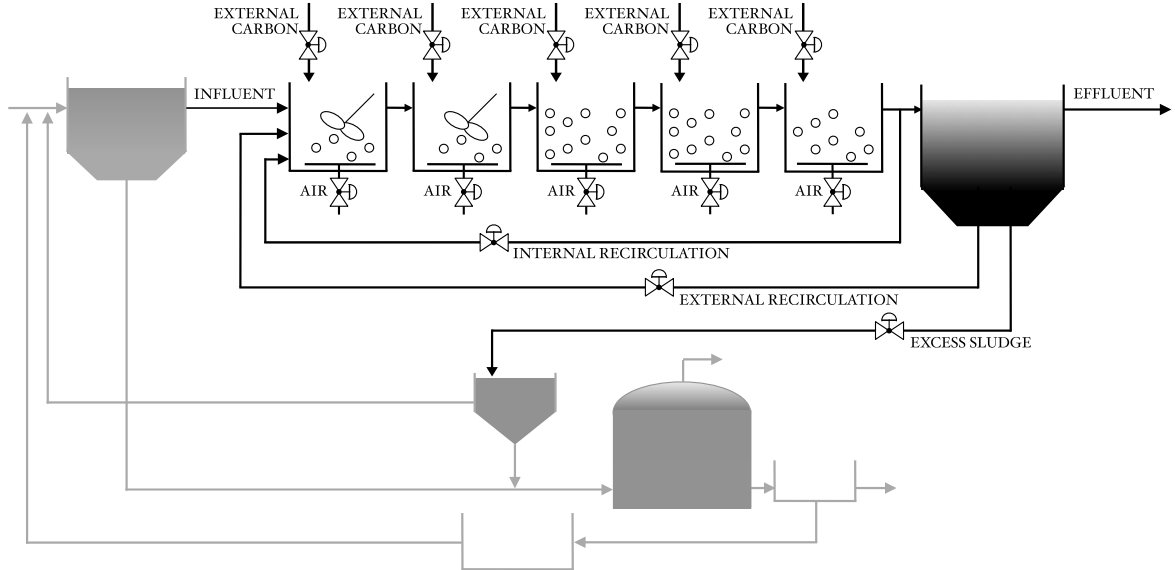
We consider the activated sludge process in a conventional biological wastewater treatment plant. Based on the simultaneous denitrification-nitrification process, bacteria reduce nitrogen present in the influent wastewater in the form of ammonia into nitrate, which is subsequently reduced into nitrogen gas to be released into the atmosphere (GRADY JR et al., 2011). The prototypical process, in Figure 1, consists of five biological reactors and a secondary clarifier.

The treatment begins with a first reactor where influent wastewater from primary sedimentation, return sludge from secondary sedimentation and internal recycle sludge are fed. The outflow from the first reactor is then sequentially fed to the downstream reactors and, eventually, from the fifth reactor to the secondary settler. Mixed liquor from the fifth reactor is recirculated into the first reactor together with the recycle sludge from secondary sedimentation, as mentioned. Excess sludge from the settler can also be removed towards another process in the facility. Oxygen is potentially added by insufflating air into each reactor. In the aerated reactors, the ammonium nitrogen ($\text{NH}_4\text{-N}$) contained in the wastewater is oxidised into nitrate nitrogen ($\text{NO}_3\text{-N}$),



which is in turn reduced into nitrogen gas (N_2) by denitrifying bacteria in the anoxic reactors. An additional carbon source can be added to each reactor independently. No other chemicals are assumed to be added to the process.

Figure 1 – Biological wastewater treatment: process layout, highlighting the activated sludge plant. The first two bio-reactors comprise the anoxic section, while the last three comprise the aerobic section.



Source: Prepared by the authors.

Each reactor is described by the Activated Sludge Model no. 1 (HENZE et al., 2000), while the settler is described using the 10-layer non-reactive model proposed by Takács et al. (1991). Under this configuration, the bio-process corresponds to the Benchmark Simulation Model no. 1 (GERNAEY et al., 2014) and hereafter will be referred to as the activated sludge plant (ASP).

In this section, we present the state-space model proposed by the Benchmark Simulation Model no. 1 (BSM1) to represent the dynamics in the activated sludge plant. Moreover, we present a collection of influent wastewater time-series suggested by the benchmark as inputs to simulate the plant, together with the data generation process that was assumed. Finally, we discuss the control objectives and performance evaluation criteria for two applications of activated sludge plants: conventional wastewater treatment and water reuse for crop irrigation.

1.3.1 Benchmark state-space model description

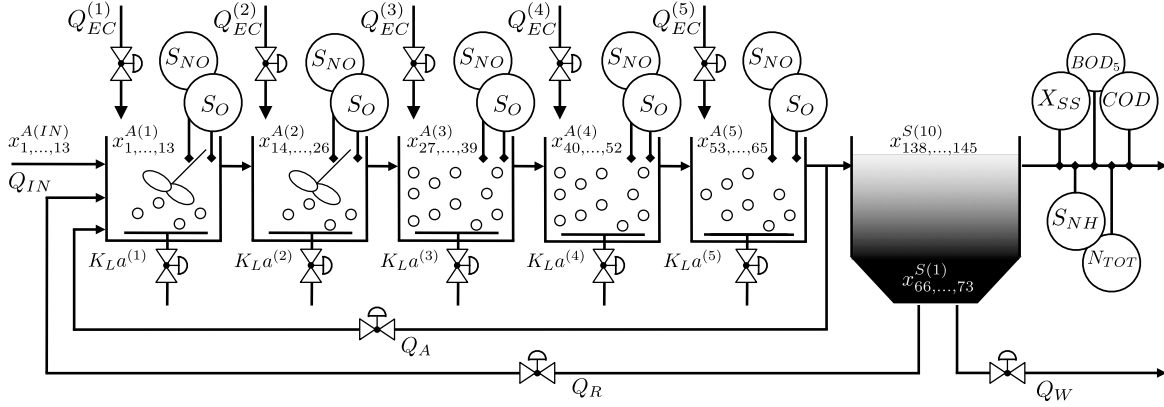
A layout of the activated sludge plant detailing the process variables is shown in Figure 2.

From the system perspective, the dynamics of each reactor $A^{(r)}$ ($r = 1, \dots, 5$) in the plant are described by 13 state variables, the vector of concentrations

$$x^{A^{(r)}} = [S_I^{A^{(r)}} \ S_S^{A^{(r)}} \ X_I^{A^{(r)}} \ X_S^{A^{(r)}} \ X_{BH}^{A^{(r)}} \ X_{BA}^{A^{(r)}} \ X_P^{A^{(r)}} \ S_O^{A^{(r)}} \ S_{NO}^{A^{(r)}} \ S_{NH}^{A^{(r)}} \ S_{ND}^{A^{(r)}} \ X_{ND}^{A^{(r)}} \ S_{ALK}^{A^{(r)}}]^\top, \quad (1)$$

and controllable inputs $u^{A^{(r)}} = [K_L a^{(r)} \ Q_{EC}^{(r)}]$, the oxygen transfer coefficient $K_L a^{(r)}$ and the external carbon source flow-rate $Q_{EC}^{(r)}$. The dynamics of each settler layer $S^{(l)}$ ($l = 1, \dots, 10$) are

Figure 2 – Activated sludge plant: process variables and their relative locations in the plant layout.



Source: Prepared by the authors.

described by 8 state variables, the vector of concentrations

$$x^{S(l)} = [X_{SS}^{S(l)} \ S_I^{S(l)} \ S_S^{S(l)} \ S_O^{S(l)} \ S_{NO}^{S(l)} \ S_{NH}^{S(l)} \ S_{ND}^{S(l)} \ S_{ALK}^{S(l)}]^\top. \quad (2)$$

Moreover, the plant is subjected to three additional controllable inputs, the internal and external sludge recycle flow-rates (Q_A and Q_R , respectively) and the wastage flow-rate Q_W , and to 14 uncontrollable inputs or disturbances, the influent flow-rate Q_{IN} and its concentrations $x^{A(IN)}$, all directly entering the first reactor. Wastewater concentrations in the internal recycle are given by $x^{A(5)}$, whereas $x^{S(1)}$ are the concentrations in the external recycle and wastage stream.

As for the measurements, we consider a typical sensor-arrangement in which we assume the existence of a set of analysers determining, in real-time, the vector of concentrations

$$y = [y^{A(1)} \ \dots \ y^{A(5)} \ X_{SS}^{S(10)} \ S_{NH}^{S(10)} \ BOD_5^{S(10)} \ COD^{S(10)} \ N_{TOT}^{S(10)}]^\top, \quad (3)$$

with $y^{A(r)} = [S_O^{A(r)} \ S_{NO}^{A(r)}]$. The effluent concentrations of biochemical oxygen demand (BOD_5), chemical oxygen demand (COD) and total nitrogen (N_{TOT}) are defined as

$$\begin{aligned} BOD_5^{S(10)} &= 0.25((1 - f_P)(X_{BH}^{S(10)} + X_{BA}^{S(10)}) + S_S^{S(10)} + X_S^{S(10)}); \\ COD^{S(10)} &= S_S^{S(10)} + S_I^{S(10)} + X_S^{S(10)} + X_I^{S(10)} + X_{BH}^{S(10)} + X_{BA}^{S(10)} + X_P^{S(10)}; \\ N_{TOT}^{S(10)} &= S_{NO}^{S(10)} + S_{NH}^{S(10)} + S_{ND}^{S(10)} + X_{ND}^{S(10)} + i_{XB}(X_{BH}^{S(10)} + X_{BA}^{S(10)}) + i_{XP}(X_P^{S(10)} + X_I^{S(10)}), \end{aligned}$$

with stoichiometric parameters (f_P , i_{XB} , and i_{XP}) given by Germaey et al. (2014). Effluent concentrations $X_a^{S(10)} = (X_{SS}^{S(10)} / X_f) X_a^{A(5)}$, for $X_a \in \{X_I, X_S, X_{BH}, X_{BA}, X_P, X_{ND}\}$, depend on the feed concentration $X_f = 0.75(X_I^{A(5)} + X_S^{A(5)} + X_{BH}^{A(5)} + X_{BA}^{A(5)} + X_P^{A(5)})$.

The state-space model for this class of ASPs is

$$\dot{x}(t) = f(x(t), u(t), w(t) | \theta_x); \quad (4a)$$

$$y(t) = g(x(t) | \theta_y), \quad (4b)$$

where, at time $t \in \mathbb{R}_{\geq 0}$, $x(t) = [x^{A(1)} \dots x^{A(5)} x^{S(1)} \dots x^{S(10)}]^\top \in \mathbb{R}_{\geq 0}^{N_x}$ is the vector of state-variables in Equations (1, 2), $y(t) \in \mathbb{R}_{\geq 0}^{N_y}$ is the vector of outputs or measurement variables in Equation (3), $u(t) = [Q_A \ Q_R \ Q_W \ u^{A(1)} \dots u^{A(5)}]^\top \in \mathbb{R}_{\geq 0}^{N_u}$ is the vector of controllable inputs, and $w(t) = [Q_{IN} \ x^{A(IN)}]^\top \in \mathbb{R}_{\geq 0}^{N_w}$ is the vector of uncontrollable inputs or disturbances.

The time-invariant dynamics $f(\cdot | \theta_x)$ and $g(\cdot | \theta_y)$ depend on a set of stoichiometric and kinetic parameters collectively denoted by the vectors θ_x and θ_y . The state-space model in Equation (4) thus consists of $N_x = 13 \times 5 + 8 \times 10 = 145$ state variables, $N_u = 3 + 5 + 5 = 13$ controllable inputs, $N_w = 1 + 13 = 14$ disturbances and $N_y = 15$ outputs. Being $N_x \gg N_u$ and $N_x \gg N_y$, the system is both strongly underactuated and strongly underobserved. The explicit notation is provided in Table 1, while the model equations and parameters are detailed in Appendix 4.

Importantly, our state-space configuration includes all the control handles suggested in the benchmark that do not require changes to the plant layout depicted in Figure 2. Moreover, we consider the possibility of having the default low-level controllers (GERNAEY et al., 2014) applied on each of the five reactors. As such, our configuration necessarily includes a sensor-arrangement that considers the measurement of $S_{NO}^{A(r)}$ and $S_O^{A(r)}$ in all reactors ($r = 1, \dots, 5$).

1.3.2 Influent wastewater data description

The influent wastewater constitutes one of the most important streams in the process. From a control perspective, these inputs correspond to exogenous disturbances that a controller should reject in order to attain its objective. In the following, the influent modelling approach and resulting time-series suggested by the benchmark are presented.

The disturbance scenarios are based on a model of urban activity such that households, industry and rain activity are assumed to be the main sources of wastewater. Specifically, diurnal and weekly patterns of waste production are designed to account for the households and industry contributions. Rainfall contributes only to the influent flow-rate, following seasonal and episodic patterns. The flow-rate and pollutants from these sources are processed by a simple sewer system from which the primary influent flow-rate, Q_{IN} and its concentrations, $x^{A(IN)}$, are composed.

The provided data collection is comprised by three 14-days scenarios (*dry weather*, *storm event*, and *rain event*) and a *long-term weather scenario*. The time-series correspond to simulations of the aforementioned influent model sampled every 15 minutes. In detail:

- *Dry weather scenario*: Depicts expected diurnal variations under normal weather condi-

Table 1 – Activated sludge plant: Process variables by location ($A(r)$, in the r -th biological reactor with $r = 1, \dots, 5$, or IN in the influent wastewater; $S(l)$ in the l -th layer of the settler with $l = 1, \dots, 10$) and type (D , disturbance; S , state variable; M measurement; and C , control).

Variable	Description	Type	Units
$S_I^{IN}, S_I^{A(r)}, S_I^{S(l)}$	Soluble inert organic matter	D, S, S	g COD m^{-3}
$S_S^{IN}, S_S^{A(r)}, S_S^{S(l)}$	Readily biodegradable substrate	D, S, S	g COD m^{-3}
$X_I^{IN}, X_I^{A(r)}$	Particulate inert organic matter	D, S	g COD m^{-3}
$X_S^{IN}, X_S^{A(r)}$	Slowly biodegradable substrate	D, S	g COD m^{-3}
$X_{BH}^{IN}, X_{BH}^{A(r)}$	Active heterotrophic biomass	D, S	g COD m^{-3}
$X_{BA}^{IN}, X_{BA}^{A(r)}$	Active autotrophic biomass	D, S	g COD m^{-3}
$X_P^{IN}, X_P^{A(r)}$	Particulate products from biomass decay	D, S	g COD m^{-3}
$S_O^{IN}, S_O^{A(r)}, S_O^{S(l)}$	Dissolved oxygen	D, S/M, S	$\text{g O}_2 \text{ m}^{-3}$
$S_{NO}^{IN}, S_{NO}^{A(r)}, S_{NO}^{S(l)}$	Nitrate and nitrite nitrogen	D, S/M, S	g N m^{-3}
$S_{NH}^{IN}, S_{NH}^{A(r)}, S_{NH}^{S(l)}$	$\text{NH}_4^+ + \text{NH}_3$ nitrogen	D, S, S/M($l = 10$)	g N m^{-3}
$S_{ND}^{IN}, S_{ND}^{A(r)}, S_{ND}^{S(l)}$	Soluble biodegradable organic nitrogen	D, S, S	g N m^{-3}
$X_{ND}^{IN}, X_{ND}^{A(r)}$	Particulate biodegradable organic nitrogen	D, S	g N m^{-3}
$S_{ALK}^{IN}, S_{ALK}^{A(r)}, S_{ALK}^{S(l)}$	Alkalinity	D, S	$\text{mol HCO}_3^- \text{ m}^{-3}$
$X_{SS}^{S(l)}$	Total suspended solids	S/M($l = 10$)	g COD m^{-3}
Q_{IN}	Influent flow-rate	D	$\text{m}^3 \text{ d}^{-1}$
Q_A	Internal recirculation flow-rate	C	$\text{m}^3 \text{ d}^{-1}$
Q_R	External recirculation flow-rate	C	$\text{m}^3 \text{ d}^{-1}$
Q_W	Wastage flow-rate	C	$\text{m}^3 \text{ d}^{-1}$
$Q_{EC}^{(r)}$	External carbon source flow-rate	C	$\text{m}^3 \text{ d}^{-1}$
$K_{La}^{(r)}$	Oxygen transfer coefficient	C	d^{-1}
$BOD_5^{S(10)}$	Biochemical oxygen demand	M	g COD m^{-3}
$COD^{S(10)}$	Chemical oxygen demand	M	g COD m^{-3}
$N_{TOT}^{S(10)}$	Total nitrogen	M	g N m^{-3}

Source: Prepared by the authors.

tions.

- *Storm event scenario*: Based on the *dry weather scenario*, with the addition of two high-intensity storm events occurring in the second week. Consequently, the scenario depicts a significant increase in suspended solids after such events, especially for the first storm.
- *Rain event scenario*: Based on the *dry weather scenario*, with the addition of a long-duration rain event in the second week. Being of low intensity, the rain only increases the flow-rate over that period without significantly affecting the suspended solids afterwards.
- *Long-term weather scenario*: Depicts expected diurnal variations over a total period of 18 months. Due to its long duration, this time-series includes seasonal patterns into the influent model (weekends, holidays, rainy and dry seasons, etc.).

Table 2 provides the average flow-rate and the flow-weighted average concentrations,

$$\text{Average concentration} = \frac{1}{T} \sum_{t=0}^T \frac{\text{Flow-rate}(t) \cdot \text{Concentration}(t)}{\text{Average flow-rate}}, \quad (5)$$

for each disturbance scenario. As the influent model assumes constant $X_{BA}^{IN}(t) = X_P^{IN}(t) = S_O^{IN}(t) = S_{NO}^{IN}(t) = 0$ and $S_{ALK}^{IN}(t) = 7$, for all $t \in \mathbb{R}_{\geq 0}$, these variables are omitted.

Table 2 – Influent time-series: Flow-weighted average influent conditions for each disturbance scenario.

Variable	Dry weather	Storm event	Rain event	Long-term	Units
Period	14	14	14	609	days
Q_{IN}	18446.33	19744.72	21319.75	20850.54	$\text{m}^3 \text{d}^{-1}$
S_I^{IN}	30	28.03	25.96	27.05	g COD m^{-3}
S_S^{IN}	69.5	64.93	60.13	57.45	g COD m^{-3}
X_I^{IN}	51.2	51.92	44.3	48.15	g COD m^{-3}
X_S^{IN}	202.32	193.32	175.05	189.55	g COD m^{-3}
X_{BH}^{IN}	28.17	27.25	24.37	26.39	g COD m^{-3}
S_{NH}^{IN}	31.56	29.48	27.3	23.55	g N m^{-3}
S_{ND}^{IN}	6.95	6.49	6.01	5.58	g N m^{-3}
X_{ND}^{IN}	10.59	10.24	9.16	8.4	g N m^{-3}

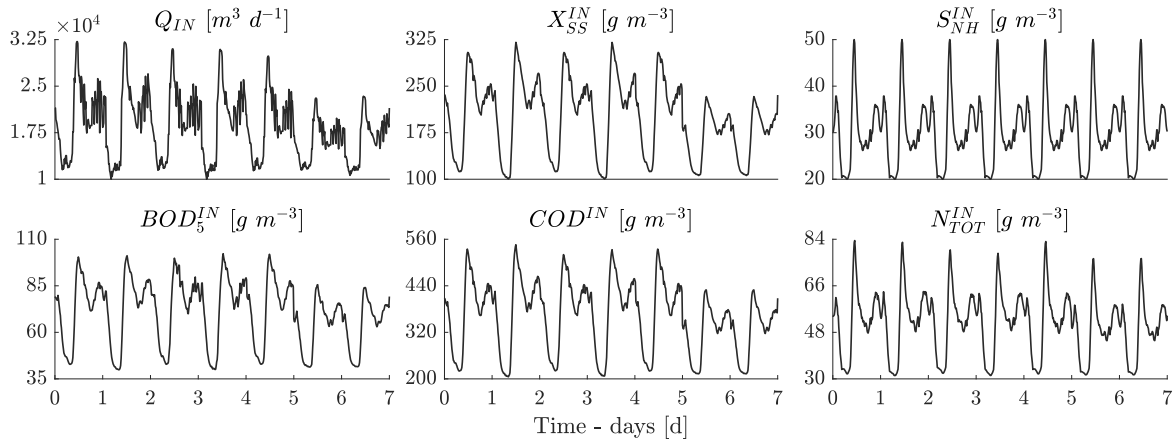
Source: Prepared by the authors.

A visualization of the first 7 days from the dry weather time-series is provided in Figure 3, in terms of the effluent measurements defined in Equation (3). The disturbance over this period is identical for the remaining short-term scenarios, as they are based on the dry weather influent. The influent total suspended solids (X_{SS}^{IN}), chemical oxygen demand (COD^{IN}), biochemical oxygen demand (BOD_5^{IN}) and total nitrogen (N_{TOT}^{IN}), are defined by

$$\begin{aligned} X_{SS}^{IN} &= 0.75(X_I^{IN} + X_S^{IN} + X_{BH}^{IN} + X_{BA}^{IN} + X_P^{IN}); \\ BOD_5^{IN} &= 0.25((1 - f_P)(X_{BH}^{IN} + X_{BA}^{IN}) + S_S^{IN} + X_S^{IN}); \\ COD^{IN} &= S_S^{IN} + S_I^{IN} + X_S^{IN} + X_I^{IN} + X_{BH}^{IN} + X_{BA}^{IN} + X_P^{IN}; \\ N_{TOT}^{IN} &= S_{NO}^{IN} + S_{NH}^{IN} + S_{ND}^{IN} + X_{ND}^{IN} + i_{XB}(X_{BH}^{IN} + X_{BA}^{IN}) + i_{XP}(X_P^{IN} + X_I^{IN}). \end{aligned} \quad (6)$$

This visualization highlights the diurnal and weekly patterns used in the influent model design. Every day, the wastewater flow-rate and its concentrations peak at mid-day, remaining at high levels until significantly decreasing at midnight. A decrease in the waste being produced can be perceived during the weekends (after 5 days), when industrial activity is expected to be smaller.

Figure 3 – Dry weather scenario, $t \in [0, 7]$: Time-series for influent flow-rate (Q_{IN}), and influent nitrogen and organic concentrations (X_{SS}^{IN} , S_{NH}^{IN} , BOD_5^{IN} , COD^{IN} , and N_{TOT}^{IN}), over a 1-week period.



Source: Prepared by the authors.

1.3.3 Process operation and control objectives

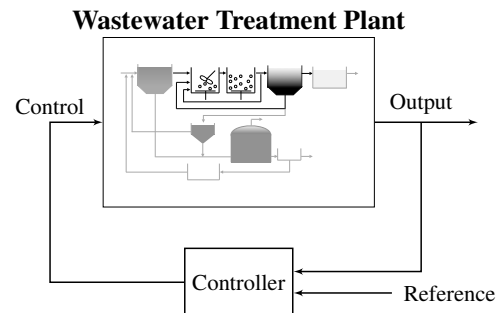
Conventionally, an activated sludge plant is operated to produce treated water by means of efficient carbon and nitrogen removal. Recently, the growing interest in wastewater reuse has encouraged different modes of operation that aim at obtaining tailored quantities of these chemicals. In this section, we detail the control objectives and performance evaluation criteria for both the conventional treatment application and a water reuse application for crop irrigation.

Conventional wastewater treatment

In conventional wastewater treatment, the general objective consists of producing effluent water satisfying, during the entire operation period, the quality upper limits shown at Table 3. These effluent limits are realistic suggestions for benchmarking, despite not corresponding to the actual requirements of a specific location. The control performance is evaluated by the number of limit violations and by the percentage of time that the effluent fails to meet the requirements.

Table 3 & Figure 4 – Treatment control: Quality limits and steady-state references for the effluent-based outputs (left), and diagram of the regulation control task (right).

Variable	Limit	Reference	Units
$X_{SS}^{S(10)}$	30	12.50	g COD m^{-3}
$S_{NH}^{S(10)}$	4	1.73	g N m^{-3}
$BOD_5^{S(10)}$	10	2.65	g COD m^{-3}
$COD^{S(10)}$	100	47.55	g COD m^{-3}
$N_{TOT}^{S(10)}$	18	14.05	g N m^{-3}



Source: Prepared by the authors.

In this work, we tackle the treatment control task by designing a feedback controller to regulate the process towards a reference steady-state satisfying the effluent requirements, as illustrated in Figure 4. For this purpose, we consider the default steady-state point $SS = (x^{SS}, u^{SS}, w^{SS}, y^{SS})$ suggested by the benchmark (GERNAEY et al., 2014). This point is obtained as the result of a 100-days open-loop simulation of the model equations (Eq. 4) with constant default values for the controllable inputs and constant influent conditions. This is a valid reference steady-state for the regulation control, as the output variables satisfy the upper quality limits (Table 3). The explicit values for all variables in the steady-state point are given in Appendix 4.

In addition to quality limits, a popular metric consists on the Effluent Quality Index (EQI),

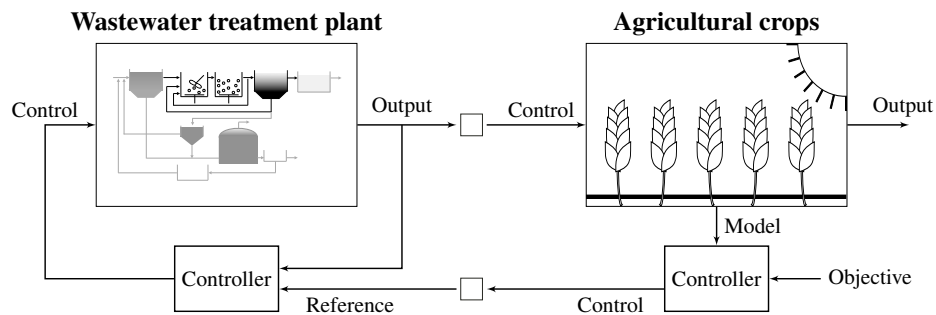
$$EQI = \frac{1}{1000T} \int_{t_0}^{t_f} (Q_{IN}(t) - Q_W(t)) \left(2X_{SS}^{S(10)}(t) + COD^{S(10)}(t) + 2BOD_5^{S(10)}(t) + 30N_{TKN}^{S(10)}(t) + 10S_{NO}^{S(10)}(t) \right) dt \quad (7)$$

over total operation period $T = (t_f - t_0)$ and given Kjeldahl nitrogen $N_{TKN}^{S(10)} = N_{TOT}^{S(10)} - S_{NO}^{S(10)}$. We consider this quantity to compare the overall effluent quality of the closed-loop control against the open-loop operation. This metric (in units of kg pollution unit d^{-1}) is proportional to the total effluent concentration of the pollutants considered relevant in most regional regulations.

Water reuse for crop irrigation

We consider the operation of activated sludge plants to produce reusable water of tailored quality for crop irrigation. We focus on soluble nitrogen as the relevant chemical for irrigation, as this nutrient is known to directly affect the growth rate for several classes of crops (PELAK et al., 2017). The control task thus consists of tracking an effluent of varying nitrogen content.

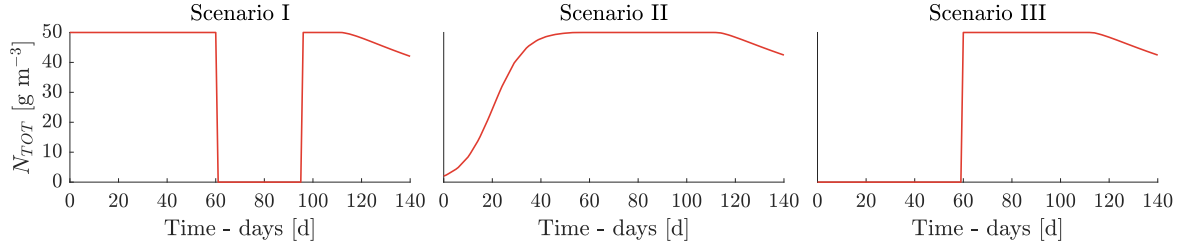
Figure 5 – Reuse control: Control hierarchy of the crop-treatment system. A fertigation plan for optimal crop growth is generated by the crop system, then imported as reference for the treatment plant.



Source: Prepared by the authors.

The reference nitrogen trajectories considered in this work are resulting from a higher-level control problem that aims at maximizing plant biomass using a simple crop growth system (NETO; HADDON, et al., 2021). The reuse control problem is then approached through a

Figure 6 – Reuse control: Nitrogen reference trajectories generated by the crop system for one growing season (140 days). Each scenario differs with respect to the initial soil nitrogen content being assumed.



Source: Prepared by the authors.

zero-offset controller that operates the treatment plant to supply total nitrogen (N_{TOT}) according to this optimal planning for crop growth. The coupling between both controllers is depicted in Figure 5. We consider three reference trajectories corresponding to different irrigation scenarios, shown in Figure. 6. These scenarios assume a normal growing season of 140 days. A detailed discussion about the computation of these references is given in Appendix 4.

The control performance is evaluated by the normalized mean-square error (NMSE),

$$J_{\text{NMSE}}(\tilde{y}, \tilde{y}^{sp}) = \frac{1}{T} \int_{t_0}^{t_f} \frac{\|\tilde{y}(t) - \tilde{y}^{sp}(t)\|^2}{\|\tilde{y}^{sp}(t)\|^2} dt, \quad (8)$$

measuring, for interval $T = t_f - t_0$, the tracking accuracy of the output variables of interest, $\tilde{y} \in \mathbb{R}^{N_{\tilde{y}}}$ ($N_{\tilde{y}} \leq N_y$), with respect to the desired reference, $\tilde{y}^{sp} \in \mathbb{R}^{N_{\tilde{y}}}$. Additionally, we introduce energy cost indices for the pumping energy (PE, in kWh d⁻¹), aeration energy (AE, in kWh d⁻¹), and carbon addition energy (CAE, in kg COD d⁻¹),

$$\text{PE} = \frac{1}{T} \int_{t_0}^{t_f} (0.004Q_A(t) + 0.008Q_R(t) + 0.05Q_W(t)) dt; \quad (9a)$$

$$\text{AE} = \frac{S_O^{sat}}{1.8(1000T)} \int_{t_0}^{t_f} \sum_{r=1}^5 V^{A(r)} K_{La}^{(r)}(t) dt; \quad (9b)$$

$$\text{CAE} = \frac{1}{1000T} \int_{t_0}^{t_f} \sum_{r=1}^5 S_S^{EC} Q_{EC}^{(r)}(t) dt, \quad (9c)$$

for oxygen saturation concentration S_O^{sat} , volumes $V^{A(r)}$, and carbon source concentration S_S^{EC} (Appendix 4). Collectively, these metrics define the operational cost index (OCI, in kWh d⁻¹),

$$\text{OCI} = \text{PE} + \text{AE} + f_{EC} \cdot \text{CAE}, \quad (10)$$

summarising the energy costs of a control strategy. The weighting factor is $f_{EC} = 3 \text{ kWh kg}^{-1}$.

2 THEORETICAL PRELIMINARIES

2.1 Dynamical models properties

We discuss general state-space representations of non-autonomous dynamical systems

$$\dot{x}(t) = f_t(x(t), u(t), w(t)|\theta_x); \quad (11a)$$

$$y(t) = g_t(x(t), u(t), w(t)|\theta_y). \quad (11b)$$

The state equation, Eq. (11a), describes how the state vector $x(t) \in \mathbb{R}^{N_x}$ evolves in time, given its current value and the controllable and uncontrollable but measurable input vectors $u(t) \in \mathbb{R}^{N_u}$ and $w(t) \in \mathbb{R}^{N_w}$, respectively. The measurement equation, Eq. (11b), describes how the state is emitted to form the measurement vector $y(t) \in \mathbb{R}^{N_y}$. The nonlinear, time-varying and parametric vector functions $f_t(\cdot|\theta_x)$ and $g_t(\cdot|\theta_y)$ define the dynamics and the measurement process, respectively. Vectors θ_x and θ_y are fixed model's parameters. We limit ourselves to autonomous functions $f(\cdot)$ and $g(\cdot)$ and no feedthrough of the inputs, $y(t) = g(x(t)|\theta_y)$. As time-invariance allows us to assume $t_0 = 0$, often we intentionally omit mentioning it.

The structural form of the state-space representation can be written using the linear model

$$\dot{x}(t) = Ax(t) + Bu(t) + Gw(t) \quad (12a)$$

$$y(t) = Cx(t) \quad (12b)$$

The structure of matrices A , B , G and C can be defined using inference diagrams in such a way that element $A_{n'_x, n_x}$ (respectively, B_{n_x, n_u} , G_{n_x, n_w} and C_{n_y, n_x}) is non-zero, and potentially unknown, whenever component x_{n_x} (u_{n_u} , w_{n_w} and again x_{n_x}) appears in the vector field $f_{n'_x}(\cdot)$ and algebraic function $g_{n_y}(\cdot)$; that is, whenever the (n'_x, n_x) -th element $\partial f_{n'_x}/\partial x_{n_x}$ (respectively, $\partial f_{n'_x}/\partial u_{n_u}$, $\partial f_{n'_x}/\partial w_{n_w}$ and $\partial g_{n_y}/\partial x_{n_x}$) in the Jacobian matrix(es) is not identically null. When the elements of A , B , G and C are either zeros or unknown, the resulting family of systems is referred to as structured dynamical system (REINSCHKE, 1988).

Under such representations, the dynamical properties of the system being studied can be characterised and discussed. By coupling controls to state variables and state variables to measurements, the notions of controllability and observability emerge as prerequisites for control and state estimation, respectively. These conditions can be relaxed in the absence of unstable modes, to derive the weaker notions of stabilisability and detectability. For linear systems, classical sufficient and necessary controllability and observability tests have been derived (KALMAN, R., 1960; CHEN, 1998). When the system is only known structurally, we have to resort to stronger notions of structural controllability and observability (LIN, 1974) and their associated sufficient and necessary conditions (LIU et al., 2011, 2013). For the sake of completeness and for notational necessity, this chapter overviews these concepts.

2.1.1 Stability

We review stability in terms of the conditions under which system Eq. (12) subjected to a bounded input produces bounded state- and bounded output-response trajectories. These two notions are often referred to as external and internal stability, the latter one being more general. For simplicity and without any loss of generality, we neglect the distinction between controls and disturbances and momentarily redefine the control matrix to be $B := [B|G]$.

A linear system with impulse response matrix $H(\cdot, \cdot) : \mathbb{R}_{\geq 0} \times \mathbb{R}_{\geq 0} \rightarrow \mathbb{R}^{N_y \times N_x}; (t, \tau) \mapsto H(t, \tau)$ is said to be stable if its output $y(t) = \int_{t_0}^t H(t, \tau)u(\tau)d\tau$ is bounded when the input $u(t)$ is bounded. This notion of external stability is defined as the existence of a finite gain $\kappa < \infty$ such that for all bounded inputs u the following relation holds

$$\|y(t)\|_{\infty} \leq \kappa \|u(t)\|_{\infty}. \quad (13)$$

External stability Eq. (13) can be verified at the system level by showing that, under some mild conditions on the smoothness of u and H , the upper bound κ for the induced matrix norm of the input-output map exists and can be used as gain in Eq. (13); that is,

$$\sup_{t \in \mathbb{R}_{\geq 0}} \left\{ \int_{t_0}^t \|H(t, \tau)\|_{\infty} d\tau \right\} = \kappa < \infty. \quad (14)$$

For a LTI system (12), $H(t, \tau) = H(t - \tau) = Ce^{A(t-\tau)}B$. Condition Eq. (14) specialises and, equivalently, it suffices to show that *i*) the impulse response is absolutely integrable and *ii*) the transfer function $H(s) = \mathcal{L}[H(t)] = C(sI - A)^{-1}B$ is Hurwitz (all the poles λ of all of its elements lie on the open left half of the complex plane):

$$i) \quad \int_{t_0}^{\infty} \|H(t)\| dt < \infty; \quad (15a)$$

$$ii) \quad \{\lambda[H(s)] \in \mathbb{C} : \text{Re}(\lambda) < 0\}. \quad (15b)$$

More generally, a linear system (A, B, C) with state transition matrix $\Phi(\cdot, \cdot) : \mathbb{R}_{\geq 0} \times \mathbb{R}_{\geq 0} \rightarrow \mathbb{R}^{N_x \times N_x}; (t, \tau) \mapsto \Phi(t, \tau)$ is stable if both its state $x(t) = \Phi(t, t_0)x(t_0) + \int_{t_0}^t \Phi(t, \tau)Bu(\tau)d\tau$ and output $y(t) = C\Phi(t, t_0)x(t_0) + C \int_{t_0}^t \Phi(t, \tau)Bu(\tau)d\tau$ responses are bounded for every bounded input $u(t)$. This notion of joint internal and external stability is defined for representations with bounded functions B and C (that is, when $\|B\|_{\infty} < \infty$ and $\|C\|_{\infty} < \infty$) as the existence of positive constants β and γ such that, for every bounded input u and every initial condition x_0 ,

$$\|x(t)\|_{\infty} \leq \beta \|x_0\| + ((\beta/\gamma)\|B\|_{\infty}) \|u(t)\|_{\infty} \quad (16a)$$

$$\|y(t)\|_{\infty} \leq (\beta\|C\|_{\infty}) \|x_0\| + ((\beta/\gamma)\|C\|_{\infty}\|B\|_{\infty}) \|u(t)\|_{\infty} \quad (16b)$$

Importantly, the definition is valid only for systems whose homogeneous part is exponentially stable with the same constants β and γ (that is, when $\|\Phi(t, \tau)\| \leq \beta e^{-\gamma(t-\tau)}$). At the system level, internal and external stability Eq. (16) can be verified by showing that the state matrix A is Hurwitz (all the eigenvalues λ lie on the open left half of the complex plane); Formally,

Lemma 2.1. (CALLIER; DESOER, 1991). *A system with a LTI representation Eq. (12) is said to be exponentially stable at the system level, or just stable, if and only if*

$$\{\lambda[A] \in \mathbb{C} : \text{Re}(\lambda) < 0\} \quad (17)$$

For the LTI system Eq. (12) where $\Phi(t, \tau)$ is the matrix exponential $e^{A(t-\tau)}$, the entries of the state transition matrix are linear combinations of the system modes. Letting $\lambda[A] = \{\lambda_{n_x}\}_{n_x=1}^{N_x}$ be the eigenvalues of matrix A , with $\{\lambda_1, \dots, \lambda_N\} \subseteq \mathbb{R}$ and $\{(\lambda_{N+1}, \lambda_{N+1}^*), \dots, (\lambda_{N+S}, \lambda_{N+S}^*)\} \subseteq \mathbb{C}$ being the eigenvalues with respective algebraic multiplicities $\mu(\lambda_{n_x})$, and given coefficients $\alpha_{n,k}^{(i,j)}, \beta_{n,k}^{(i,j)}, \phi_{n,k}^{(i,j)} \in \mathbb{R}$, each (i, j) -th entry in transition matrix $\Phi(t, \tau) = e^{A(t-\tau)}$ is of the form

$$\begin{aligned} \left[e^{A(t-\tau)} \right]_{i,j} &= \sum_{n=1}^N \sum_{k=0}^{\mu(\lambda_n)-1} \left(\alpha_{n,k}^{(i,j)} (t-\tau)^k \right) e^{\lambda_n(t-\tau)} \\ &+ \sum_{n=N+1}^{N+S} \sum_{k=0}^{\mu(\lambda_n)-1} \left(\beta_{n,k}^{(i,j)} (t-\tau)^k \cos(\text{Im}(\lambda_n)(t-\tau) + \phi_{n,k}^{(i,j)}) \right) e^{\text{Re}(\lambda_n)(t-\tau)}. \end{aligned} \quad (18)$$

The condition Eq. (17) implies that $\lim_{t \rightarrow \infty} [\Phi(t, \tau)]_{i,j} = 0$, for all (i, j) . Therefore, it is possible to verify exponential stability at the system level since that, for any fixed $\tau \leq t$, the homogeneous part is strictly decreasing with $\max_t \|\Phi(t, \tau)\| = \|\Phi(\tau, \tau)\| \leq \beta$ and $\lim_{t \rightarrow \infty} \|\Phi(t, \tau)\| = 0$.

2.1.2 Controllability and observability

A system is said to be full-state controllable if it is possible to steer its state vector from any initial value to any final value in finite time, whereas it is said to be full-state observable if it is possible to uniquely determine its initial state from a sequence of measurements over a finite time interval. These notions are overviewed and classical necessary and sufficient conditions are given for LTI systems. For uncertain systems, the stronger sufficient and necessary structural conditions are reviewed. Due to the duality between both properties, this section focus on the definitions concerning only controllability, thus avoiding repetitive statements. For the sake of completeness, the observability counterparts are presented in Appendix 4.

Classical controllability

Let the controllability Gramian of the pair (A, B) be the $N_x \times N_x$ symmetric matrix

$$W_c(t) = \int_0^t e^{A\tau} B B^T e^{A^T \tau} d\tau, \quad (19)$$

a sufficient and necessary controllability condition is $\det(W_c(t)) \neq 0, \forall t > 0$. The computation of Gramian-based criteria in Eq. (19) is straightforward but unpractical. Equivalent criteria can be defined in terms of the system's controllability matrix (KALMAN, R., 1960).

Let $\mathcal{C} = [B \ AB \ A^2B \ \dots \ A^{N_x-1}B]$ be the $N_x \times (N_x \times N_u)$ controllability matrix of the system. A sufficient and necessary condition for controllability is

$$\text{rank}(\mathcal{C}) = N_x. \quad (20)$$

The criterion in Eq. (20) is more direct and, for low-dimensional systems, its evaluation only requires a small number of matrix multiplications. However, the computation of matrix \mathcal{C} can still be troublesome when the dimensionality of the state vector is large. This limitation is due to numerical over- and under-flow that may result from computing large powers of A and A^\top .

A scalable alternative that overcomes the limitations of both Gramian-based and Kalman's rank criteria is provided by the Popov-Belevitch-Hautus (PBH) test. Necessary and sufficient conditions are given by the following lemma:

Lemma 2.2. (HAUTUS, 1970). *The following statements are all equivalent:*

$$\text{I. The pair } (A, B) \text{ is controllable} \quad (21a)$$

$$\text{II. } \text{rank}\left(\begin{bmatrix} \lambda I - A & B \end{bmatrix}\right) = N_x, \forall \lambda \in \mathbb{C}; \quad (21b)$$

$$\text{III. } \text{rank}\left(\begin{bmatrix} \lambda_i I - A & B \end{bmatrix}\right) = N_x, \forall \lambda_i \in \sigma(A) \subset \mathbb{C}. \quad (21c)$$

Based on Lemma 2.2, the pair (A, B) is said to be controllable if and only if, for each eigenvalue $\lambda_i \in \sigma(A)$ (that is, when $\text{rank}(\lambda_i I - A) < N_x$), the columns of B have at least one component in the direction $v_i \in \mathbb{R}^{N_x}$, v_i being the eigenvector of A associated to λ_i ; The eigenvectors v_i for which $\text{rank}([\lambda_i I - A \ B]) < N_x$ indicate state-space directions that are uncontrollable with the controls determined by B .

Since controllability is invariant with respect to similarity transformations represented by nonsingular matrices $P \in \mathbb{R}^{N_x \times N_x}$, the following holds:

- Pair (A, B) is controllable if and only if pair $(A', B') = (P^{-1}AP, P^{-1}B)$ is controllable;

Controllability metrics

Full-state controllability is a binary property. Starting from the seminal work by Müller and Weber (1972), various scalar metrics have been proposed to quantify the difficulty of the control task. We overview energy-related metrics recently proposed by Pasqualetti et al. (2014) and Summers et al. (2016) for the controllability of LTI systems.

Define the quadratic control and measurement energies

$$E_c(u(t), t | R) = \int_0^t u(\tau)^\top R u(\tau) d\tau = \|u(t)\|_R^2; \quad (22a)$$

$$E_o(y(t), t | Q) = \int_0^t y(\tau)^\top Q y(\tau) d\tau = \|y(t)\|_Q^2. \quad (22b)$$

In optimal quadratic regulation, we search for a controller that minimises the sum of these energies, for some user-defined positive definite weighting matrices $R \in \mathbb{R}^{N_x \times N_x}$ and $Q \in \mathbb{R}^{N_y \times N_y}$. When minimised individually with identity matrix $R = I_u$, the unweighted control energy determines

- $\tilde{u}(t) = B^\top e^{A^\top(t_f-t)} W_c^{-1}(t_f) (x(t_f) - e^{At_f} x(0))$, the control from $x(0)$ to $x(t_f)$ of minimum L_2 -effort $E_c^*(t | \tilde{u}(t)) = (x(t_f) - e^{At_f} x(0))^\top W_c^{-1}(t) (x(t_f) - e^{At_f} x(0))$;

Finite- and infinite-horizon controllability metrics can thus be derived from Eq. (19). The eigenvectors $\{v_{n_x}(\lambda_{n_x}^c)\}_{n_x=1}^{N_x}$ associated with the eigenvalues $\lambda_{n_x}^c \in \sigma(W_c(t))$ correspond to state-space directions that require increasingly larger control energy the smaller $\lambda_{n_x}^c$. The control effort associated with pair (A, B) can thus be quantified by single scalars defined from the spectrum $\sigma(W_c(t)) = \{\lambda_{n_x}^c\}_{n_x=1}^{N_x}$. Because the infinite-time Gramian, $W_c(\infty)$, always exists for Hurwitz systems, Eq. (17), and its computation can be performed efficiently by solving a Lyapunov equation (BENNER et al., 2008), we overview only a number of infinite-time metrics. Their finite-time counterparts are evaluated by integrating Eq. (19).

Definition 2.1. (Energy-related controllability metrics, (SUMMERS et al., 2016)) Let $W_c(\infty)$ be the solution of $AW_c(\infty) + W_c(\infty)A^\top + BB^\top = 0$. The control effort for the pair (A, B) can be quantified according to the following scalar metrics:

- I. $\text{trace}(W_c(\infty))$: Inversely related to the control effort averaged over all state-space directions;
- II. $\text{trace}(W_c^\dagger(\infty))$: Related to the control effort averaged over all directions in the state-space;
- III. $\log(\det(W_c(\infty)))$: Related to the volume of a N_x -dimensional hyper-ellipsoid whose points are reachable with one unit or less of control energy;
- IV. $\lambda_{\min}^c(W_c(\infty))$: Inversely related to the control energy along the least controllable eigen-direction.

The control effort associated to attempting to control the full-state by only controlling one individual state variable x_{n_x} at a time is quantified by

$$C_c(n_x) = \text{trace}(W_{c,n_x}(\infty)). \quad (23)$$

This non-negative quantity, the average controllability centrality (SUMMERS et al., 2016), is

computed by assuming a single control that actuates only on the n_x -th state variable: That is, when $B = e_{n_x}$, a unit vector in the standard basis of \mathbb{R}^{N_x} . The infinite-horizon controllability Gramians $W_{c,n_x}(\infty) \in \mathbb{R}^{N_x \times N_x}$ are computed independently for each $n_x \in \{1, \dots, N_x\}$ by solving the Lyapunov equations $AW_{c,n_x}(\infty) + W_{c,n_x}(\infty)A^\top = -e_{n_x}e_{n_x}^\top$.

Structural controllability

Structural analysis aims at assessing a family of systems with the same structure. As it encodes the relationships between state-, control- and output-variables, analysing a structured system assess the controllability and observability properties of each possible realisation from the family of systems it represents. The dynamics and measurement process of a structured dynamical system (A, B, C) can be studied by mapping its state and output equations onto the digraph

$$\mathcal{G} = (\mathcal{V}, \mathcal{E}), \quad (24)$$

where the vertex set $\mathcal{V} = \mathcal{V}_A \cup \mathcal{V}_B \cup \mathcal{V}_C$ consists of the union of vertex sets $\mathcal{V}_A = \{x_1, \dots, x_{N_x}\}$ of state, $\mathcal{V}_B = \{u_1, \dots, u_{N_u}\}$ of control, and $\mathcal{V}_C = \{y_1, \dots, y_{N_y}\}$ of output components. The edge set $\mathcal{E} = \mathcal{E}_A \cup \mathcal{E}_B \cup \mathcal{E}_C$ is the union of set $\mathcal{E}_A = \{(x_{n_x}, x_{n'_x}) \mid A_{n'_x, n_x} \neq 0\}$ of directed edges between state component vertices, set $\mathcal{E}_B = \{(u_{n_u}, x_{n_x}) \mid B_{n_x, n_u} \neq 0\}$ of directed edges between state and control component vertices, and set $\mathcal{E}_C = \{(x_{n_x}, y_{n_y}) \mid C_{n_y, n_x} \neq 0\}$ of directed edges between state and output component vertices.

Specifically, the structural controllability of the family of systems with dynamics represented by pair (A, B) can be studied through its associated directed subgraph $\mathcal{G}_c = (\mathcal{V}_c, \mathcal{E}_c)$, defined by the vertex set $\mathcal{V}_c = \mathcal{V}_A \cup \mathcal{V}_B$ and the edge set $\mathcal{E}_c = \mathcal{E}_A \cup \mathcal{E}_B$. The pair (A, B) is said to be structurally controllable if the nonzero elements of A and B can be set in such a way that the system is controllable in the classical sense. Formally, we have the definition

Definition 2.2. (Structural Controllability, (LIN, 1974)). The pair (A, B) is said to be structurally controllable if and only if there exists a controllable pair (\bar{A}, \bar{B}) of same dimension and structure of pair (A, B) such that $\|\bar{A} - A\| < \varepsilon$ and $\|\bar{B} - B\| < \varepsilon$, for an arbitrarily small $\varepsilon > 0$.

Two pairs (A, B) and (\bar{A}, \bar{B}) have the same structure if they have the same dimensions and each element $A_{n_1, n_2} \neq 0$ (respectively, $B_{n_x, n_u} \neq 0$) whenever $\bar{A}_{n_1, n_2} \neq 0$ (respectively, $\bar{B}_{n_x, n_u} \neq 0$). The necessary and sufficient conditions for structural controllability are the following:

Lemma 2.3. (LIN, 1974). Let $\mathcal{G}_c = (\mathcal{V}_c, \mathcal{E}_c)$ be the directed network associated to the pair (A, B) . The pair (A, B) is said to be structurally controllable if and only if the following conditions hold:

- (Accessibility) For every state-node $x_{n_x} \in \mathcal{V}_A$ there exists at least one directed path starting from any control-node $u_{n_u} \in \mathcal{V}_B$ to x_{n_x} .

- (Dilation-free) For every $\mathcal{S} \subseteq \mathcal{V}_A$, $|T(\mathcal{S})| \geq |\mathcal{S}|$, where $T(\mathcal{S}) = \{v_j \in \mathcal{V}_c \mid x_{n_x} \in \mathcal{S} \wedge (v_j, x_{n_x}) \in \mathcal{E}_c\}$ denotes a neighbourhood set for \mathcal{S} .

The first condition can be verified by identifying the state vertices that are accessible from each possible origin vertex (a control): Any graph search algorithm can be used for the task (CORMEN et al., 2009). The second condition can be verified by forming a maximum matching $\mathcal{M} \subseteq \Gamma$ of an equivalent bipartite graph $\mathcal{K} = (\mathcal{V}_A^+, \mathcal{V}_A^-, \Gamma)$ and then checking that all unmatched state vertices $x_j \in \mathcal{V}_A^-$ are directly connected to distinct control vertices in $\mathcal{G}_c = (\mathcal{V}_c, \mathcal{E}_c)$ (LIU et al., 2011). The maximum matching problem consists of identifying a (possibly not unique) subset of edges without common vertices that has maximum cardinality. The bipartite graph $\mathcal{K} = (\mathcal{V}_A^+, \mathcal{V}_A^-, \Gamma)$ is defined by the disjoint and independent vertex sets $\mathcal{V}_A^+ = \{x_1^+, \dots, x_{N_x}^+\}$ and $\mathcal{V}_A^- = \{x_1^-, \dots, x_{N_x}^-\}$, and by the undirected edge set $\Gamma = \{(x_{n_1}^+, x_{n_2}^-) \mid (x_{n_1}, x_{n_2}) \in \mathcal{E}_c\}$. Distinct control nodes linked to unmatched state vertices form a \mathcal{V}_A^- -perfect matching. A guarantee of the dilation-free condition thus follows from the Hall's theorem (HALL, 1935).

2.1.3 Reduced-order models and stabilisability

A system which is not controllable can be decomposed into controllable and not controllable parts by a similarity transformation $P_c \in \mathbb{R}^{N_x \times N_x}$. In this section, we overview the Kalman decomposition theorem for obtaining minimal realisations of LTI systems from such transformation. For uncontrollable systems, the weaker property of stabilisability is also overviewed.

Kalman decomposition theorem

Let $S \in \mathbb{R}^{N_x \times N_x}$ and $T \in \mathbb{R}^{N_x \times N_x}$ be a pair of transformation matrices satisfying $ST = I$. The linear transformation $\tilde{x} = Sx$ resulting in the state-space representation

$$\begin{aligned}\dot{\tilde{x}}(t) &= \tilde{A}\tilde{x}(t) + \tilde{B}u(t) \\ y(t) &= \tilde{C}\tilde{x}(t),\end{aligned}$$

with $\tilde{A} \in \mathbb{R}^{N_{\tilde{x}} \times N_{\tilde{x}}} = SAT$, $\tilde{B} \in \mathbb{R}^{N_{\tilde{x}} \times N_u} = SB$, and $\tilde{C} \in \mathbb{R}^{N_y \times N_{\tilde{x}}} = CT$, is considered a $N_{\tilde{x}}$ -order reduced model of the full-order model (A, B, C) whenever $N_{\tilde{x}} < N_x$. The quality of the reduced-order model $(\tilde{A}, \tilde{B}, \tilde{C})$ can be assessed in terms of the approximation error

$$\|\tilde{G} - G\|_{\mathcal{H}_\infty} \|u\|_{\mathcal{L}_2} \quad (\forall u \in \mathbb{R}^{N_u}),$$

for the input-output maps $\tilde{G}(s) = \tilde{C}(sI - \tilde{A})^{-1}\tilde{B}$ and $G(s) = C(sI - A)^{-1}B$.

A perfect reduced-order model can be obtained by means of computing the minimal realisation of (A, B, C) using the Kalman decomposition theorem:

Lemma 2.4. (Minimal Realisation, (KALMAN, R. E., 1963)). Let \mathcal{C} and \mathcal{O} be, respectively,

the controllability and observability matrix of a full-order model (A, B, C) , with $\text{rank}(\mathcal{C}) = N_{\mathcal{C}}$, $\text{rank}(\mathcal{O}) = N_{\mathcal{O}}$ and $\text{rank}([\mathcal{C} \ \mathcal{O}^T]) = N_{\mathcal{C}\mathcal{O}}$. Now, let $\tilde{x} = [x_{co} \ x_{\bar{c}o} \ x_{c\bar{o}} \ x_{\bar{c}\bar{o}}]^T = P^{-1}x$ be a linear transformation converting (A, B, C) into Kalman's canonical form

$$\begin{bmatrix} \dot{x}_{co}(t) \\ \dot{x}_{c\bar{o}}(t) \\ \dot{x}_{\bar{c}o}(t) \\ \dot{x}_{\bar{c}\bar{o}}(t) \end{bmatrix} = \begin{bmatrix} A_{co} & 0 & A_{13} & 0 \\ A_{21} & A_{c\bar{o}} & A_{23} & A_{24} \\ 0 & 0 & A_{\bar{c}o} & 0 \\ 0 & 0 & A_{43} & A_{\bar{c}\bar{o}} \end{bmatrix} \begin{bmatrix} x_{co}(t) \\ x_{c\bar{o}}(t) \\ x_{\bar{c}o}(t) \\ x_{\bar{c}\bar{o}}(t) \end{bmatrix} + \begin{bmatrix} B_{co} \\ B_{c\bar{o}} \\ 0 \\ 0 \end{bmatrix} u(t)$$

$$y(t) = \begin{bmatrix} C_{co} & 0 & C_{\bar{c}o} & 0 \end{bmatrix} \tilde{x}(t).$$

The minimal realisation (A_{co}, B_{co}, C_{co}) is a reduced model of order $N_{x_{co}} = N_{\mathcal{C}} + N_{\mathcal{O}} - N_{\mathcal{C}\mathcal{O}}$.

The minimal realisation is a reduced model of (A, B, C) which is both controllable and observable. This model can be efficiently obtained even for high-dimensional state-spaces, as the actual computation of matrices \mathcal{C} and \mathcal{O} can be avoided (VAN DOOREN, 1981). Moreover, $\tilde{G}(s) = C_{co}(sI - A_{co})^{-1}B_{co} = C(sI - A)^{-1}B = G(s)$, such that this realisation is a perfect approximation with error $\|\tilde{G} - G\|_{\mathcal{H}_{\infty}} \|u\|_{\mathcal{L}_2} = 0$, for all $u \in \mathbb{R}^{N_u}$. However, the minimal realisation has full-order $N_{x_{co}} = N_x$ whenever (A, B, C) is both controllable and observable.

Stabilizability

A system is said stabilizable if it possible to steer its state vector from any initial state to the zero-state (a steady-state, for linearised systems). This condition is often perceived as a weaker alternative to full-state controllability. Formally,

Definition 2.3. (Stabilizability). The pair (A, B) is said to be stabilizable if, given any initial state $x(0)$, it is possible to design an input $u(t)$ such that $x(t) \rightarrow 0$ as $t \rightarrow \infty$.

Sufficient and necessary conditions for stabilizability can be derived from the Kalman canonical decomposition of the system. Let $\mathcal{C} = [B \ AB \ A^2B \ \dots \ A^{N_x-1}B]$ be the $\mathbb{R}^{N_x \times N_x N_u}$ controllability matrix of a system (A, B) , with $\text{rank}(\mathcal{C}) = N_{x_c} \leq N_x$. There exists a nonsingular matrix $P_c \in \mathbb{R}^{N_x \times N_x}$, whose first N_{x_c} columns are the linearly independent columns of \mathcal{C} , such that the transformation $\tilde{x} = P_c^{-1}x$ has a state equation in the form

$$\begin{bmatrix} \dot{\tilde{x}}_c(t) \\ \dot{\tilde{x}}_{\bar{c}}(t) \end{bmatrix} = \begin{bmatrix} A_c & A_{12} \\ 0 & A_{\bar{c}} \end{bmatrix} \begin{bmatrix} \tilde{x}_c(t) \\ \tilde{x}_{\bar{c}}(t) \end{bmatrix} + \begin{bmatrix} B_c \\ 0 \end{bmatrix} u(t),$$

with $\tilde{x}_c(t) \in \mathbb{R}^{N_1}$ and $\tilde{x}_{\bar{c}}(t) \in \mathbb{R}^{(N_x - N_1)}$. A sufficient and necessary condition for stabilizability is that $\text{Re}(\lambda_j) < 0$ for all $\lambda_j \in \sigma(A_{\bar{c}}) \subset \sigma(A)$ (CHEN, 1998). Although straightforward, this criterion is unpractical for high-dimensional systems as the design of P_c requires the computation of the full controllability matrix $\mathcal{C} = [B \ AB \ A^2B \ \dots \ A^{N_x-1}B]$.

A scalable alternative is given by the Popov-Belevitch-Hautus (PBH) stabilizability test, based on the Hautus lemma:

Lemma 2.5. (HAUTUS, 1970). Let $\sigma(A) = \{\lambda_i\}_{i=1}^{N_x}$ be the spectrum of A and $\tilde{\sigma}(A) = \{\lambda_i \in \sigma(A) \mid \text{Re}(\lambda_i) \geq 0\}$ be the set of eigenvalues with positive real part. The statement ‘the pair (A, B) is stabilizable’ is equivalent to the following statements:

$$\text{I. } \text{rank}\left(\begin{bmatrix} \lambda I - A & B \end{bmatrix}\right) = N_x, \forall \lambda \in \mathbb{C}; \quad (25a)$$

$$\text{II. } \text{rank}\left(\begin{bmatrix} \lambda_i I - A & B \end{bmatrix}\right) = N_x, \forall \lambda_i \in \tilde{\sigma}(A) \subset \mathbb{C}. \quad (25b)$$

Thus, the pair (A, B) is stabilizable if and only if, for each unstable eigenvalue λ_i of A (that is, when $\text{Re}(\lambda_i) \geq 0$ and $\text{rank}(\lambda_i I - A) < N_x$), the columns of B have at least one component in the direction $v_i \in \mathbb{R}^{N_x}$, v_i being the eigenvector of A associated to λ_i . Importantly, every system (A, B) with a Hurwitz matrix A is consequently stabilizable, since $\tilde{\sigma}(A) = \emptyset$.

2.2 Model predictive control

We discuss the design of optimal controls $u(t) = \pi(x(t)|\theta_u)$ that transfers a system from initial state $x(t_0)$ to a desired state $x(t_f)$ by means of predictive control. Specifically, we aim at obtaining the optimal control $u^*(\cdot) : \mathbb{R}_{\geq 0} \rightarrow \mathbb{R}^{N_u}$, and resulting optimal state trajectory $x^*(\cdot) : \mathbb{R}_{\geq 0} \rightarrow \mathbb{R}^{N_x}$, that solves finite-horizon optimal control problems (OCP) in the form

$$\min_{x(\cdot), u(\cdot)} J(x(\cdot), u(\cdot)) = \int_{t_0}^{t_f} L(x(t), u(t)) dt + L_f(x(t_f)) \quad (26a)$$

$$\text{s.t. } \dot{x}(t) = f(x(t), u(t), w(t)|\theta_x), \quad (26b)$$

$$x(t) \in \mathcal{X}, \quad u(t) \in \mathcal{U}, \quad (26c)$$

$$\Phi(x(t_0), x(t_f)) = 0. \quad (26d)$$

The functions $L(\cdot, \cdot) : \mathbb{R}^{N_x} \times \mathbb{R}^{N_u} \rightarrow \mathbb{R}_{\geq 0}$ and $L_f(\cdot) : \mathbb{R}^{N_x} \rightarrow \mathbb{R}_{\geq 0}$ define, respectively, the stage and terminal cost functions. The sets \mathcal{X} and \mathcal{U} characterise the constraints to the state and control trajectories, respectively. The vector-valued function $\Phi(\cdot, \cdot) : \mathbb{R}^{N_x} \times \mathbb{R}^{N_x} \rightarrow \mathbb{R}^{N_\Phi}$ defines N_Φ equality constraints on the initial state $x(t_0)$ and terminal $x(t_f)$, and their combinations.

In this section, we review the *discretise-then-optimize* approach of solving OCPs, and then we overview the Model Predictive Control (MPC) strategy as a closed-loop controller. We also discuss the constrained affine quadratic regulator (c-AQR) class of OCPs arising from a specific choice of cost and constraints functions. Finally, a zero-offset MPC formulation is proposed to deal with regulation and reference tracking control tasks using linearisations of nonlinear models.

2.2.1 Discretise-then-optimise and the direct method

In general, solving optimisation Eq. (26) requires solving a two-value boundary-value problem for the Hamiltonian system defined by state-equation $\dot{x}(t) = (\partial H / \partial \lambda)$ and adjoint-state equation $\dot{\lambda}(t) = -(\partial H / \partial x)$, with $H = J(\cdot) + \lambda^\top f(\cdot) + \mu^\top h(\cdot)$ being the augmented Hamiltonian (KIRK, 2004). The vector-valued function $h(\cdot) : \mathbb{R}^{N_x} \times \mathbb{R}^{N_u} \rightarrow \mathbb{R}^{N_\mu}$ refers to the inequality constraints used to represent \mathcal{X} and \mathcal{U} . Although this approach (known as the *indirect approach*) leads to the optimal control function, $u^*(\cdot)$, its solutions are often only computationally feasible under reasonably strict conditions (e.g., small-scale linear unconstrained systems).

In the direction of a more practical approach to solve general OCPs, we focus on the *discretise-then-optimise* approach. For each time interval $t \in [t_k, t_{k+1})$, we consider piecewise constant inputs $u(t) = u(t_k)$ and $w(t) = w(t_k)$, with $t_k = k\Delta t$ the k -th time instant given period $\Delta t > 0$. The state dynamics can thus be represented in discrete-time by the transition function

$$x_{k+1} = f_{\Delta t}(x_k, u_k, w_k | \theta_x) = x_k + \int_{t_k}^{t_{k+1}} f(x(\tau), u_k, w_k | \theta_x) d\tau, \quad (27)$$

with $x_k = x(k\Delta t)$, $u_k = u(k\Delta t)$, and $w_k = w(k\Delta t)$. The discrete-time output equation is given by $y_k = y(k\Delta t) = g(x_k | \theta_y)$. Under this discrete-time representation, the control horizon can be partitioned into $N = \lfloor (t_f - t_0) / \Delta t \rfloor$ intervals as $T = \{[t_n, t_{n+1}]\}_{n=0}^N$ such that the integral term in the objective functional $J(x, u)$, Eq. (26), can be approximated by the left Riemann sum

$$\int_{t_0}^{t_f} L(x(t), u(t)) dt \approx \Delta t \sum_{n=0}^{N-1} L(x(t_n), u(t_n)) = \Delta t \sum_{n=0}^{N-1} L(x_n, u_n) \propto \sum_{n=0}^{N-1} L(x_n, u_n).$$

Similarly, the terminal cost is directly $L_f(x(t_f)) = L_f(x_N)$. Considering such approximations, the general problem in Eq. (26) reduces to a finite-dimensional optimisation over the sequence of control actions (u_0, \dots, u_{N-1}) and states (x_0, \dots, x_N) . We formally define this class of OCPs:

Definition 2.4. (Discrete-time optimal control problem). Consider a system with dynamics represented by $x_{n+1} = f_{\Delta t}(x_n, u_n, w_n | \theta_x)$. For cost functions $L(\cdot, \cdot) : \mathbb{R}^{N_x} \times \mathbb{R}^{N_u} \rightarrow \mathbb{R}_{\geq 0}$ and $L_f(\cdot) : \mathbb{R}^{N_x} \rightarrow \mathbb{R}_{\geq 0}$, constraint sets \mathcal{X} and \mathcal{U} , and equality conditions $\Phi(\cdot, \cdot) : \mathbb{R}^{N_x} \times \mathbb{R}^{N_x} \rightarrow \mathbb{R}^{N_\Phi}$, a discrete-time optimal control problem is defined as an optimisation problem in the form

$$\min_{\substack{x_0, \dots, x_N, \\ u_0, \dots, u_{N-1}}} J_{\Delta t}(x, u) = \sum_{n=0}^{N-1} L(x_n, u_n) + L_f(x_N) \quad (28a)$$

$$\text{s.t.} \quad x_{n+1} = f_{\Delta t}(x_n, u_n, w_n | \theta_x), \quad (28b)$$

$$\forall n \in [0, N-1] \quad x_n \in \mathcal{X}, \quad u_n \in \mathcal{U}, \quad (28c)$$

$$\Phi(x_0, x_N) = 0. \quad (28d)$$

The optimisation in Definition. 2.4 is solved by transcribing the problem into a standard nonlinear program (NLP) from which candidate solutions satisfying optimality conditions can be obtained using numerical methods. This is known as the *direct approach* to optimal control (BETTS, 2010). Specifically, consider the constrained nonlinear program,

$$\min_{x,u} J_{\Delta t}(x,u) \quad (29a)$$

$$\text{s.t. } G(x,u) = 0, \quad H(x,u) \leq 0, \quad (29b)$$

where $x = (x_0, \dots, x_N) \in \mathbb{R}^{(N)N_x}$ and $u = (u_0, \dots, u_{N-1}) \in \mathbb{R}^{(N-1)N_u}$ are the decision vectors, function $G(x,u) : \mathbb{R}^{(N)N_x} \times \mathbb{R}^{(N-1)N_u} \rightarrow \mathbb{R}^{N+N_\Phi}$ is obtained by collecting all dynamical constraints in Eq. (28b) and conditions Eq. (28d), and $H(x,u) : \mathbb{R}^{(N)N_x} \times \mathbb{R}^{(N-1)N_u} \rightarrow \mathbb{R}^{N_\mu}$ represents both constraint sets \mathcal{X} and \mathcal{U} in Eq. (28c). A candidate solution for Eq. (29) can be obtained by solving the first-order Karush-Kuhn-Tucker (KKT) optimality conditions,

$$\nabla_{(x,u)} \mathcal{L}(x,u,\lambda,\mu) = 0 \quad (30a)$$

$$G(x,u) = 0, \quad H(x,u) \leq 0, \quad (30b)$$

$$\mu \geq 0, \quad \mu_j H_j(x,u) = 0 \quad (j = 1, \dots, N_\mu), \quad (30c)$$

with Lagrangian function $\mathcal{L}(x,u,\lambda,\mu) = J_{\Delta t}(x,u) + \lambda^\top G(x,u) + \mu^\top H(x,u)$ defined given the Lagrange multipliers $\lambda = [\lambda_0 \dots \lambda_{N-1+N_\Phi}]^\top \in \mathbb{R}^{N+N_\Phi}$ and $\mu = [\mu_0 \dots \mu_{N_\mu}]^\top \in \mathbb{R}^{N_\mu+1}$. In general, the KKT conditions are solved using Newton-type methods, including active-set methods to deal with Eqs. (30b, 30c), the inequality constraints (BETTS, 2010).

For unconstrained terminal states, $\Phi(x_0, x_N) = \Phi_0(x_0)$, and inequalities $H_n(x,u) = H_n(x_n, u_n)$, $n = 1, \dots, N-1$, the KKT conditions for the NLP from Definition 2.4 have a specific structure:

Lemma 2.6. (*KKT Conditions for the OCP*). *Considering the NLP in Eq (29) constructed by the OCP in Definition 2.4, the KKT conditions (with indices $n = 0, \dots, N-1$) are given by*

$$\lambda_N = \nabla_{x_N} L_f(x_N), \quad (31a)$$

$$\lambda_n = \nabla_{x_n} L(x_n, u_n) + \left(\frac{\partial f_{\Delta t}}{\partial x_n} \right)^\top \Big|_{(x_n, u_n, w_n)} \lambda_{n+1} + \left(\frac{\partial H}{\partial x_n} \right)^\top \Big|_{(x_n, u_n)} \mu_n, \quad (31b)$$

$$0 = \nabla_{u_n} L(x_n, u_n) + \left(\frac{\partial f_{\Delta t}}{\partial u_n} \right)^\top \Big|_{(x_n, u_n, w_n)} \lambda_{n+1} + \left(\frac{\partial H}{\partial u_n} \right)^\top \Big|_{(x_n, u_n)} \mu_n, \quad (31c)$$

$$\Phi_0(x_0) = 0, \quad x_{n+1} - f_{\Delta t}(x_n, u_n, w_n | \theta_x) = 0, \quad H(x,u) \leq 0, \quad (31d)$$

$$\mu \geq 0, \quad \mu_n H_n(x_n, u_n) = 0. \quad (31e)$$

We denote Eqs. (31a, 31b) and Eq. (31c) respectively as the adjoint and control equations. These conditions show that the Lagrangian $\mathcal{L}(\cdot)$ is a partially separable function (GRIEWANK; TOINT, 1982). Thus, this function admits a decomposition $\mathcal{L}(x,u,\lambda,\mu) =$

$\sum_{n=0}^N \mathcal{L}_n(x_n, u_n, \lambda, \mu)$, with each partial function $\mathcal{L}_n(x_n, u_n, \lambda, \mu)$ depending only on the n -th state and input vectors. This important property leads to the realisation that the OCP in Definition 2.4 characterise sparse optimisation problems. Specifically, it is possible to verify that the Hessian $\nabla^2 \mathcal{L}$ has a block-diagonal structure. As a consequence, the direct approach can benefit from sparsity-exploiting algorithms to efficiently solve for optimal controls $(u_0^*, \dots, u_{N-1}^*)$ and states (x_0^*, \dots, x_N^*) .

Despite the sparsity pattern, the optimisation problems described are still problematic for large-scale state-spaces as the total number of decision variables, $(N)N_x + (N-1)N_u$, is considerably large. Alternatively, it is possible to simplify the problem by considering the recursive formula

$$x_{n+1} = f_{\Delta t}^n(x_0, u_0, \dots, u_n) = \begin{cases} f_{\Delta t}(f_{\Delta t}^{n-1}(x_0, u_0, \dots, u_{n-1}), u_n, w_n) & n > 0 \\ x_0 & n = 0 \end{cases}, \quad (32)$$

the forward simulation of $f_{\Delta t}(\cdot)$ starting at initial state x_0 . Thus, dependence on intermediate states (x_1, \dots, x_N) can be removed from the objective functional in Eq. (28a) by rewriting it as

$$J_{\Delta t}(x_0, u) = \sum_{n=0}^{N-1} L(f_{\Delta t}^{n-1}(x_0, u_0, \dots, u_{n-1}), u_n) + L_f(f_{\Delta t}^{N-1}(x_0, u_0, \dots, u_{N-1})).$$

For this reduced optimisation, now defined for only $N_x + (N-1)N_u$ decision variables, each Newton's method iteration consists on first computing (x_1, \dots, x_N) by forward simulation (and computing $(\lambda_N, \dots, \lambda_0)$ by backwards simulation) then updating $(x_0, u_0, \dots, u_{N-1})$. This method is thus named the *sequential approach*, whereas directly solving Lemma 2.6 is denoted the *simultaneous approach*. The sequential approach is preferable over the simultaneous approach specially for strongly underactuated systems, i.e., when $N_x \gg N_u$. Additionally, the optimisation can be further simplified when initial state is fixed by $\Phi(x_0, x_N) = x_0 - \hat{x}_0$, for a given \hat{x}_0 .

In this work, all optimal control problems are solved using the sequential approach. For notation simplicity, we keep the dynamical constraints in the OCP definitions (Eq (28b)) to denote the model that is implicitly being used for forward simulation.

2.2.2 Receding-horizon control

A controller based on the optimal controls $(u_0^*, \dots, u_{N-1}^*)$ solving the aforementioned OCPs is inherently open-loop: The actions are applied without monitoring the actual evolution of the system. In reality, such controllers are prone to fail reaching the desired state due to plant-model-mismatch (BORRELLI et al., 2017). Moreover, the optimisation problem in Definition 2.4 makes the unrealistic assumption that future disturbances, w_n ($n = 0, \dots, N$), are known. In this work, we consider the closed-loop strategy known as Receding-Horizon Control (RHC), or

Model Predictive Control (MPC), which provides a framework to deal with these issues.

The MPC strategy consists of, at every instant $k \in \mathbb{N}$, solving the OCP in Eq. (28) for the control horizon indexed by $n \in [k, k+N]$, then applying only the first control action to the process. The initial state at each control horizon is fixed by $\Phi(x_k, x_{k+N}) = x_k - \hat{x}_k$, with \hat{x}_k assumed to be directly measured from the process. Thus, the strategy allows for re-optimising control actions whenever the actual state deviates from the predicted trajectory. Moreover, disturbances are held constant over each horizon, $w_n = \hat{w}_k$ ($n = k, \dots, k+N$), with \hat{w}_k known. This accounts for the future disturbances being unknown. To satisfy a realistic setup, disturbances are assumed to be measured given sampling period $\Delta t_w \geq 0$ such that $\hat{w}_k = w(\lfloor \frac{k\Delta t}{\Delta t_w} \rfloor \Delta t_w)$. Formally:

Definition 2.5. (Model predictive control, MPC). Consider the conditions presented in Definition 2.4. Given (\hat{x}_k, \hat{w}_k) , the model predictive control (MPC) strategy consists in solving, for each time instant $k \in \mathbb{N}$, optimal control problems in the form

$$\min_{\substack{x_k, \dots, x_{k+N}, \\ u_k, \dots, u_{k+N-1}}} J_{\text{MPC}}(x, u) = \sum_{n=k}^{k+N-1} L(x_n, u_n) + L_f(x_{k+N}) \quad (33a)$$

$$\text{s.t.} \quad x_{n+1} = f_{\Delta t}(x_n, u_n, \hat{w}_k | \theta_x), \quad (33b)$$

$$\forall n \in [k, k+N] \quad x_n \in \mathcal{X}, \quad u_n \in \mathcal{U}, \quad (33c)$$

$$x_k = \hat{x}_k, \quad (33d)$$

then applying only the first optimal action, u_k^* , to the actual process.

This strategy corresponds to an implicit state-feedback control law $\pi(\hat{x}_k, \hat{w}_k | \theta_u) = u_k^*$, with $(u_k^*, \dots, u_{k+N-1}^*)$ an optimal solution for Eq. (33) given initial state \hat{x}_k , disturbance \hat{w}_k , and the set of parameters θ_u related to the constraint sets and cost functions.

Constrained affine quadratic regulator (c-AQR)

We discuss a class of optimal control problems arising from a specific choice of dynamical models and cost functions. Specifically, we consider state-space models with affine dynamics $\dot{x}(t) = z + Ax(t) + Bu(t) + Gw(t)$. In this case, an analytical solution of the transition function $f_{\Delta t}(\cdot | \theta_x)$, Eq. (27), leads directly to the discrete-time affine state-space

$$x_{k+1} = z_{\Delta t} + A_{\Delta t}x_k + B_{\Delta t}u_k + G_{\Delta t}w_k, \quad (34)$$

with matrices $A_{\Delta t} = e^{A\Delta t}$, $B_{\Delta t} = S_{\Delta t}B$, $G_{\Delta t} = S_{\Delta t}G$, and vector $z_{\Delta t} = S_{\Delta t}z$, given auxiliary matrix $S_{\Delta t} = A^{-1}(e^{A\Delta t} - I)$. A derivation of such representation is presented in the Appendix 4. The

recursive formula in Eq. (32) also admits an analytical solution in case of affine models,

$$x_{n+1} = f_{\Delta t}^n(x_0, u_0, \dots, u_n) = A_{\Delta t}^{n+1}x_0 + \sum_{k=0}^n A_{\Delta t}^k B_{\Delta t} u_{n-k+1} + \sum_{k=0}^n A_{\Delta t}^k G_{\Delta t} w_{n-k+1} + \sum_{k=0}^n A_{\Delta t}^k z_{\Delta t}.$$

We select the quadratic costs $L(\cdot, \cdot) = \|x_n - x_n^{sp}\|_Q^2 + \|u_n - u_n^{sp}\|_R^2$ and $L_f(\cdot) = \|x_{k+N} - x_{k+N}^{sp}\|_{Q_f}^2$, given state (x_n^{sp}) and input (u_n^{sp}) references, and symmetric weighting matrices $Q, Q_f \succeq 0$ and $R \succ 0$. Moreover, we assume that the constraint sets \mathcal{X} and \mathcal{U} are convex, so that they can be represented by linear inequalities $\mathcal{X} = \{x \in \mathbb{R}^{N_x} \mid H_x x \leq h_x\}$ and $\mathcal{U} = \{u \in \mathbb{R}^{N_u} \mid H_u u \leq h_u\}$.

Definition 2.6. (Constrained affine quadratic regulator, c-AQR). Consider a system represented by Eq. (34). For quadratic cost functions $L(x_n, u_n) = \|x_n - x_n^{sp}\|_Q^2 + \|u_n - u_n^{sp}\|_R^2$ and $L_f(x_{k+N}) = \|x_{k+N} - x_{k+N}^{sp}\|_{Q_f}^2$, convex constraint sets \mathcal{X} and \mathcal{U} , and initial condition $\Phi(\cdot) = x_k - \hat{x}_k$, the constrained affine quadratic regulator (c-AQR) defines optimal control problems in the form

$$\min_{\substack{x_k, \dots, x_{k+N}, \\ u_k, \dots, u_{k+N-1}}} J_{\text{AQR}}(x, u) = \sum_{n=k}^{k+N-1} (\|x_n - x_n^{sp}\|_Q^2 + \|u_n - u_n^{sp}\|_R^2) + \|x_{k+N} - x_{k+N}^{sp}\|_{Q_f}^2 \quad (35a)$$

$$\text{s.t.} \quad x_{n+1} = z_{\Delta t} + A_{\Delta t} x_n + B_{\Delta t} u_n + G_{\Delta t} \hat{w}_k, \quad (35b)$$

$$\forall n \in [k, k+N] \quad H_x x_n \leq h_x, \quad H_u u_n \leq h_u, \quad (35c)$$

$$x_k = \hat{x}_k. \quad (35d)$$

The weighting matrices $Q, Q_f \succeq 0$ and $R \succ 0$ are used to control the importance of specific state and control variables in the minimization. A common choice is $Q = Q_f = C^T C$, such that

$$\|x_n - x_n^{sp}\|_{C^T C}^2 = (x_n - x_n^{sp})^T C^T C (x_n - x_n^{sp}) = (y_n - y_n^{sp})^T (y_n - y_n^{sp}) = \|y_n - y_n^{sp}\|_{I_{N_y}}^2,$$

with $y_n^{sp} = C x_n^{sp}$. This choice is motivated by expressing the minimisation in terms of quadratic measurement and control energies (see Section 2.1.2), and for ensuring closed-loop stability when (A, B) is stabilizable and (A, C) is detectable (MAYNE et al., 2000). Thus, the closed-loop $x_{n+1} = f_{\Delta t}(x_n, \pi(x_n, 0 | \theta_u), 0 | \theta_x) = A_{\Delta t} x_n + B \pi(x_n, 0 | \theta_u)$ is able to stabilise the system around each desired set-point (x_n^{sp}, u_n^{sp}) . In the case of uncertain systems, this stability property holds when disturbances are sufficiently small, while additional conditions are needed otherwise. Without loss of generality, we will consider $Q = Q_f = C^T Q_y C$, for symmetric $Q_y \succeq 0$ weighting specific output variables, such that $L(x_n, u_n) = \|y_n - y_n^{sp}\|_{Q_y}^2 + \|u_n - u_n^{sp}\|_R^2$ and $L_f(x_{k+N}) = L(x_{k+N}, 0)$.

The transcription of a c-AQR to a standard nonlinear program specialises:

Theorem 2.7. (*c-AQR Transcription*). Consider the optimal control problem in Definition. 2.6.

The described optimization can be converted into a quadratic program

$$\min_U \quad U^\top H U + g^\top U + r \quad (36a)$$

$$s.t. \quad E_u U \leq e_u \quad (36b)$$

with decision vector $U = (x_k, \dots, x_{k+N}, u_k, \dots, u_{k+N-1}) \in \mathbb{R}^{(N)N_x + (N-1)N_u}$ and symmetric matrix $H = H^\top \succeq 0$. Assuming the sequential approach, the problem reduces to decision vector $U = (u_k, \dots, u_{k+N-1}) \in \mathbb{R}^{(N-1)N_u}$ and positive definite matrix $H = H^\top \succ 0$.

A proof of this Theorem is provided in Appendix 4. Quadratic programs comprise a well-studied class of nonlinear optimisation problems that are common in optimal control problems. Moreover, the QP described in Theorem 2.7 is a convex optimisation problem: Optimal solutions can be efficiently obtained even for very large-scale systems (BOYD; VANDENBERGHE, 2004).

2.2.3 Zero-offset affine quadratic regulator

The main goal in most control applications is to drive a system to desired states, known as set-points, while rejecting disturbances that might cause offset from these objectives. In the class of applications known as *regulation control*, the goal is to stabilize the system around a single fixed set-point $SP = (x^{SP}, u^{SP})$, at all times. Conversely, control problems known as *reference tracking control* are concerned with reaching set-points $SP = \{(x_m^{SP}, u_m^{SP})\}_{m=0}^M$, sampled from reference trajectories $x_m^{SP} = x^{SP}((m+1)\Delta t_{sp})$ and $u_m^{SP} = u^{SP}((m+1)\Delta t_{sp})$ with period $\Delta t_{sp} > 0$.

In both cases, the control objectives are translated into optimal control problems that minimise the offsets $L(x_n, u_n) = \|x_n - x_n^{SP}\|_Q^2 + \|u_n - u_n^{SP}\|_R^2$, described in Section 2.2.2. For systems described by nonlinear dynamics $f_{\Delta t}(x_n, u_n, w_n | \theta_x)$, this approach requires affine approximations of the state equations to be used in the dynamical constraints (GROS et al., 2020). In regulation control, the intuitive solution is to consider the linearisation around the fixed-point $P := (x^{SP}, u^{SP}, w^{SP}, y^{SP})$,

$$\dot{x}(t) = z_f + A\Delta x(t) + B\Delta u(t) + G\Delta w(t), \quad (37)$$

with the Jacobian matrices $A = (\partial f / \partial x)|_P \in \mathbb{R}^{N_x \times N_x}$, $B = (\partial f / \partial u)|_P \in \mathbb{R}^{N_x \times N_u}$, $G = (\partial f / \partial w)|_P \in \mathbb{R}^{N_x \times N_w}$, and constant vector $z_f = f(x^{SP}, u^{SP}, w^{SP} | \theta_x) \in \mathbb{R}^{N_x}$, evaluated at such point. The variable $\Delta x(t) = x(t) - x^{SP}$ (respectively, $\Delta u(t) = u(t) - u^{SP}$ and $\Delta w(t) = w(t) - w^{SP}$) is the state (control and disturbance) deviation from the linearisation point. Moreover, all constant terms are accumulated in $\tilde{z}_f = z_f - (Ax^{SP} + Bu^{SP} + Gw^{SP})$, leading to the affine form

$$\dot{x}(t) = \tilde{z}_f + Ax(t) + Bu(t) + Gw(t), \quad (38)$$

which can then be discretised as $x_{n+1} = \tilde{z}_{f\Delta t} + A_{\Delta t}x_n + B_{\Delta t}u_n + G_{\Delta t}w_n$ according to Eq. (34).

Similarly, the usual solution for reference tracking is to consider the collection of linear approximations around each fixed-point $P_m := (x_m^{sp}, u_m^{sp}, w_m^{sp}, y_m^{sp})$, discretised as

$$x_{n+1} = \tilde{z}_{f\Delta t}^{(m)} + A^{(m)}x_n + B^{(m)}u_n + G^{(m)}w_n, \quad (39)$$

from Jacobian matrices $A^{(m)} = (\partial f / \partial x)|_{P_m}$, $B^{(m)} = (\partial f / \partial u)|_{P_m}$, and $G^{(m)} = (\partial f / \partial w)|_{P_m}$, and constant vector $\tilde{z}_{f\Delta t}^{(m)} = f(x_m^{sp}, u_m^{sp}, w_m^{sp} | \theta_x) - (A^{(m)}x_m^{sp} + B^{(m)}u_m^{sp} + G^{(m)}w_m^{sp})$. We collect all approximations Eq. (39) into a single piecewise affine state equation,

$$x_{n+1} = \sum_{m=0}^M \mathbb{I}_{m=\lfloor \frac{n\Delta t}{\Delta t_{sp}} \rfloor} (\tilde{z}_{f\Delta t}^{(m)} + A^{(m)}x_n + B^{(m)}u_n + G^{(m)}w_n) \quad (40)$$

where \mathbb{I}_S is the indicator function with $\mathbb{I}_S = 1$ if statement S is true, and $\mathbb{I}_S = 0$ otherwise. This equation “selects” only the m -th state-space $(A^{(m)}, B^{(m)}, G^{(m)})$ for which $m = \lfloor \frac{n\Delta t}{\Delta t_{sp}} \rfloor$. Note that the regulation control task is a special case of reference tracking with $SP = \{x_m^{sp}, u_m^{sp}\}_{m=0}^0$ and $\Delta t_{sp} = t_f - t_0$. We use this representation to define the general zero-offset AQR formulation:

Definition 2.7. (Zero-offset AQR). Consider a system represented by Eq. (40), given the set-points $P_m := (x_m^{sp}, u_m^{sp}, w_m^{sp}, y_m^{sp})$. For cost functions $L(x_n, u_n) = \|x_n - \hat{x}_n^{sp}\|_Q^2 + \|u_n - \hat{u}_n^{sp}\|_R^2$ and $L_f(x_{k+N}) = \|x_{k+N} - \hat{x}_{k+N}^{sp}\|_{Q_f}^2$, with $\hat{x}_n^{sp} = x^{sp}(\lfloor \frac{(n+1)\Delta t}{\Delta t_{sp}} \rfloor \Delta t_{sp})$ and $\hat{u}_n^{sp} = u^{sp}(\lfloor \frac{(n+1)\Delta t}{\Delta t_{sp}} \rfloor \Delta t_{sp})$, the Zero-offset AQR defines optimal control problems in the form

$$\min_{\substack{x_k, \dots, x_{k+N}, \\ u_k, \dots, u_{k+N-1}}} J_{Z\text{-AQR}}(x, u) = \sum_{n=k}^{k+N-1} (\|x_n - \hat{x}_n^{sp}\|_Q^2 + \|u_n - \hat{u}_n^{sp}\|_R^2) + \|x_{k+N} - \hat{x}_{k+N}^{sp}\|_{Q_f}^2 \quad (41a)$$

$$\text{s.t. } \forall n \in [k, k+N] \quad x_{n+1} = \sum_{m=0}^M \mathbb{I}_{m=\lfloor \frac{n\Delta t}{\Delta t_{sp}} \rfloor} (\tilde{z}_{f\Delta t}^{(m)} + A^{(m)}x_n + B^{(m)}u_n + G^{(m)}\hat{w}_k), \quad (41b)$$

$$H_x x_n \leq h_x, \quad H_u u_n \leq h_u, \quad (41c)$$

$$x_k = \hat{x}_k. \quad (41d)$$

As only a single affine model is active during each n -th time instant, this controller shares the same properties as the c-AQR in Section 2.2.2. In general, the set-points (x_m^{sp}, u_m^{sp}) from linearisation points $P_m = (x_m^{sp}, u_m^{sp}, w_m^{sp}, y_m^{sp})$ are selected to be steady-states, i.e., $f(x_m^{sp}, u_m^{sp}, w_m^{sp} | \theta_x) = 0$ for a fixed disturbance w_m^{sp} . During operation, it is also possible to update all linearisations at each n -th time instant by having $w_m^{sp} = \hat{w}_n = w(\lfloor \frac{n\Delta t}{\Delta t_w} \rfloor \Delta t_w)$, the last available measurement. This ensures that the linear approximations take into account the true disturbance values.

In practice, references are not provided for each state-variable, but rather only for a subset of output variables, $\tilde{y}_m^{sp} = Hg(x_m^{sp} | \theta_y) \in \mathbb{R}^{N_{\tilde{y}}}$. Matrix $H \in \{0, 1\}^{N_{\tilde{y}} \times N_y}$ selects the $N_{\tilde{y}} \leq N_y$ outputs of interest. Note that fact is specially true for large-scale systems, in which tailoring references

for each individual variable is a daunting task. In case the references are provided in the form of continuous-time trajectories, the collection of set-points $\{(y_m^{SP}, u_m^{SP})\}_{m=0}^M$ are sampled from $y_m^{SP} = y^{SP}((m+1)\Delta t_{sp})$ and $u_m^{SP} = u^{SP}((m+1)\Delta t_{sp})$. In such cases, state and input set-points satisfying the desired output references are computed according to the nonlinear optimisation:

Definition 2.8. (Reference steady-state optimisation). For a reference output $\tilde{y}_m^{SP} \in \mathbb{R}^{N_y}$ and input $\hat{u}_m^{SP} \in \mathbb{R}^{N_u}$, and given symmetric weighting matrices $W_y, W_u \succeq 0$ and disturbances $\hat{w}^{SP} \in \mathbb{R}^{N_w}$, the linearisation point $P_m = (x_m^{SP}, u_m^{SP}, \hat{w}_m^{SP}, y_m^{SP})$ is the pair (x_m^{SP}, u_m^{SP}) that solves

$$\min_{x_m^{SP}, u_m^{SP}} J_{SP}(x_m^{SP}, u_m^{SP}) = \|Hg(x_m | \theta_y) - \tilde{y}_m^{SP}\|_{W_y}^2 + \|u_m^{SP} - \hat{u}_m^{SP}\|_{W_u}^2 \quad (42a)$$

$$\text{s.t. } 0 = f(x^{SP}, u^{SP}, \hat{w}^{SP} | \theta_x), \quad (42b)$$

$$x_m^{SP} \in \mathcal{X}^{SP}, \quad u_m^{SP} \in \mathcal{U}^{SP}. \quad (42c)$$

In this optimisation, matrices W_y and W_u control the trade-off between satisfying the desired reference and allowing deviations from a specific control configuration, respectively. The optimisation with $W_u = 0$ obtains any steady-state satisfying the reference. Conversely, selecting $W_u \succ 0$ and $u_m^{SP} = 0$ leads to a pair (x_m^{SP}, u_m^{SP}) of minimum L_2 control effort that is close enough to set-point \tilde{y}_m^{SP} . Moreover, it is possible to relax the constraint Eq. (42b) as $\|f(x^{SP}, u^{SP}, \hat{w}^{SP} | \theta_x)\|^2 \leq \varepsilon$, for any $\varepsilon > 0$, when feasible steady-states satisfying the output requirements are non-existent.

2.3 Moving horizon estimation

In reality, dynamical models are always uncertain and the internal state of a system is unknown but partially observed through the measurements, i.e., it is a latent variable. We thus concern ourselves with the state estimation task for systems described the stochastic state-space

$$\dot{x}(t) = f(x(t), u(t), w(t) | \theta_x); \quad (43a)$$

$$y(t) = g(x(t), v(t) | \theta_y), \quad (43b)$$

with process noise $w(t) \stackrel{i.i.d}{\sim} p_w(w(t) | \theta_w)$ and measurement noise $v(t) \stackrel{i.i.d}{\sim} p_v(v(t) | \theta_v)$. The first random variable summarises the uncertainty on the state dynamics due to exogenous disturbances and plant-model mismatch, while the latter models the uncertainty in the measurements due to noisy sensors. This model leads to $x(t) \sim p_x(x(t) | u(t), w(t), \theta_x)$, the latent variable to be estimated, and $y(t) \sim p_y(y(t) | x(t), v(t), \theta_y)$, for which sensor data is available. We limit ourselves to measurement processes with additive noise, i.e., $y(t) = g(x(t), v(t) | \theta_y) = g(x(t) | \theta_y) + v(t)$.

In this section, we formulate the state estimation task of reconstructing the internal state of system through partial noisy measurements as a *maximum a posteriori* (MAP) estimation task. We adopt a *discretise-then-optimize* approach of solving optimal state estimation (OEP)

problems, and then we overview the Moving Horizon Estimation (MHE) strategy as a closed-loop estimator. Additionally, we discuss the constrained affine Gauss-Markov (c-AGM) estimator arising from specific assumptions over the stochastic model and probabilistic distributions.

2.3.1 Inference problem and MAP estimation

We assume a discrete measurement process in which observations are available given a period $\Delta t > 0$, such that $y_k = y(k\Delta t)$. Thus, for each time interval $t \in [t_k, t_{k+1})$, we consider piecewise constant inputs $w(t) = w(t_k)$ and $u(t) = u(t_k)$, with $t_k = k\Delta t$ the k -th time instant at which a measurement $y(t_k)$ is received. As in Section 2.2.1, the discrete-time state dynamics are

$$x_{k+1} = f_{\Delta t}(x_k, u_k, w_k | \theta_x) = x_k + \int_{t_k}^{t_{k+1}} f(x(\tau), u_k, w_k | \theta_x) d\tau, \quad (44)$$

with $x_k = x(k\Delta t)$, $u_k = u(k\Delta t)$ and $w_k = w(k\Delta t)$. The discrete-time stochastic state-space is

$$x_{k+1} = f_{\Delta t}(x_k, u_k, w_k | \theta_x); \quad (45a)$$

$$y_k = g(x_k | \theta_y) + v_k. \quad (45b)$$

with process noise $w_k \stackrel{i.i.d.}{\sim} p_{w_k}(w_k | \theta_w)$ and measurement noise $v_k \stackrel{i.i.d.}{\sim} p_{v_k}(v_k | \theta_v)$, and given initial state $x_0 \sim p_{x_0}(x_0 | \theta_{x_0})$. The model Eq. (45) can be interpreted as a Hidden Markov Model (HMM), in which $X = \{x_0, x_1, \dots\}$ is a Markov chain of latent variables and $Y = \{y_0, y_1, \dots\}$ are the corresponding observations (BISHOP, 2006). Specifically, the Markov property determines

- $p(x_{k+1} | x_0, \dots, x_k, u_0, \dots, u_k, w_0, \dots, w_k) = p(x_{k+1} | x_k, u_k, w_k)$, the *transition distribution* modelling the probability of reaching x_{k+1} from (x_k, u_k, w_k) .
- $p(y_k | x_0, \dots, x_k) = p(y_k | x_k)$, the *emission distribution* modelling the probability of the measurement y_k being emitted from the state x_k .

The state estimation problem translates to the inference problem of determining the distribution $P(x, w | y) = p(x_0, \dots, x_{k+1}, w_0, \dots, w_k | y_0, \dots, y_k)$, the probability of a trajectory given the measurements. Considering a Bayesian treatment, this distribution is computed as the posterior

$$P(x, w | y) = \frac{p(y_0, \dots, y_k | x_0, \dots, x_{k+1}, w_0, \dots, w_k) p(x_0, \dots, x_k, w_0, \dots, w_k)}{p(y_0, \dots, y_k)}, \quad (46)$$

where $p(y_0, \dots, y_k | x_0, \dots, x_{k+1}, w_0, \dots, w_k)$ and $p(x_0, \dots, x_{k+1}, w_0, \dots, w_k)$ are known as the likelihood and prior distributions, respectively, and we omit the known (u_0, \dots, u_k) for notation simplicity. In general, the distribution $P(x, w | y)$ is numerically approximated (e.g., using Markov Chain Monte Carlo methods), as analytical solutions only exist under specific conditions (MAYBECK, 1979). Instead of determining $P(x, w | y)$, we focus on obtaining an optimal estimate

$(\hat{x}_0, \dots, \hat{x}_{k+1}, \hat{w}_0, \dots, \hat{w}_k)$ by solving the *maximum a posteriori* (MAP) estimation problem

$$\max_{\substack{x_0, \dots, x_{k+1}, \\ w_0, \dots, w_k}} \tilde{P}(x, w|y) = p(y_0, \dots, y_k | x_0, \dots, x_{k+1}, w_0, \dots, w_k) p(x_0, \dots, x_k, w_0, \dots, w_k), \quad (47)$$

with $\tilde{P}(x, w|y) \propto P(x, w|y)$ as $p(y_0, \dots, y_k)$ is constant. The estimate $(\hat{x}_0, \dots, \hat{x}_{k+1}, \hat{w}_0, \dots, \hat{w}_k)$ corresponds to one of the modes from the posterior distribution $P(x, w|y)$. This maximisation can also be written in terms of the known distributions $p_{x_0}(x_0|\theta_{x_0})$, $p_{v_k}(v_k|\theta_v)$ and $p_{w_k}(w_k|\theta_w)$:

Lemma 2.8. (*Maximum a posteriori estimate*). Consider the HMM described in Eq. (45), with $x_0 \sim p_{x_0}(x_0|\theta_{x_0})$, $v_k \stackrel{i.i.d}{\sim} p_{v_k}(v_k|\theta_v)$ and $w_k \stackrel{i.i.d}{\sim} p_{w_k}(w_k|\theta_w)$. The maximum a posteriori (MAP) estimate from the posterior probability $P(x, w|y)$ is the solution of

$$\max_{\substack{x_0, \dots, x_{k+1}, \\ w_0, \dots, w_k}} \tilde{P}(x, w|y) = p_{x_0}(x_0) \prod_{n=0}^k p_v(v_n|\theta_v) p_w(w_n|\theta_w) \quad (48a)$$

$$\text{s.t.} \quad x_{n+1} = f_{\Delta t}(x_n, u_n, w_n | \theta_x), \quad (48b)$$

$$\forall n \in [0, k] \quad x_n \in \mathcal{X}, \quad w_n \in \mathcal{W}. \quad (48c)$$

A detailed derivation is provided in Appendix 4. Furthermore, we note that the maximisation in Lemma 2.8 is equivalent to minimising the negative of the log-posterior distribution,

$$\min_{\substack{x_0, \dots, x_{k+1}, \\ w_0, \dots, w_k}} -\log \tilde{P}(x, w|y) = -\log p_{x_0}(x_0) - \sum_{n=0}^k (\log p_v(v_n) + \log p_w(w_n)),$$

under the same constraints. Motivated by this new cost functional, we limit ourselves to the case of distributions from the exponential family, $p_{x_0}(x_0|\theta_{x_0}) = e^{-L_0(x_0|\theta_{x_0})}$, $p_{v_k}(v_k|\theta_v) = e^{-L_v(v_k|\theta_v)} = e^{-L_v(y_k - g(x_k)|\theta_v)}$ and $p_{w_k}(w_k|\theta_w) = e^{-L_w(w_k|\theta_w)}$. Under such assumptions, the cost functional is

$$J_{\Delta t}(x, w|y) \triangleq -\log \tilde{P}(x, w|y) = L_0(x_0|\theta_{x_0}) + \sum_{n=0}^k (L_v(y_n - g(x_n)|\theta_v) + L_w(w_n|\theta_w)).$$

Moreover, let $L(x_n, w_n) = L_v(y_n - g(x_n)|\theta_v) + L_w(w_n|\theta_w)$ denote the stage cost function. The resulting optimisation is denoted as an optimal estimation problem (OEP). Formally:

Definition 2.9. (Discrete-time optimal estimation problem). Consider a system represented by Eq. (45). For $x_0 \sim e^{-L_0(x_0|\theta_{x_0})}$, $v_k \stackrel{i.i.d}{\sim} e^{-L_v(y_k - g(x_k)|\theta_v)}$ and $w_k \stackrel{i.i.d}{\sim} e^{-L_w(w_k|\theta_w)}$, and support sets \mathcal{X} and \mathcal{W} , a optimal estimation problem is defined as an optimisation problem in the form

$$\min_{\substack{x_0, \dots, x_{k+1}, \\ w_0, \dots, w_k}} J_{\Delta t}(x, w|y) = L_0(x_0) + \sum_{n=0}^k L(x_n, w_n) \quad (49a)$$

$$\text{s.t.} \quad x_{n+1} = f_{\Delta t}(x_n, u_n, w_n | \theta_x), \quad (49b)$$

$$\forall n \in [0, k] \quad x_n \in \mathcal{X}, \quad w_n \in \mathcal{W}. \quad (49c)$$

The optimisation in Definition. 2.9 has similar form to the optimal control problems presented in Chapter 2.2. Thus, the same solution approaches can be applied. The OEP is solved by the *direct approach* of transcribing the problem into a standard nonlinear program (NLP), then solving it numerically. Specifically, consider the constrained nonlinear program,

$$\min_{x, w} J_{\Delta t}(x, w) \quad (50a)$$

$$\text{s.t.} \quad G(x, w) = 0, \quad H(x, w) \leq 0, \quad (50b)$$

where $x = (x_0, \dots, x_{k+1}) \in \mathbb{R}^{(k+1)N_x}$ and $w = (w_0, \dots, w_k) \in \mathbb{R}^{kN_w}$ are the decision vectors, function $G(x, w) : \mathbb{R}^{(k+1)N_x} \times \mathbb{R}^{kN_w} \rightarrow \mathbb{R}^k$ is obtained by collecting all dynamical constraints in Eq. (49b), and $H(x, w) : \mathbb{R}^{(k+1)N_x} \times \mathbb{R}^{kN_w} \rightarrow \mathbb{R}^{N_\mu}$ represents both constraint sets \mathcal{X} and \mathcal{W} in Eq. (49c). A candidate solution is obtained from the Karush-Kuhn-Tucker (KKT) conditions,

$$\nabla \mathcal{L}(x, w, \lambda, \mu) = 0 \quad (51a)$$

$$G(x, w) = 0, \quad H(x, w) \leq 0, \quad (51b)$$

$$\mu \geq 0, \quad \mu_j H_j(x, w) = 0 \quad (j = 1, \dots, N_\mu), \quad (51c)$$

with Lagrangian function $\mathcal{L}(x, w, \lambda, \mu) = J_{\Delta t}(x, w) + \lambda^\top G(x, w) + \mu^\top H(x, w)$ defined given the Lagrange multipliers $\lambda = [\lambda_0 \dots \lambda_k]^\top \in \mathbb{R}^{k+1}$ and $\mu = [\mu_0 \dots \mu_{N_\mu}]^\top \in \mathbb{R}^{N_\mu+1}$. Considering inequalities $H_n(x, w) = H_n(x_n, w_n)$, $n = 0, \dots, k$, the KKT conditions for the NLP transcribed from Definition 2.9 have a specific structure:

Lemma 2.9. (*KKT Conditions for the OEP*). *Considering the NLP in Eq (50) constructed by the OEP in Definition 2.9, the KKT conditions (with indices $n = 0, \dots, k$) are given by*

$$\lambda_0 = \nabla_{x_0} L_0(x_0), \quad (52a)$$

$$\lambda_n = \nabla_{x_n} L(x_n, w_n) + \left(\frac{\partial f_{\Delta t}}{\partial x_n} \right)^\top \Big|_{(x_n, u_n, w_n)} \lambda_{n+1} + \left(\frac{\partial H}{\partial x_n} \right)^\top \Big|_{(x_n, w_n)} \mu_n, \quad (52b)$$

$$0 = \nabla_{w_n} L(x_n, w_n) + \left(\frac{\partial f_{\Delta t}}{\partial w_n} \right)^\top \Big|_{(x_n, u_n, w_n)} \lambda_{n+1} + \left(\frac{\partial H}{\partial w_n} \right)^\top \Big|_{(x_n, w_n)} \mu_n, \quad (52c)$$

$$0 = x_{n+1} - f_{\Delta t}(x_n, u_n, w_n | \theta_x), \quad H(x, w) \leq 0, \quad (52d)$$

$$\mu \geq 0, \quad \mu_n H_n(x_n, w_n) = 0. \quad (52e)$$

We denote Eqs. (52a, 52b) and Eq. (52c) as the adjoint and noise equations, respectively. As in Section 2.2.1, the Lagrangian is a partially separable function admitting a decomposition $\mathcal{L}(x, w, \lambda, \mu) = \sum_{n=0}^k \mathcal{L}_n(x_n, w_n, \lambda, \mu)$. Thus, also the OEP in Definition 2.9 characterise sparse

optimisation problems. Specifically, it is possible to verify that the Hessian $\nabla^2 \mathcal{L}$ has a block-diagonal structure. As a consequence, the direct approach can benefit from sparsity-exploiting algorithms to efficiently solve for optimal estimates $(\hat{w}_1^*, \dots, \hat{w}_k^*)$ and state $(\hat{x}_0^*, \dots, \hat{x}_{k+1}^*)$.

Despite the sparsity pattern, the optimisation problems described are still problematic for large-scale state-spaces as the total number of decision variables, $(k+1)N_x + kN_w$, is considerably large. Alternatively, it is possible to simplify the problem by considering the recursive formula

$$x_{n+1} = f_{\Delta t}^n(x_0, w_0, \dots, w_n) = \begin{cases} f_{\Delta t}(f_{\Delta t}^{n-1}(x_0, w_0, \dots, w_{n-1}), u_n, w_n) & n > 0 \\ x_0 & n = 0 \end{cases}, \quad (53)$$

the forward simulation of $f_{\Delta t}(\cdot)$ starting at initial state x_0 . Thus, dependence on intermediate states (x_1, \dots, x_{k+1}) can be removed from the objective functional Eq. (49a) by rewriting it as

$$J_{\Delta t}(x_0, w|y) = L_0(x_0) + \sum_{n=0}^k L(f_{\Delta t}^{n-1}(x_0, w_0, \dots, w_{n-1}), w_n)$$

For this reduced optimisation, now defined for only $N_x + kN_w$ decision variables, each Newton's method iteration consists on the sequential approach of first computing (x_1, \dots, x_{k+1}) and $(\lambda_0, \dots, \lambda_k)$ by forward simulation, then updating (x_0, w_1, \dots, w_k) . This is preferable over the simultaneous approach when the number of disturbance variables is small, i.e., when $N_x \gg N_w$.

2.3.2 Moving horizon estimation strategy

Unlike the open-loop OCP of Chapter 2.2, obtaining the current disturbance \hat{w}_k and state \hat{x}_k estimates from the OEP is already performed in a closed-loop fashion, as the optimisation is solved at each k -th time instant. This approach, known as the *full information problem*, suffers from the fact that the size of the estimation horizon, and thus the number of decision variables $(k+1)N_x + kN_w$, is not fixed. As a result, the complexity of solving the OEP scales at least linearly with time. This raises obvious technical problems (e.g., increasing computer burden) and also introduces issues for the initial state sensitivity when the sequential approach is used.

We approach this issue by relying on a Moving Horizon Estimation (MHE) strategy. Consider the separation of the cost functional in Definition 2.9 into time intervals $[0, k-N]$ and $[k-N+1, k]$,

$$J_{\Delta t}(x, w|y) = \left(L_0(x_0) + \sum_{n=0}^{k-N} L(x_n, w_n) \right) + \sum_{n=k-N+1}^k L(x_n, w_n),$$

from which we define $\Phi(x_0, w_1, \dots, w_{k-N}) = L_0(x_0) + \sum_{n=0}^{k-N} L(x_n, w_n)$. The estimation horizon can thus be truncated by considering an approximation for $\Phi(\cdot)$ depending only on a fixed number of variables. We consider a MHE strategy of approximating $\Phi(\cdot) \approx L_0(x_{k-N+1})$, assuming that

all information about (x_0, \dots, x_{k-N}) and (w_0, \dots, w_{k-N}) is summarised in the state x_{k-N+1} . Implicitly, the uncertainty about each initial state is given by $x_{k-N+1} \sim p_{x_0}(x_{k-N+1} | \theta_{x_0})$.

Definition 2.10. (Moving horizon estimation, MHE). Consider the conditions presented in Definition 2.9. The moving horizon estimation (MHE) strategy consists in solving, for each time instant $k \in \mathbb{N}$, optimal estimation problems in the form

$$\min_{\substack{x_{k-N+1}, \dots, x_{k+1} \\ w_{k-N+1}, \dots, w_k}} J_{\text{MHE}}(x, w | y) = L_0(x_{k-N+1}) + \sum_{n=k-N+1}^k L(x_n, w_n) \quad (54a)$$

$$\text{s.t.} \quad x_{n+1} = f_{\Delta t}(x_n, u_n, w_n | \theta_x), \quad (54b)$$

$$\forall n \in [k-N+1, k] \quad x_n \in \mathcal{X}, \quad w_n \in \mathcal{W}. \quad (54c)$$

In the sequential method, intermediate estimates $(\hat{x}_{k-N+2}, \dots, \hat{x}_{k+1})$ are obtained by forward simulating $f_{\Delta t}(\cdot)$ using $(\hat{x}_{k-N+1}, \hat{w}_{k-N+1}, \dots, \hat{w}_k)$. The moving-horizon strategy thus corresponds to an implicit state-estimation function $\pi(y_{k-N+1}, \dots, y_k | \theta_w) = \hat{x}_k$, with $(\hat{x}_{k-N+1}, \hat{w}_{k-N+1}, \dots, \hat{w}_k)$ an optimal solution for Eq. (54) given measurements (y_{k-N+1}, \dots, y_k) , and the set of parameters θ_w related to the probabilistic distributions and support sets.

Constrained affine Gauss-Markov estimator (c-AGM)

We discuss a class of optimal estimation problems arising from a specific choice of models and probabilistic distributions. As in Section 2.2.2, we consider affine state-space models with dynamics $\dot{x}(t) = z + Ax(t) + Bu(t) + Gw(t)$ and outputs $y(t) = Cx(t) + v(t)$. A transition function $f_{\Delta t}(\cdot | \theta_x)$, Eq. (44) is again obtained analytically, leading to the discrete-time state-space

$$x_{k+1} = z_{\Delta t} + A_{\Delta t}x_k + B_{\Delta t}u_k + G_{\Delta t}w_k, \quad (55a)$$

$$y_k = C_{\Delta}x_k + v_k, \quad (55b)$$

with matrices $A_{\Delta t} = e^{A\Delta t}$, $B_{\Delta t} = S_{\Delta t}B$, $G_{\Delta t} = S_{\Delta t}G$ and $C_{\Delta t} = C$, and vector $z_{\Delta t} = S_{\Delta t}z$, given auxiliary matrix $S_{\Delta t} = A^{-1}(e^{A\Delta t} - I)$. Again, the recursive formula in Eq. (32) is

$$x_{n+1} = f_{\Delta t}^n(x_0, u_0, \dots, u_n) = A_{\Delta t}^{n+1}x_0 + \sum_{k=0}^n A_{\Delta t}^k B_{\Delta t} u_{n-k+1} + \sum_{k=0}^n A_{\Delta t}^k G_{\Delta t} w_{n-k+1} + \sum_{k=0}^n A_{\Delta t}^k z_{\Delta t}.$$

We assume Gaussian distributions $x_{k-N+1} \sim \mathcal{N}(\bar{x}_{k-N+1}, Q_{x_0})$, $w_n \stackrel{i.i.d}{\sim} \mathcal{N}(\bar{w}_n, R_w)$, and $v_n \stackrel{i.i.d}{\sim} \mathcal{N}(0, Q_v)$, given means \bar{x}_{k-N} and \bar{w}_n ($n = k-N+1, \dots, k$), and covariance matrices (Q_{x_0}, Q_v, R_w) . As a consequence, the states are distributed as $x_n \sim \mathcal{N}(\bar{x}_n, Q_{x_n})$, for all $n = k-N+1, \dots, k+1$, and Eq. (55) characterise a Gauss-Markov process $X = \{x_n\}_{k-N+1}^k$. Moreover, we assume that the constraint sets \mathcal{X} and \mathcal{W} are convex, so that they can be represented by linear inequalities $\mathcal{X} = \{x \in \mathbb{R}^{N_x} \mid H_x x \leq h_x\}$ and $\mathcal{W} = \{w \in \mathbb{R}^{N_w} \mid H_w w \leq h_w\}$. We define the MHE problem:

Definition 2.11. (Constrained affine Gauss-Markov estimator, c-AGM). Consider a system represented by Eq. (45). For $x_{k-N+1} \sim \mathcal{N}(\bar{x}_{k-N+1}, Q_{x_0})$, $w_n \sim \mathcal{N}(\bar{w}_n, R_w)$, $v_n \sim \mathcal{N}(0, Q_v)$, and convex support sets \mathcal{X} and \mathcal{W} , the constrained affine Gauss-Markov estimator (c-AGM) defines optimal estimation problems in the form

$$\min_{\substack{x_{k-N+1}, \dots, x_{k+1} \\ w_{k-N+1}, \dots, w_k}} J_{\text{AGM}}(\cdot) = \|x_{k-N+1} - \bar{x}_{k-N+1}\|_{Q_{x_0}^{-1}}^2 + \sum_{n=k-N+1}^k \left(\|y_n - Cx_n\|_{Q_v^{-1}}^2 + \|w_n - \bar{w}_n\|_{R_w^{-1}}^2 \right) \quad (56a)$$

$$\text{s.t.} \quad x_{n+1} = z_{\Delta t} + A_{\Delta t}x_n + B_{\Delta t}u_n + G_{\Delta t}w_n, \quad \forall n \in [k-N+1, k] \quad (56b)$$

$$H_x x_n \leq h_x, \quad H_w w_n \leq h_w. \quad (56c)$$

From the optimisation perspective, weighting matrices Q_v^{-1} and R_w^{-1} penalise the mismatches between outputs Cx_n and measurements y_n , and the deviations of estimated disturbances w_n from means \bar{w}_n , respectively. Due to the recursive nature of the moving-horizon strategy, the intuitive choice for the initial state and disturbance means are the estimates from the previous estimation horizon, i.e., $\bar{x}_{k-N+1} = \hat{x}_{k-N+1}$ and $\bar{w}_n = \hat{w}_n$ ($n = k-N+1, \dots, k-1$), and repeated $\bar{w}_k = \hat{w}_{k-1}$ for the new disturbance vector. This choice recursively satisfy

$$L_0(x_{k-N+1}) \leq \min_{\substack{x_{k-2N+1}, \dots, x_{k-N+1}, \\ w_{k-2N+1}, \dots, w_{k-N}}} L_0(x_{k-2N+1}) + \sum_{n=k-2N+1}^{k-N} L(x_n, w_n).$$

For detectable systems, this condition ensures stability for the MHE (RAO et al., 2003). This is analogous to the stabilizability condition for closed-loop stable MPC controllers (Section 2.2.2).

The transcription of a c-AGM to a standard nonlinear program specialises:

Theorem 2.10. (*c-AGM Transcription*) Consider the optimal estimation problem in Definition 2.11. The described optimization can be converted into a quadratic program

$$\min_W W^T H W + g^T W + r \quad (57a)$$

$$\text{s.t.} \quad E_w W \leq e_w, \quad (57b)$$

with decision vector $W = (x_{k-N+1}, \dots, x_{k+1}, w_{k-N+1}, \dots, w_k) \in \mathbb{R}^{(N)N_x + (N-1)N_w}$ and symmetric matrix $H = H^T \succeq 0$. Assuming the sequential approach, the problem reduces to decision vector $W = (x_{k-N+1}, w_{k-N+1}, \dots, w_k) \in \mathbb{R}^{N_x + (N-1)N_w}$ and positive semi-definite matrix $H = H^T \succeq 0$.

A proof of this theorem is provided in Appendix 4. As already discussed, quadratic programs comprise a well-studied class of nonlinear optimisation problems that are common in control problems. The QP described in Theorem 2.10 is a convex optimisation problem: Optimal estimates can be efficiently obtained even for very large-scale systems.

For systems described by nonlinear dynamics $x_{n+1} = f_{\Delta t}(x_n, u_n, w_n | \theta_x)$, the c-AGM requires affine approximations of the state-equations to be used as dynamical constraints, as in Section 2.2.3. In this case, the approximations are to be taken over the most likely trajectory, rather than for specific set-points satisfying some requirements. An intuitive choice is to consider the linearisations around fixed-points $P_n := \{(\hat{x}_n, u_n, \hat{w}_n, \hat{y}_n)\}_{n=k-N+1}^k$,

$$\dot{x}(t) = z_f^{(n)} + A^{(n)} \Delta x(t) + B^{(n)} \Delta u(t) + G^{(n)} \Delta w(t), \quad (58a)$$

$$y(t) = C^{(n)} x(t) + v(t), \quad (58b)$$

for $\{(\hat{x}_n, \hat{w}_n)\}_{n=k-N}^{k-1}$ the estimates from the previous horizon, with the Jacobian matrices $A = (\partial f / \partial x)|_{P(n)} \in \mathbb{R}^{N_x \times N_x}$, $B = (\partial f / \partial u)|_{P(n)} \in \mathbb{R}^{N_x \times N_u}$, $G = (\partial f / \partial w)|_{P(n)} \in \mathbb{R}^{N_x \times N_w}$, and $C = (\partial g / \partial x)|_{P(n)} \in \mathbb{R}^{N_y \times N_x}$, and constant vector $z_f = f(x^{sp}, u^{sp}, w^{sp} | \theta_x) \in \mathbb{R}^{N_x}$. The last fixed-point pair is fixed as $(\hat{x}_k, \hat{w}_k) = (\hat{x}_{k-1}, \hat{w}_{k-1})$. We simplify the model by collecting all constant terms in $\tilde{z}_f = z_f - (A^{(n)} \hat{x}_n + B^{(n)} u_n + G^{(n)} \hat{w}_n)$, then discretising it as

$$x_{n+1} = z_{f_{\Delta t}}^{(n)} + A_{\Delta t}^{(n)} x_n + B_{\Delta t}^{(n)} u_n + G_{\Delta t}^{(n)} w_n, \quad (59a)$$

$$y_n = C_{\Delta t}^{(n)} x_n + v_n. \quad (59b)$$

As the linearisation changes every time-step, this representation consists on a time-varying affine state-space model. We thus consider Eq. (59) for the dynamical constraints in Eq. (56b).

2.4 Output model predictive control

The model predictive controllers described in Chapter 2.2 assumes that the state- and disturbance-vectors are directly accessible. This unrealistic assumption motivates the discussions on moving horizon estimators in Chapter 2.3. In this section, we discuss the Output Model Predictive Control (Output-MPC) strategy that combines both optimal control and estimation methods to perform predictive control when only noisy measurements of the process state are available.

Considering the system described by an stochastic state-space model

$$\dot{x}(t) = f(x(t), u(t), w(t) | \theta_x); \quad (60a)$$

$$y(t) = g(x(t) | \theta_y) + v(t), \quad (60b)$$

with process noise $w(t) \sim p_w(w(t) | \theta_w)$ and measurement noise $v(t) \sim p_v(v(t) | \theta_v)$, optimal controllers and estimators are obtained using the discretise-then-optimise strategies described in Sections 2.2 and 2.3, respectively. The controller considers a discretisation of Eq. (60) based on piecewise constant inputs $u(t) = u(t_k)$ and $w(t) = w(t_k)$, for $t \in [t_k, t_{k+1})$, where $t_k = \Delta t$ is the k -th time instant given the period $\Delta t > 0$. Similarly, the estimator considers the same discretisation

for a different $\Delta t_e > 0$, corresponding to the measurement process sampling period. At each time instant $t_k = k\Delta t$, the output MPC strategy consists on first estimating (\hat{x}_k, \hat{w}_k) by solving an OEP (Definition 2.9) for the estimation horizon $t \in [(k-N_e+1)\Delta t_e, k\Delta t_e]$ of size N_e , then solving an OCP (Definition 2.4) for the control horizon $t \in [k\Delta t, (k+N)\Delta t]$ of size N using (\hat{x}_k, \hat{w}_k) as initial conditions. Formally, this controller is defined by:

Definition 2.12. (Output model predictive control, Output MPC). Consider the conditions presented in Definitions 2.4 and 2.9. For each time instant $k \in \mathbb{N}$, the output model predictive control (Output-MPC) strategy consists on first solving the optimal estimation problem

$$\min_{\substack{x_{k-N_e+1}, \dots, x_{k+1} \\ w_{k-N_e+1}, \dots, w_k}} J_{\text{MHE}}(x, w|y) = L_0(x_{k-N_e+1}) + \sum_{n=k-N_e+1}^k L(x_n, w_n) \quad (61a)$$

$$\text{s.t.} \quad x_{n+1} = f_{\Delta t_e}(x_n, u_n, w_n | \theta_x), \quad \forall n \in [k-N_e+1, k] \quad (61b)$$

$$x_n \in \mathcal{X}, \quad w_n \in \mathcal{W}, \quad (61c)$$

to obtain estimates (\hat{x}_k, \hat{w}_k) , then solving the optimal control problem

$$\min_{\substack{x_k, \dots, x_{k+N} \\ u_k, \dots, u_{k+N-1}}} J_{\text{MPC}}(x, u) = \sum_{n=k}^{k+N-1} L(x_n, u_n) + L_f(x_{k+N}) \quad (62a)$$

$$\text{s.t.} \quad x_{n+1} = f_{\Delta t}(x_n, u_n, \hat{w}_k | \theta_x), \quad \forall n \in [k, k+N] \quad (62b)$$

$$x_n \in \mathcal{X}, \quad u_n \in \mathcal{U}, \quad (62c)$$

$$x_k = \hat{x}_k, \quad (62d)$$

and applying only the first optimal action, u_k^* , to the actual process.

In this optimal control strategy, all the conditions and properties stated in Sections 2.2.2 and 2.3.2 still follow. Namely, the optimisations are solved using the direct approach of transcribing each problem as a nonlinear program, then solving it numerically. Moreover, both the controller and the estimator have desirable stability properties for stabilizable and detectable systems (or, equivalently, stable systems). In the following, we discuss the output affine quadratic regulator resulting from the combination of a c-AQR (Section 2.2.2) and a c-AGM (Section 2.3.2).

2.4.1 Output affine quadratic regulator (Output-AQR)

A specific class of output predictive controllers arise from the usual choice of cost functions and constraints. Specifically, we are concerned with stochastic affine state-space models

$$\dot{x}(t) = z + Ax(t) + Bu(t) + Gw(t),$$

$$y(t) = Cx(t) + v(t),$$

from which a discrete-time realisations with dynamics $x_{k+1} = z_{\Delta t} + A_{\Delta t}x_k + B_{\Delta t}u_k + G_{\Delta t}w_k$ and outputs $y_k = C_{\Delta}x_k + v_k$ are obtained as in Eqs. (34) and (55).

We assume a controller based on quadratic costs functions $L(\cdot, \cdot) = \|x_n - x_n^{SP}\|_Q^2 + \|u_n - u_n^{SP}\|_R^2$ and $L_f(\cdot) = \|x_{k+N} - x_{k+N}^{SP}\|_{Q_f}^2$, given state (x_n^{SP}) and input (u_n^{SP}) references, and symmetric weighting matrices $Q, Q_f \succeq 0$ and $R \succ 0$. Moreover, we assume Gaussian distributions $x_{k-N_e+1} \sim \mathcal{N}(\bar{x}_{k-N_e+1}, Q_{x_0})$, $v_n \stackrel{i.i.d}{\sim} \mathcal{N}(0, Q_v)$, and $w_n \stackrel{i.i.d}{\sim} \mathcal{N}(\bar{w}_n, R_w)$, given means \bar{x}_{k-N_e} and \bar{w}_n ($n = k-N_e+1, \dots, k$) and covariance matrices (Q_{x_0}, Q_v, R_w). Finally, the constraint sets \mathcal{X} , \mathcal{U} , and \mathcal{W} are assumed convex, so that they can be represented by linear inequalities $\mathcal{X} = \{x \in \mathbb{R}^{N_x} \mid H_x x \leq h_x\}$, $\mathcal{U} = \{u \in \mathbb{R}^{N_u} \mid H_u u \leq h_u\}$ and $\mathcal{W} = \{w \in \mathbb{R}^{N_w} \mid H_w w \leq h_w\}$. Under such conditions, we formally define the constrained output affine quadratic regulator:

Definition 2.13. (Output affine quadratic regulator, Output c-AQR). Consider the system described by Eq. (63). Let $x_{k-N_e+1} \sim \mathcal{N}(\bar{x}_{k-N_e+1}, Q_{x_0})$, $w_n \sim \mathcal{N}(\bar{w}_n, R_w)$ and $v_n \sim \mathcal{N}(0, Q_v)$, assume cost functions $L(\cdot, \cdot) = \|x_n - x_n^{SP}\|_Q^2 + \|u_n - u_n^{SP}\|_R^2$ and $L_f(\cdot) = \|x_{k+N} - x_{k+N}^{SP}\|_{Q_f}^2$, and convex sets \mathcal{X} , \mathcal{U} and \mathcal{W} . For each time instant $k \in \mathbb{N}$, the output affine quadratic regulator (Output-AQR) strategy consists on first solving the optimal estimation problem

$$\min_{\substack{x_{k-N_e+1}, \dots, x_{k+1}, \\ w_{k-N_e+1}, \dots, w_k}} J_{AGM}(\cdot) = \|x_{k-N_e+1} - \bar{x}_{k-N_e+1}\|_{Q_{x_0}^{-1}}^2 + \sum_{n=k-N_e+1}^k \left(\|y_n - Cx_n\|_{Q_v^{-1}}^2 + \|w_n - \bar{w}_n\|_{R_w^{-1}}^2 \right) \quad (64a)$$

$$\text{s.t.} \quad x_{n+1} = z_{\Delta t_e} + A_{\Delta t_e}x_n + B_{\Delta t_e}u_n + G_{\Delta t_e}w_k, \quad (64b)$$

$$\forall n \in [k-N_e+1, k] \quad H_x x_n \leq h_x, \quad H_w w_n \leq h_w, \quad (64c)$$

to obtain estimates (\hat{x}_k, \hat{w}_k) , then solving the optimal control problem

$$\min_{\substack{x_k, \dots, x_{k+N}, \\ u_k, \dots, u_{k+N-1}}} J_{AQR}(\cdot) = \sum_{n=k}^{k+N-1} \left(\|x_n - x_n^{SP}\|_Q^2 + \|u_n - u_n^{SP}\|_R^2 \right) + \|x_{k+N} - x_{k+N}^{SP}\|_{Q_f}^2 \quad (65a)$$

$$\text{s.t.} \quad x_{n+1} = z_{\Delta t} + A_{\Delta t}x_n + B_{\Delta t}u_n + G_{\Delta t}\hat{w}_k, \quad (65b)$$

$$\forall n \in [k, k+N] \quad H_x x_n \leq h_x, \quad H_u u_n \leq h_u, \quad (65c)$$

$$x_k = \hat{x}_k, \quad (65d)$$

and applying only the first optimal action, u_k^* , to the actual process.

As in the previous sections, both problems in Definition 2.13 are transcribed into convex quadratic optimisation problems (see Lemmas 2.7 and 2.10). For nonlinear systems, the dynamic constraint of the OCP, Eq. (65b), is represented by a collection of linearisations $\{(A_{\Delta t}^{(k)}, B_{\Delta t}^{(k)}, G_{\Delta t}^{(k)})\}_{k=0}^K$ according to the choice of set-points described in Section 2.2.3. Moreover, the dynamic constraint of the OEP, Eq. (64b), is represented by the time-varying state-space from linearisations $(A_{\Delta t_e}^{(n)}, B_{\Delta t_e}^{(n)}, G_{\Delta t_e}^{(n)}, C_{\Delta t_e}^{(n)})$ based on the previous MHE estimates (Section 2.3.2).

3 RESULTS AND DISCUSSIONS

3.1 Analysis of activated sludge plant models

In this section, we analyse the full-state controllability and full-state observability properties for the class of activated sludge plants represented by Eq. (4) defined in Chapter 1.3. The discussion starts with the structural controllability and observability analysis for matrices (A, B, C) describing the structure of the system. Then, a classical analysis of stability, controllability, and observability, is performed for a suggested linearisation described by matrices (A^{SS}, B^{SS}, C^{SS}) . Finally, a minimal realisation based on this linearisation is used to discuss the controllability and observability of the system in qualitative terms.

3.1.1 Structural controllability and observability analysis

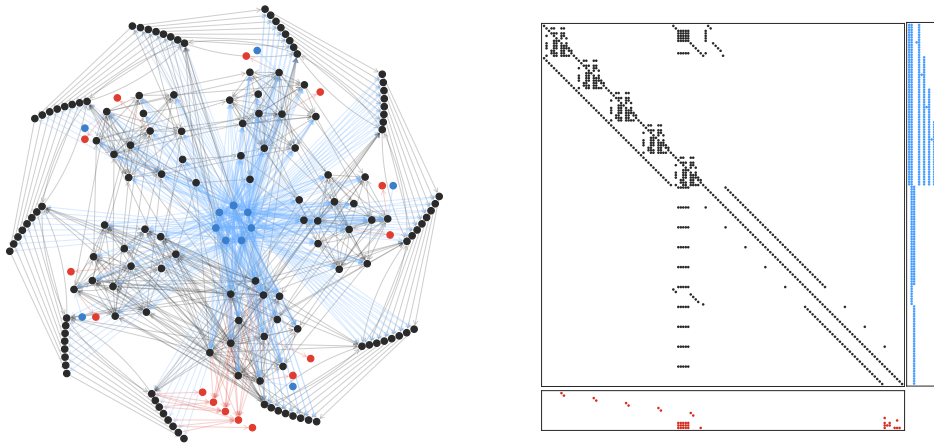
For the activated sludge plant $\dot{x}(t) = f(x(t), u(t), w(t) | \theta_x)$ with measurements $y(t) = g(x(t) | \theta_y)$ the structural matrices $A \in \mathbb{R}^{N_x \times N_x}$, $B \in \mathbb{R}^{N_x \times N_u}$, and $C \in \mathbb{R}^{N_y \times N_x}$ are obtained from the Jacobians $A = \partial f / \partial x$, $B = \partial f / \partial u$, $C = \partial g / \partial x$, with $N_x = 145$, $N_u = 13$ and $N_y = 15$. The associated digraph $\mathcal{G} = (\mathcal{V}, \mathcal{E})$, Figure 7, is defined by the vertex set

$$\mathcal{V} = \mathcal{V}_A \cup \mathcal{V}_B \cup \mathcal{V}_C = \{x_1, \dots, x_{N_x}\} \cup \{u_1, \dots, u_{N_u}\} \cup \{y_1, \dots, y_{N_y}\}$$

and the directed edge set

$$\mathcal{E} = \mathcal{E}_A \cup \mathcal{E}_B \cup \mathcal{E}_C = \{(x_j, x_i) \mid A_{i,j} \neq 0\} \cup \{(u_k, x_i) \mid B_{i,k} \neq 0\} \cup \{(x_j, y_k) \mid C_{k,j} \neq 0\}.$$

Figure 7 – Network $\mathcal{G} = (\mathcal{V}, \mathcal{E})$ (left panel) associated to structured system (A, B, C) (right panels). State vertices $x_i \in \mathcal{V}_A$ are in black, input vertices $u_k \in \mathcal{V}_B$ are in blue, and output vertices $y_k \in \mathcal{V}_C$ are in red. State-state edges $(x_i, x_j) \in \mathcal{E}_A$, input-state edges $(u_k, x_j) \in \mathcal{E}_B$, and state-output edges $(x_i, y_k) \in \mathcal{E}_C$ are dyed to match the corresponding entries in (A, B, C) . To reduce clutter, state self-loops are omitted.



Source: Prepared by the authors.

In the following we discuss the structural controllability and observability of the plant through pairs (A, B) and (A, C) , and associated digraphs $\mathcal{G}_c = (\mathcal{V}_c, \mathcal{E}_c)$ and $\mathcal{G}_o = (\mathcal{V}_o, \mathcal{E}_o)$, respectively.

The structural pair (A, B) associates with the subgraph $\mathcal{G}_c = (\mathcal{V}_c, \mathcal{E}_c)$, with $\mathcal{V}_c = \mathcal{V}_A \cup \mathcal{V}_B$ and $\mathcal{E}_c = \mathcal{E}_A \cup \mathcal{E}_B$. The topology of $\mathcal{G}_c = (\mathcal{V}_c, \mathcal{E}_c)$ indicates that pair (A, B) is structurally controllable (Lemma 2.3). The accessibility condition is satisfied since all state vertices are reachable from a control vertex. Specifically, it is easy to see how they all are reachable through one-edge paths starting from control vertex Q_R or Q_W . The dilation-free condition is satisfied through a perfect matching \mathcal{M} of size $|\mathcal{M}| = N_x$ formed by choosing every state vertex's self-loop, thus leaving no vertex unmatched. A perfect matching such as \mathcal{M} ensures the dilation-free condition and suggests that controls are only needed to ensure accessibility. Being structurally controllable, the system is also full-state controllable in a classical sense for almost all realisations of A and B .

The structural pair (A, C) associates with the subgraph $\mathcal{G}_o = (\mathcal{V}_o, \mathcal{E}_o)$, with $\mathcal{V}_o = \mathcal{V}_A \cup \mathcal{V}_C$ and $\mathcal{E}_o = \mathcal{E}_A \cup \mathcal{E}_C$. The topology of $\mathcal{G}_o = (\mathcal{V}_o, \mathcal{E}_o)$ indicates that pair (A, C) is structurally unobservable (Lemma .2). As there are no paths from state vertices $\{S_{ALK}^{A(r)}\}_{r=1}^5$, $\{S_{ALK}^{S(l)}\}_{l=1}^{10}$ and $\{S_O^{S(l)}\}_{l=7}^{10}$ to any of the output vertices, the accessibility condition is not satisfied. Conversely, the dilation-free condition is satisfied by the same perfect matching \mathcal{M} of size $|\mathcal{M}| = N_x$ as before, obtained by choosing every state vertex's self-loop. The lack of structural observability implies that the system is also not full-state observable in a classical sense.

We conclude that, for the activated sludge plant in Eq. (4), it is possible to design a control $u(t)$ that transfers the plant to a desired state, in finite time, for almost any realisation of (A, B) . It is not possible, however, to determine initial state $x(0)$, and thus neither intermediate states $x(t)$, starting from a measurement $y(t_f)$. Thus, it is also not possible to design a full-state-observer based on existing measurements, no matter what realisation of (A, C) is used. Being of structural nature, these conclusions are valid also in a classical sense, whatever the model linearisation.

3.1.2 Stability, controllability and observability analysis

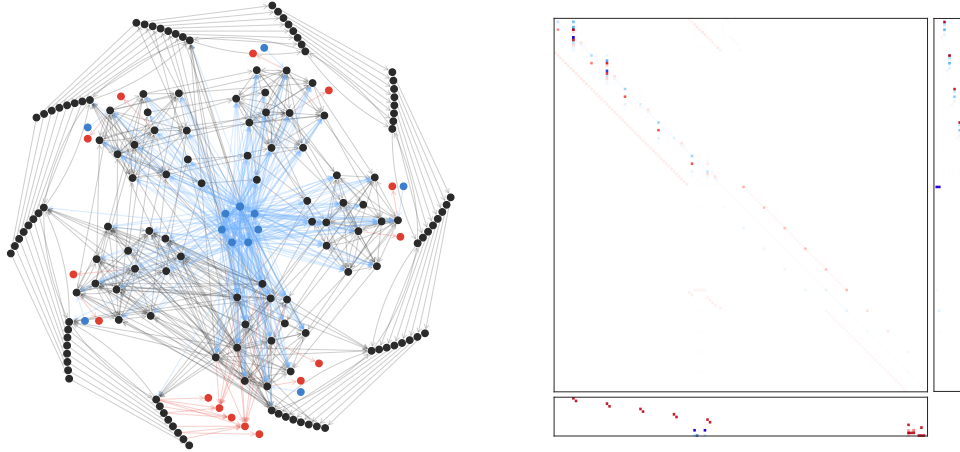
We now consider the linearisation (A^{SS}, B^{SS}, C^{SS}) , corresponding to the benchmark fixed point $SS := (x^{SS}, u^{SS}, w^{SS}, y^{SS})$ presented in Section 1.3.3. This linearisation is commonly utilised in the literature and constitutes the default configuration of the BSM1. The matrices $A^{SS} \in \mathbb{R}^{N_x \times N_x}$, $B^{SS} \in \mathbb{R}^{N_x \times N_u}$, and $C^{SS} \in \mathbb{R}^{N_y \times N_x}$ are obtained from the Jacobians evaluated at such equilibrium point $A^{SS} = (\partial f / \partial x)|_{SS}$, $B^{SS} = (\partial f / \partial u)|_{SS}$, $C^{SS} = (\partial g / \partial x)|_{SS}$. The, now weighted, associated digraph $\mathcal{G}_{SS} = (\mathcal{V}_{SS}, \mathcal{E}_{SS})$, in Figure 8, is defined by the vertex set

$$\mathcal{V} = \mathcal{V}_{A^{SS}} \cup \mathcal{V}_{B^{SS}} \cup \mathcal{V}_{C^{SS}} = \{x_1, \dots, x_{N_x}\} \cup \{u_1, \dots, u_{N_u}\} \cup \{y_1, \dots, y_{N_y}\}$$

and the directed edge set

$$\mathcal{E} = \mathcal{E}_{A^{SS}} \cup \mathcal{E}_{B^{SS}} \cup \mathcal{E}_{C^{SS}} = \{(x_j, x_i) \mid A_{i,j}^{SS} \neq 0\} \cup \{(u_k, x_i) \mid B_{i,k}^{SS} \neq 0\} \cup \{(x_j, y_k) \mid C_{k,j}^{SS} \neq 0\}.$$

Figure 8 – Network $\mathcal{G}_{SS} = (\mathcal{V}_{SS}, \mathcal{E}_{SS})$ (left) associated to linearisation (A^{SS}, B^{SS}, C^{SS}) (right). State vertices $x_i \in \mathcal{V}_{A^{SS}}$ and state-state edges $(x_i, x_j) \in \mathcal{E}_{A^{SS}}$ are in black, input vertices $u_k \in \mathcal{V}_{B^{SS}}$ and input-state edges $(u_k, x_j) \in \mathcal{E}_{B^{SS}}$ are in blue, and output vertices $y_k \in \mathcal{V}_{C^{SS}}$ and state-output edges $(x_i, y_k) \in \mathcal{E}_{C^{SS}}$ are in red. State self-loops have been omitted.

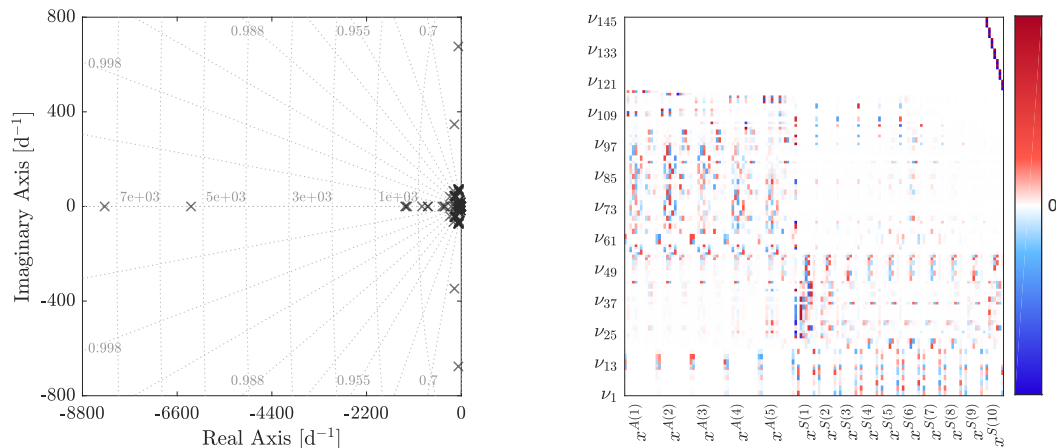


Source: Prepared by the authors.

In the following, we discuss the stability of this system and then we discuss its controllability and observability on both structural and conventional sense.

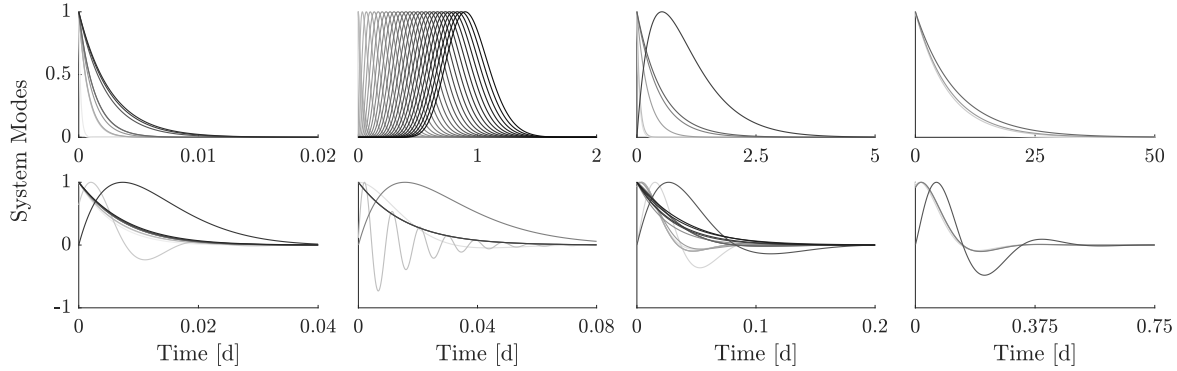
The spectrum of A^{SS} , in Figure 9, consists of 69 distinct eigenvalues and associated eigenvectors, $\sigma(A^{SS}) = \{\lambda_i(A^{SS}), v_i(\lambda_i)\}_{i=1}^{69}$, with $\{\lambda_1, \dots, \lambda_{31}\} \subset \mathbb{R}$ and $\{(\lambda_{32}, \lambda_{32}^*), \dots, (\lambda_{69}, \lambda_{69}^*)\} \subset \mathbb{C}$. Five complex conjugate pairs of eigenvalues have algebraic multiplicity equal to two and two distinct real eigenvalues have algebraic multiplicities equal to two and twenty-eight, respectively. The distribution of the eigenvalues in the complex plane shows that most of the system modes have relatively slow time constants. Moreover, the majority of eigenvalues are still close to the

Figure 9 – Spectrum $\sigma(A^{SS})$: Eigenvalues $\lambda_i \in \sigma(A^{SS})$, left, and associated eigenvectors $v_i(\lambda_i)$, right. The grid in the complex plane displays lines corresponding to constant damping factors (diagonal lines) and natural frequencies (vertical lines, in rad/days) for the associated system modes.



Source: Prepared by the authors.

Figure 10 – Time evolution of the normalised system modes $\frac{t^k e^{\lambda_i t}}{\max_t t^k e^{\lambda_i t}}$ ($k = 0, \dots, \mu(\lambda_i) - 1$) for the real eigenvalues (top plots) and complex conjugated pairs of eigenvalues (bottom plots) from the spectrum $\sigma(A^{SS}) = \{\lambda_i, v_i(\lambda_i)\}_{i=1}^{N_x}$. The curves are grouped based on each mode's time constant $\tau_i = 1/\text{Re}[\lambda_i]$.



Source: Prepared by the authors.

real axis, indicating that pseudo-oscillatory behaviour in the system modes is not expressive.

Being $\text{Re}(\lambda_i) < 0$ for all $\lambda_i \in \sigma(A^{SS})$, then A^{SS} is a stable matrix and the linear system (A^{SS}, B^{SS}, C^{SS}) is asymptotically stable (Lemma 2.1). This result can also be visualized through the simulation of individual system modes, shown in Figure 10. As the unforced evolution of the system, for any initial state $x(0)$, is a linear combination of system modes, the fact that all curves converge to zero directly implies that the system is asymptotically stable.

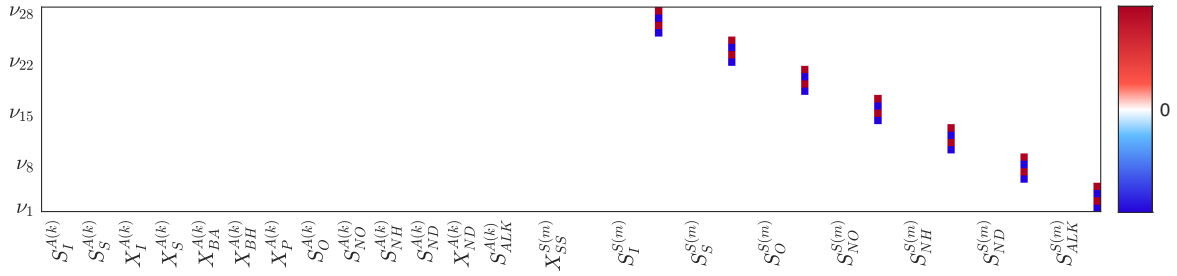
Controllability analysis

The controllability of this system is assessed through pair (A^{SS}, B^{SS}) and associated digraph $\mathcal{G}_{c^{SS}} = (\mathcal{V}_{c^{SS}}, \mathcal{E}_{c^{SS}})$, with $\mathcal{V}_{c^{SS}} = \mathcal{V}_{A^{SS}} \cup \mathcal{V}_{B^{SS}}$ and $\mathcal{E}_{c^{SS}} = \mathcal{E}_{A^{SS}} \cup \mathcal{E}_{B^{SS}}$. As expected, the topology of $\mathcal{G}_{c^{SS}} = (\mathcal{V}_{c^{SS}}, \mathcal{E}_{c^{SS}})$ indicates that (A^{SS}, B^{SS}) is full-state controllable in a structural sense (Lemma 2.3). Thus, for the activated sludge plant with dynamics described by (A^{SS}, B^{SS}) , it is possible to design a control $u(t)$ that transfers the plant to a desired state, in finite time.

As the pair (A^{SS}, B^{SS}) corresponds to the linear time-invariant approximation of Eq. (4a) in the neighbourhood of steady-state point $SS := (x^{SS}, u^{SS}, w^{SS}, y^{SS})$, it is possible to analyse its full-state controllability in a conventional sense. We have just shown that pair (A^{SS}, B^{SS}) is full-state controllable in the structural sense. The classical counterpart of this result can only be verified using the PBH controllability test (Lemma 2.2), as an accurate computation of the controllability matrix $\mathcal{C} = [B^{SS} \ A^{SS} B^{SS} \ \dots \ (A^{SS})^{N_x-1} B^{SS}]$ is unfeasible.

Surprisingly, the PBH test shows that the pair is not full-state controllable in the classical sense, as a real eigenvalue with algebraic multiplicity equal to twenty-eight leads to a rank-deficient matrix $[\lambda_i I - A^{SS} \ B^{SS}]$. The twenty-eight associated eigenvectors are shown in Figure 11. Interestingly, note that the non-zero entries of these eigenvectors correspond to state variables relative to soluble matter in the settler's last layer. This indicates that it is not possible to design

Figure 11 – Pair (A^{SS}, B^{SS}) : Eigenvectors $v_i(\lambda_i)$ for $\lambda_i \in \sigma(A^{SS})$ with $\text{rank}([\lambda_i I - A^{SS} \ B^{SS}]) < N_x$.



Source: Prepared by the authors.

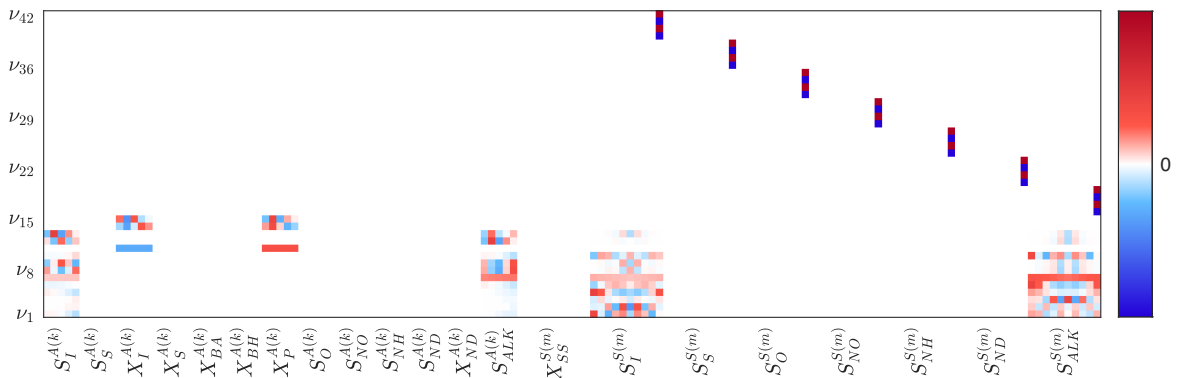
a control $u(t)$ capable of enforcing a desired profile of soluble concentrations in the settler. Moreover, since A^{SS} is a stable matrix, the eigenvalue failing the PBH test satisfies $\text{Re}(\lambda_i) < 0$ such that the pair (A^{SS}, B^{SS}) is thus characterised as stabilizable (Lemma 2.5).

Observability analysis

Furthermore, the observability of this system is assessed through pair (A^{SS}, C^{SS}) and associated digraph $\mathcal{G}_{oss} = (\mathcal{V}_{oss}, \mathcal{E}_{oss})$, with $\mathcal{V}_{oss} = \mathcal{V}_{Ass} \cup \mathcal{V}_{Css}$ and $\mathcal{E}_{oss} = \mathcal{E}_{Ass} \cup \mathcal{E}_{Css}$. As expected, the observability digraph $\mathcal{G}_{oss} = (\mathcal{V}_{oss}, \mathcal{E}_{oss})$ indicates that also the pair (A^{SS}, C^{SS}) is not full-state observable in a structural sense, as there is still no directed path from the state vertices $\{S_{ALK}^{A(r)}\}_{r=1}^5$, $\{S_{ALK}^{S(l)}\}_{l=1}^{10}$ and $\{S_O^{S(l)}\}_{l=7}^{10}$ to any of the output vertices.

For completeness, we also analyse the full-state observability of (A^{SS}, C^{SS}) in a conventional sense, as it also corresponds to the linear time-invariant approximation of Eq. (4) in the neighbourhood of steady-state point $SS := (x^{SS}, u^{SS}, w^{SS}, y^{SS})$. We have just shown that (A^{SS}, C^{SS}) is unobservable in a structural sense. We verify this result using the PBH observability test (Lemma .1), as an accurate computation of the observability matrix $\mathcal{O} = [C^{SS^T} \ A^{SS^T} \ C^{SS^T} \ \dots \ (A^{SS^T})^{N_x-1} C^{SS^T}]^T$ is also unfeasible in this case.

Figure 12 – Pair (A^{SS}, C^{SS}) : Eigenvectors $v_i(\lambda_i)$ for $\lambda_i \in \sigma(A^{SS})$ with $\text{rank}([\lambda_i I - A^{SS^T} \ C^{SS^T}]^T) < N_x$.



Source: Prepared by the authors.

The test confirms that the pair (A^{SS}, C^{SS}) is not full-state observable, as ten distinct eigenval-

ues, including two real values with multiplicities equal to two and twenty-eight, respectively, and five complex conjugated pairs with multiplicities equal to two, all lead to rank-deficient matrices $[\lambda_i I - A^{SS\top} C^{SS\top}]^\top$. The forty-three eigenvectors associated to such eigenvalues are shown in Figure 12. As before, the non-zero entries of the twenty-eight eigenvectors associated to one of the real eigenvalues refer to state variables relative to effluent soluble matter. From the remaining fifteen eigenvectors, three have non-zero entries only at state variables $\{X_I^{A(r)}, X_P^{A(r)}\}_{r=1}^5$, while the remaining twelve have non-zero entries only at state variables $\{S_I^{A(r)}, S_{ALK}^{A(r)}\}_{r=1}^5$ and $\{S_I^{S(l)}, S_{ALK}^{S(l)}\}_{l=1}^{10}$. Interestingly, these correspond to concentrations of non-reacting matter within the process. Moreover, since A^{SS} is a stable matrix, all eigenvalues failing the PBH test satisfy $\text{Re}(\lambda_i) < 0$ such that pair (A^{SS}, C^{SS}) is thus characterised as detectable (Lemma .3).

We conclude that, for the activated sludge plant described by the linearisation (A^{SS}, B^{SS}, C^{SS}) , it is not possible to design a control $u(t)$ that transfers the plant to a desired state $x(t_f)$ in a given finite time. Moreover, it is also not possible to determine the initial state $x(0)$, and thus neither intermediate states $x(t)$, starting from measurement $y(t_f)$.

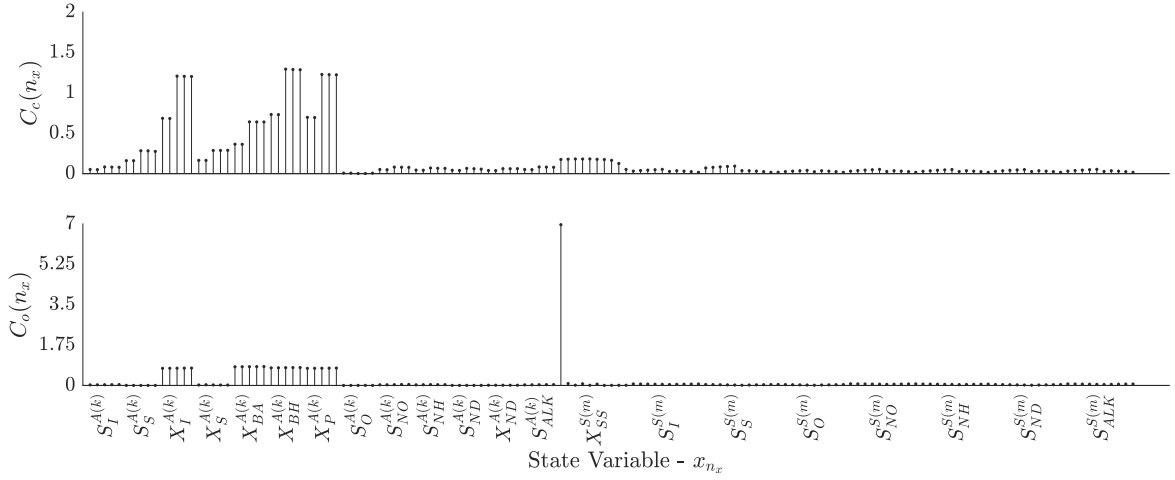
Minimal realisation and energy-related metrics

In this section, we provide a qualitative analysis of controllability and observability. We start by analysing the effort associated with controlling or observing each state variable individually, and then proceed to analyse the entire system using a minimal realisation of the linearisation (A^{SS}, B^{SS}, C^{SS}) corresponding to the default fixed point $SS := (x^{SS}, u^{SS}, w^{SS}, y^{SS})$.

Considering the linearisation (A^{SS}, B^{SS}, C^{SS}) , the average energy required to respectively control or reconstruct the full-state by directly controlling or measuring only one individual state variable is quantified by its average controllability and average observability centralities (Section 2.1.2). The results (Figure 13) show that the energy required to control the entire state-space is among the lowest if we were to actuate on some control only affecting biomass concentrations $(X_{BH}^{A(r)}, X_{BA}^{A(r)}, \text{ and } X_P^{A(r)})$ or particulate inert organic matter $(X_I^{A(r)})$ on the reactors. This reflects the fact that such variables are central to the process, but will evolve slowly if not directly controlled. Conversely, the energy required by the system would be the highest if we were to actuate on some control only affecting dissolved oxygen $(S_O^{A(r)})$. However, it is worth mentioning that it is still possible to control $S_O^{A(r)}$ (through $K_{La}^{A(r)}$), while individually controlling any of the concentrations $X_{BH}^{A(r)}, X_{BA}^{A(r)}, X_P^{A(r)}$, or $X_I^{A(r)}$, is practically unfeasible. The analysis also shows that acting directly on most state variables on the reactors lead to less demanding full-state controls than directly acting on any state variables within the settler.

Moreover, the results show that the effort required to reconstruct the entire state-space is the lowest if we were to directly measure the concentration of suspended solids in the bottom of the settler $(X_{SS}^{S(1)})$. Additionally, the effort required is also among the lowest if we were to directly measure the biomass concentrations $(X_{BH}^{A(r)}, X_{BA}^{A(r)}, \text{ and } X_P^{A(r)})$ and particulate inert organic matter

Figure 13 – System (A^{SS}, B^{SS}, C^{SS}) : Average controllability centrality $C_C(n_x)$, top, and average observability centrality $C_o(n_x)$, bottom, associated to each state variable.



Source: Prepared by the authors.

$(X_I^{A(r)})$ in the reactors. Again, this reflects how these variables are central to the process such that reconstructing the state-vector is more demanding if they are not measured. In practice, only the concentrations of dissolved oxygen ($S_O^{A(r)}$) and nitrate and nitrite nitrogen ($S_{NO}^{A(r)}$) in each reactor, along with $\text{NH}_4^+ + \text{NH}_3$ nitrogen in the top layer of the settler ($S_{NH}^{S(10)}$), are directly measured. Conversely, these variables are associated with the highest measurement effort if used individually to reconstruct the entire state of the process.

Now, we analyse the compound energy-related metrics for the control and measurement configuration of the activated sludge plant. Being the linearisation both uncontrollable and unobservable, the metrics computed for the Gramians of (A^{SS}, B^{SS}, C^{SS}) will obviously conclude that its control or state reconstruction are high-demanding. Thus, we turn to analyse the minimal realisation of (A^{SS}, B^{SS}, C^{SS}) as it preserves the input-output behaviour of the process. The minimal realisation of (A^{SS}, B^{SS}, C^{SS}) , Lemma 2.4, is represented as

$$\begin{aligned}\dot{x}_{co}(t) &= A_{co}x_{co}(t) + B_{co}u(t) \\ y(t) &= C_{co}x_{co}(t),\end{aligned}$$

with $A_{co} \in \mathbb{R}^{N_{xco} \times N_{xco}}$, $B_{co} \in \mathbb{R}^{N_{xco} \times N_u}$ and $C_{co} \in \mathbb{R}^{N_y \times N_{xco}}$, for $N_{xco} = 117$. As $\sigma(A_{co}) \subseteq \sigma(A^{SS})$ it follows that $\text{Re}(\lambda_i) < 0$ for all $\lambda_i \in \sigma(A_{co})$, and thus (A_{co}, B_{co}, C_{co}) is a stable system.

Considering this model, we analysed the energy-related metrics defined for the infinite-horizon controllability ($W_c(\infty)$) and observability ($W_o(\infty)$) Gramians (Section 2.1.2). As the system is Hurwitz, these Gramians are computed by solving Lyapunov equations $A_{co}W_c(\infty) + W_c(\infty)A_{co}^\top = -B_{co}B_{co}^\top$ and $W_o(\infty)A_{co}^\top + A_{co}W_o(\infty) = -C_{co}^\top C_{co}$. The metrics, Table 4, reveal that controlling and observing this system are energy demanding tasks even for the minimal realisation. Specifically, the fact that $\lambda_{\min}(W_c(\infty))$ and $\lambda_{\min}(W_o(\infty))$ are approximately zero implies that

there exists state-space directions which are practically uncontrollable and unobservable.

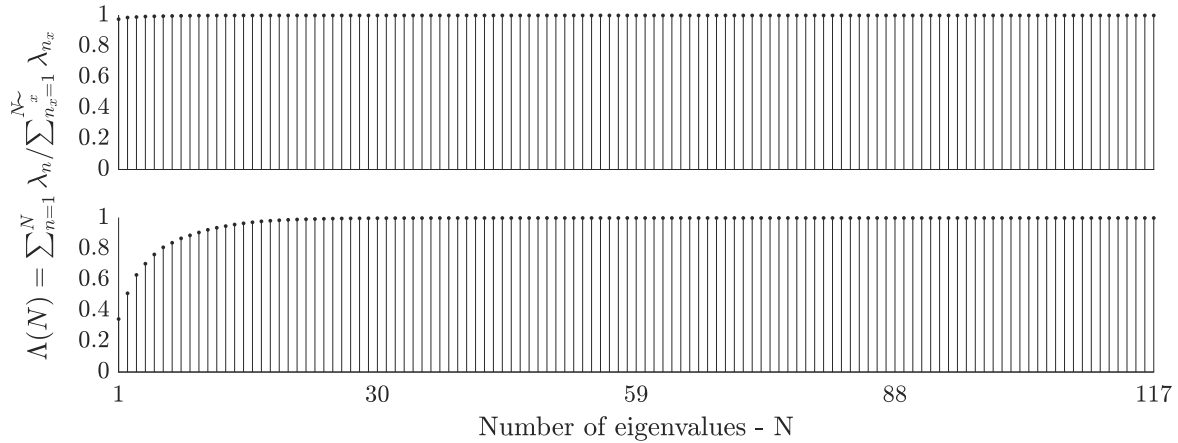
Table 4 – System (A_{co}, B_{co}, C_{co}) : Energy-related metrics.

	$\text{tr}(W)$	$\text{tr}(W^\dagger)$	$\log(\det(W))$	$\lambda_{\min}(W)$
$W_c(\infty)$	$1.23 \cdot 10^5$	$1.36 \cdot 10^9$	$-\infty$	$1.01 \cdot 10^{-11}$
$W_o(\infty)$	0.52	$6.76 \cdot 10^{14}$	$-\infty$	$5.69 \cdot 10^{-19}$

Source: Prepared by the authors.

We can conclude that, although controllable and observable, the realisation (A_{co}, B_{co}, C_{co}) requires a very large control and measurement effort in order to access the full state-space. The cumulative coverage of state-space is shown in Fig. 14 in terms of normalised cumulative sum $(\Lambda(N) = \sum_{n=1}^N \lambda_n / \sum_{n_x=1}^{N_{xco}} \lambda_{n_x})$ for the (sorted) eigenvalues of $W_c(\infty)$ and $W_o(\infty)$. The results imply that most control and output energy are comprised within a small number of directions.

Figure 14 – System (A_{co}, B_{co}, C_{co}) : Cumulative sum $\Lambda(N)$ for the eigenvalues of the infinite-horizon controllability Gramian $W_c(\infty)$, top, and observability Gramian $W_o(\infty)$, bottom.



Source: Prepared by the authors.

Contradiction between structural and conventional results

When analysing the controllability of the complete system we have shown that (A^{SS}, B^{SS}, C^{SS}) is controllable in a structural sense but not in the classical sense. This apparent contradiction can be explained from the analysis of the dilation-free condition applied to network $\mathcal{G}_{c^{SS}} = (\mathcal{V}_{c^{SS}}, \mathcal{E}_{c^{SS}})$. Specifically, as the existence of a self-loop for each state vertex is sufficient to satisfy this condition, the input vertices are needed only to satisfy the accessibility condition. Whenever some of the self-loop weights are equal, the dilation-free condition will underestimate the controls needed for full-state controllability (ZHAO et al., 2015). This is the case for (A^{SS}, B^{SS}) , where all reactors' non-reacting components (respectively, all settler's soluble components) from the same unit (layer) always have identical self-dynamics.

Consider the non-reacting components $S_a^{A(r)}$ ($S_a \in \{S_I, S_{ALK}\}$) and $X_b^{A(r)}$ ($X_b \in \{X_I, X_P\}$) in the r -th reactor. Their dynamics are each represented in Eq. (4a) by first-order differential

equations of the forms $\dot{S}_a^{A(r)} = Q^{A(r)}(S_a^{A(r-1)} - S_a^{A(r)}) - (Q_{EC}^{(r)}/V^{(r)})S_a^{A(r)} + R_a^{(r)}$ and $\dot{X}_b^{A(r)} = Q^{A(r)}(X_b^{A(r-1)} - X_b^{A(r)}) - (Q_{EC}^{(r)}/V^{(r)})X_b^{A(r)} + R_b^{(r)}$ for $r = 1, \dots, 5$. $Q^{A(r)}$ denotes the influent flow-rate to the r -th reactor and both $R_a^{(r)}$ and $R_b^{(r)}$ indicates the contribution from process reactions. The model assumes the same influent flow-rate, $\{Q^{A(r)} = (Q_A + Q_R + Q_{IN} + \sum_{j=1}^{r-1} Q_{EC}^{(j)})/V_A^{(r)}\}_{r=1}^5$, with constant volumes $V_A^{(r)}$. As these components represent non-reacting matter, $\partial R_a^{(r)}/\partial S_a^{A(r)} = \partial R_b^{(r)}/\partial X_b^{A(r)} = 0$. For the relevant entries in the Jacobian $\partial f/\partial x$ of the dynamics,

$$\left. \frac{\partial \dot{S}_a^{A(r)}}{\partial S_a^{A(r)}} \right|_{SS} = \left. \frac{\partial \dot{X}_b^{A(r)}}{\partial X_b^{A(r)}} \right|_{SS} = - \left. \frac{Q_A + Q_R + Q_{IN} + \sum_{j=1}^r Q_{EC}^{(j)}}{V_A^{(r)}} \right|_{SS},$$

which is equal for all reactors ($r = 1, \dots, 5$), whatever the fixed-point.

Similarly, the dynamics of soluble components $S_c^{S(l)}$ ($S_c \in \{S_I, S_S, S_O, S_{NO}, S_{NH}, S_{ND}, S_{ALK}\}$) in the l -th layer of the settler are each represented in Eq. (4a) by first-order differential equations of the form $\dot{S}_c^{S(l)} = Q^{S(l)}(S_c^{S(l-1)} - S_c^{S(l)})$, for $l = 1, \dots, 10$. $Q^{S(l)}$ denotes the influent flow-rate to the l -th layer. The model assumes a same influent flow-rate for all upper layers, $\{Q^{S(l)} = (Q_{IN} - Q_W)/V_S^{(l)}\}_{l=7}^{10}$, for all lower layers, $\{Q^{S(l)} = (Q_R + Q_W)/V_S^{(l)}\}_{l=1}^5$, and for the feed layer we have $Q^{S(6)} = (Q_{IN} + Q_R)/V_S^{(6)}$. The model also assumes constant volumes $V_S^{(l)} = 600 \text{ m}^3$. For the relevant entries in the Jacobian $\partial f/\partial x$ of the dynamics,

$$\left. \frac{\partial \dot{S}_c^{S(l)}}{\partial S_c^{S(l)}} \right|_{SS} = \begin{cases} (Q_W - Q_{IN})/V_S^{(l)} \Big|_{SS} & l = 7, \dots, 10 \\ -(Q_{IN} + Q_R)/V_S^{(l)} \Big|_{SS} & l = 6 \\ -(Q_R + Q_W)/V_S^{(l)} \Big|_{SS} & l = 1, \dots, 5 \end{cases},$$

which is equal for all components, independently of the fixed-point adopted for linearisation.

3.2 Wastewater treatment: regulation

In this section, we present the simulation results obtained for the predictive control of the activated sludge plant for the conventional wastewater treatment task. For the sake of comparison, the open-loop simulation of the process is presented first. We then consider a model predictive controller that regulates the process towards a steady-state satisfying effluent quality requirements (see Section 1.3.3). We first consider a predictive control in which the process state is assumed to be known, then we design an output predictive control strategy in which the state is estimated. Finally, control performances are evaluated under the short-term disturbance regimes (*dry weather*, *storm event*, and *rain event*) in terms of the effluent quality index (EQI) and compliance with the quality limits. For brevity, the discussion focuses on the *storm event* influent scenario, as it is considered to be the most challenging disturbance scenario.

3.2.1 Open-loop: simulation and state-estimation

We assume the open-loop input configuration considered in the conventional benchmark suggested steady-state $SS = (x^{SS}, u^{SS}, w^{SS}, y^{SS})$, shown in Table 5. This setup refers to the common layout of an activated sludge plant: reactors A(1) and A(2) are always anoxic, whereas reactors A(3) to A(5) are aerated. External recirculation is set $Q_R = Q_{IN}^{SS}$, the influent flow-rate assumed in the operating point, and $Q_A = 3Q_R$. No external carbon is added to the reactors.

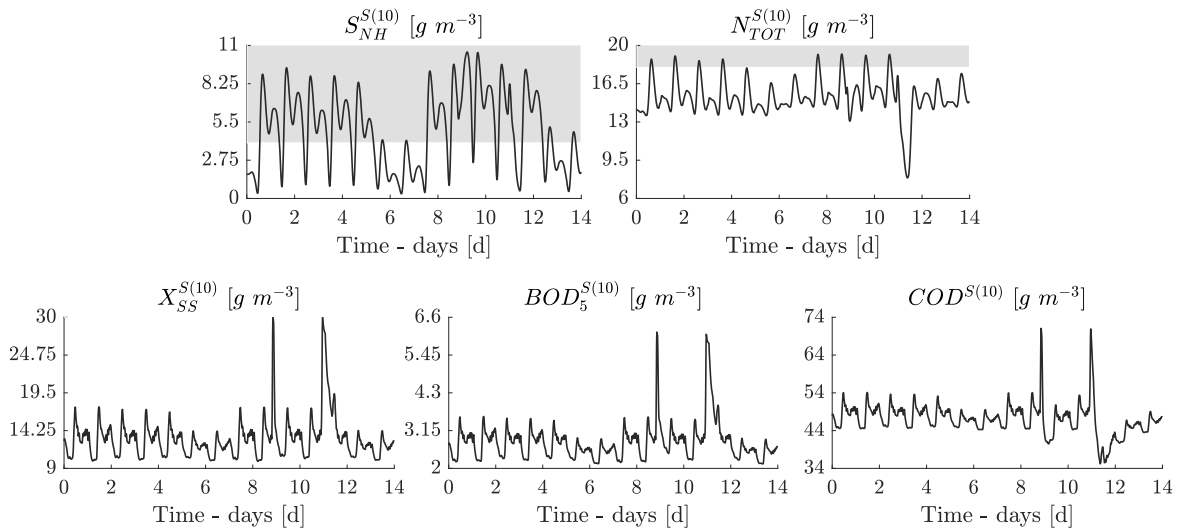
Table 5 – Activated sludge plant: controllable inputs for the default open-loop operation.

Q_A	Q_R	Q_W	$K_{La}^{(1)}$	$K_{La}^{(2)}$	$K_{La}^{(3)}$	$K_{La}^{(4)}$	$K_{La}^{(5)}$	$Q_{EC}^{(1\sim 5)}$
55338	18446	385	0	0	240	240	84	0

Source: Prepared by the author.

The simulation results for the effluent-based output variables are shown in Figure 15. Under open-loop conditions, we note that the output variables related to nitrogen concentrations, $S_{NH}^{S(10)}$ and $N_{TOT}^{S(10)}$, frequently violates their respective quality limits. Specifically, the concentrations of ammonia nitrogen, $S_{NH}^{S(10)}$, remain over the allowed limit for the majority of the simulation period. Conversely, the concentrations of organic-related matter, $X_{SS}^{S(10)}$, $BOD_5^{S(10)}$ and $COD^{S(10)}$, satisfy the quality constraints even without closed-loop control. This demonstrates the efficiency of the settler in clarifying the effluent water of particulate matter, while soluble nitrogen still requires a controller that rejects the influent disturbances. Moreover, we note that the concentration $X_{SS}^{S(10)}$ does reach the constraint (30 g m^{-3}) during the storm events, in $t \in [8, 12]$, but remains on violation for a negligible period of time.

Figure 15 – Open-loop simulation: Effluent-based output variables corresponding to nitrogen components, top panels, and organic matter, bottom panels. Shaded areas denote the values above the quality limits.



Source: Prepared by the author.

State estimation via Moving Horizon Estimation

We now consider the moving horizon estimation over the open-loop operation of the process. We assume constraints $X_{BA}^{IN} = X_P^{IN} = S_O^{IN} = S_{NO}^{IN} = 0 \text{ g m}^{-3}$ and $S_{ALK}^{IN} = 7 \text{ mol HCO}_3^- \text{ m}^{-3}$, as these disturbance variables are constant whatever the influent scenario (Section 1.3.2). For the activated sludge plant and measurement process in Eq. (4), the linear models $(A^{(n)}, B^{(n)}, G^{(n)}, C^{(n)})$ are computed around each horizon estimates $P_n := (\hat{x}_n, u_n, \hat{w}_n, \hat{y}_n)$. The dynamics $f_{\Delta t_e}(\cdot | \theta_x)$ in Eq. (45) are evaluated from $(A^{(n)}, B^{(n)}, G^{(n)}, C^{(n)})$ with sampling period of $\Delta t_e = (1/96)\text{d}$. The estimator assumes a stochastic representation of the plant with process disturbances $w_n \stackrel{i.i.d}{\sim} \mathcal{N}(\bar{w}_n, R_w)$ and measurement noise $v_n \stackrel{i.i.d}{\sim} \mathcal{N}(0, Q_v)$, given covariance matrices

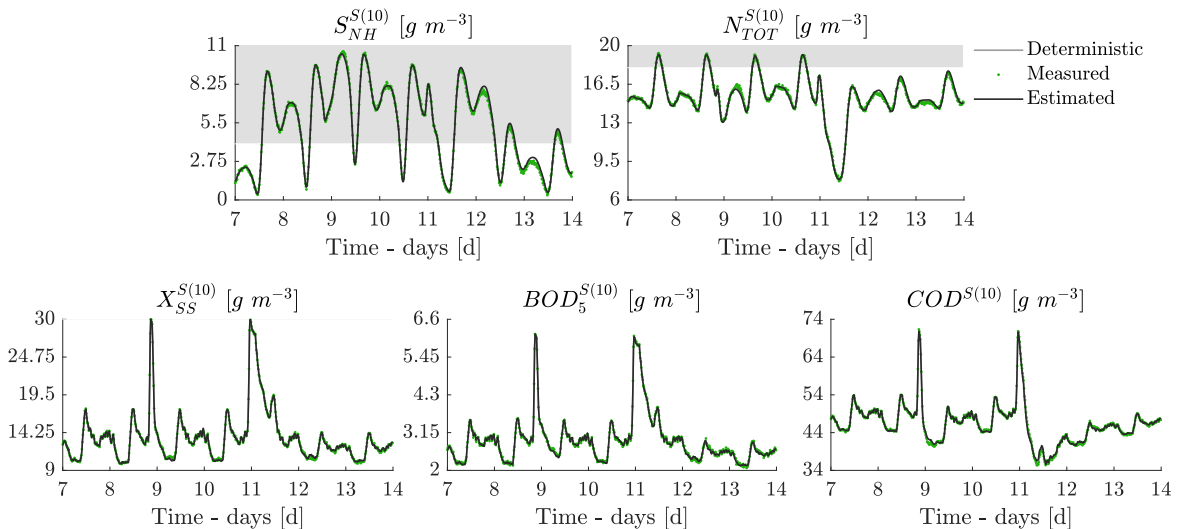
$$R_w = \text{diag}[9 \cdot 10^7 \ 5 \ 50 \ 10^3 \ 75 \ 10^3 \ 10 \ 2 \ 9];$$

$$Q_v = \text{diag}[0.001I_5 \ 0.006I_5 \ 0.01 \ 0.009 \ 0.001 \ 0.03 \ 0.01].$$

The estimation horizon, Eq. (54), is set to 3 hours, or $N_e = 12$. We define the initial state uncertainty by assuming $x_{k-N_e+1} \sim \mathcal{N}(\bar{x}_{k-N_e+1}, Q_{x_0})$ with covariance matrix $Q_{x_0} = \text{diag}[0.001(x^{SS})^2]$ and mean $\bar{x}_{k-N_e+1} \in \mathbb{R}^{N_x}$ fixed at the state estimate from the previous iteration, $\bar{x}_{k-N_e+1} = \hat{x}_{k-N_e+1}$, or $\bar{x}_0 = x^{SS}$ for the first estimation horizon.

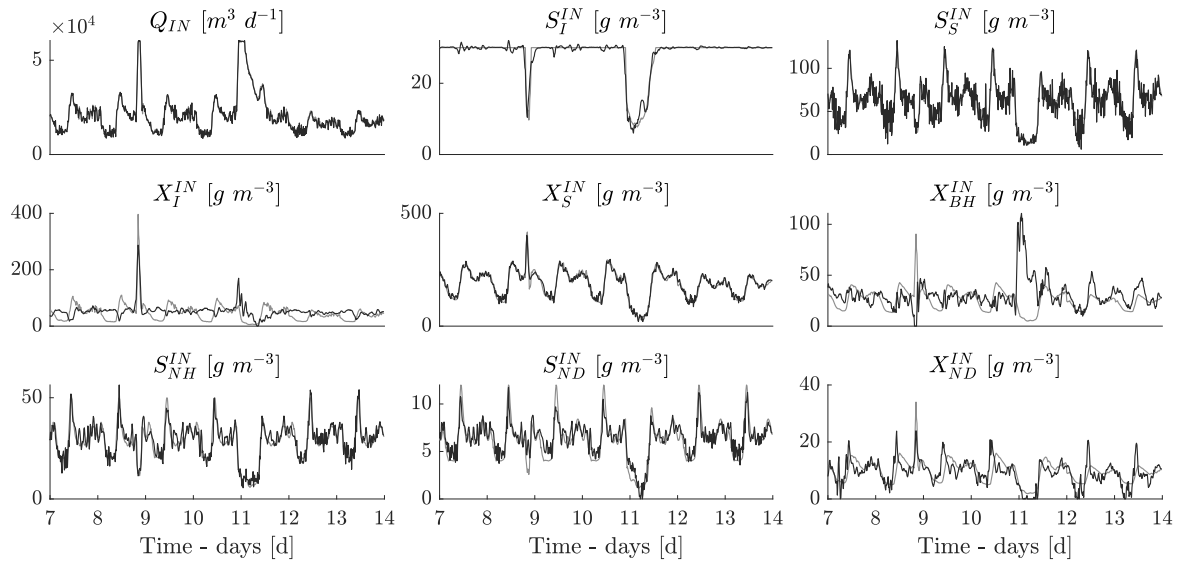
The results are shown in Figure 16 with respect to the usual effluent measurements of interest. We focus on the second week period, $t \in [7, 14]$, when the storm events occur. This visualization shows that the MHE estimator is capable to reconstruct approximately the true output of the plant from the noisy measurements. We note a decrease in the estimation performance only for $COD^{S(10)}$ at $t \in [11, 12.5]$, corresponding to the storm events. Conversely, the remaining output variables estimates show high accuracy even during such period.

Figure 16 – Open-loop simulation, $t \in [7, 14]$: Estimation of the effluent-based output variables.



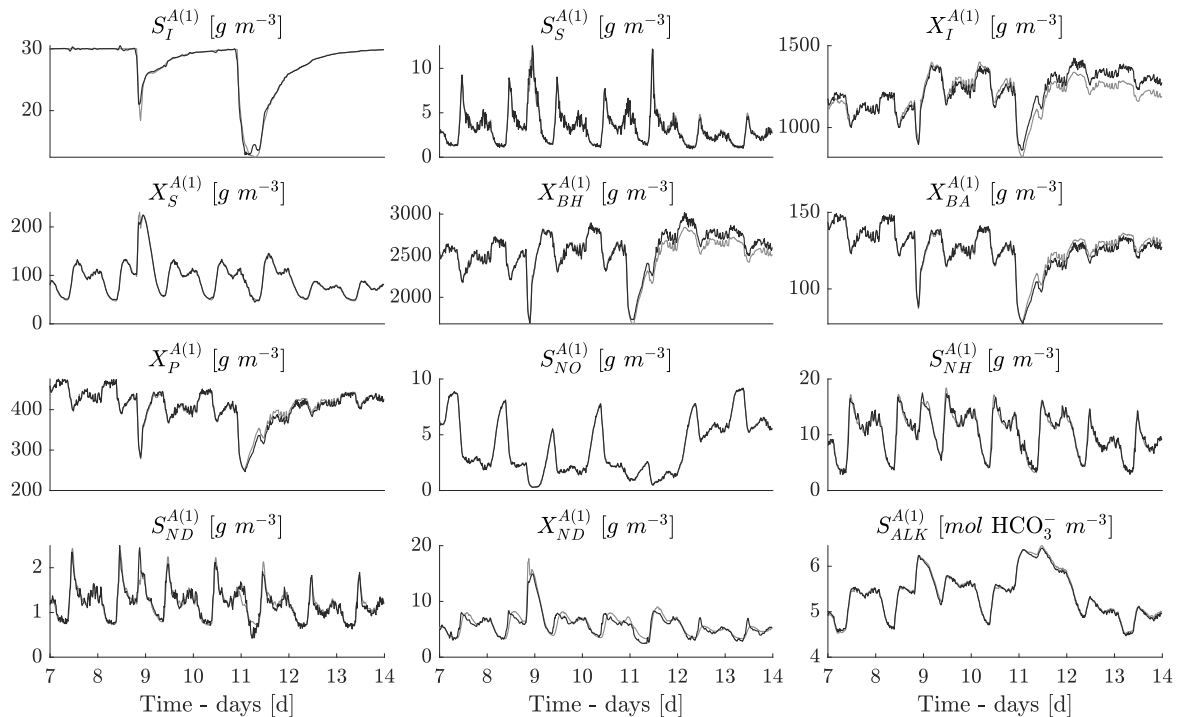
Source: Prepared by the author.

Figure 17 – Open-loop, $t \in [7, 14]$: Estimates (black) and true values (grey) for influent flow-rate Q_{IN} and concentrations $x^{A(IN)}$. Concentrations $X_{BA}^{IN} = X_P^{IN} = S_O^{IN} = S_{NO}^{IN} = 0$ and $S_{ALK}^{IN} = 7$ are omitted.



Source: Prepared by the author.

Figure 18 – Open-loop, $t \in [7, 14]$: Estimates (black) and true values (grey) for the chemical concentrations in the first reactor, $x^{A(1)}$. As $S_O^{A(1)} \approx 0$, this variable is omitted.



Source: Prepared by the author.

Furthermore, the disturbance and state estimates obtained from the MHE are shown in Figures 17 and 18, respectively. Again, the visualizations show an overall good performance of the estimator in reconstructing the true values of the disturbance and state variables. We note

Table 6 – MHE: Output, disturbance and state estimation accuracies ($J_{\text{NMSE}}(y, \hat{y})$, $J_{\text{NMSE}}(w, \hat{w})$, and $J_{\text{NMSE}}(x, \hat{x})$, respectively), under the different disturbance regimes.

	Dry Weather			Storm event			Rain event		
	(y, \hat{y})	(w, \hat{w})	(x, \hat{x})	(y, \hat{y})	(w, \hat{w})	(x, \hat{x})	(y, \hat{y})	(w, \hat{w})	(x, \hat{x})
$J_{\text{NMSE}}(\cdot)$	1.15e-05	0.0046	0.0001	4.45e-05	0.0050	0.0006	7.83e-05	0.0049	0.0030

Source: Prepared by the author.

that only the estimation of disturbance variables X_I^{IN} and X_{BH}^{IN} are of poor quality. Interestingly, the estimates for concentrations $X_I^{A(r)}$ ($r = 1, \dots, 5$) are less accurate than the estimates for the remaining state variables. These variables, corresponding to non-reactive matter in the reactors, are decoupled from remaining state variables in the reactors, and the estimator is unable to reconstruct their true value due to the poor performance in reconstructing the influent X_I^{IN} . Moreover, the concentrations $X_I^{A(r)}$ are amongst the variables which are nonzero entries for the eigenvectors for which the associated eigenvalues fails a PBH Observability test (Section 3.1.2).

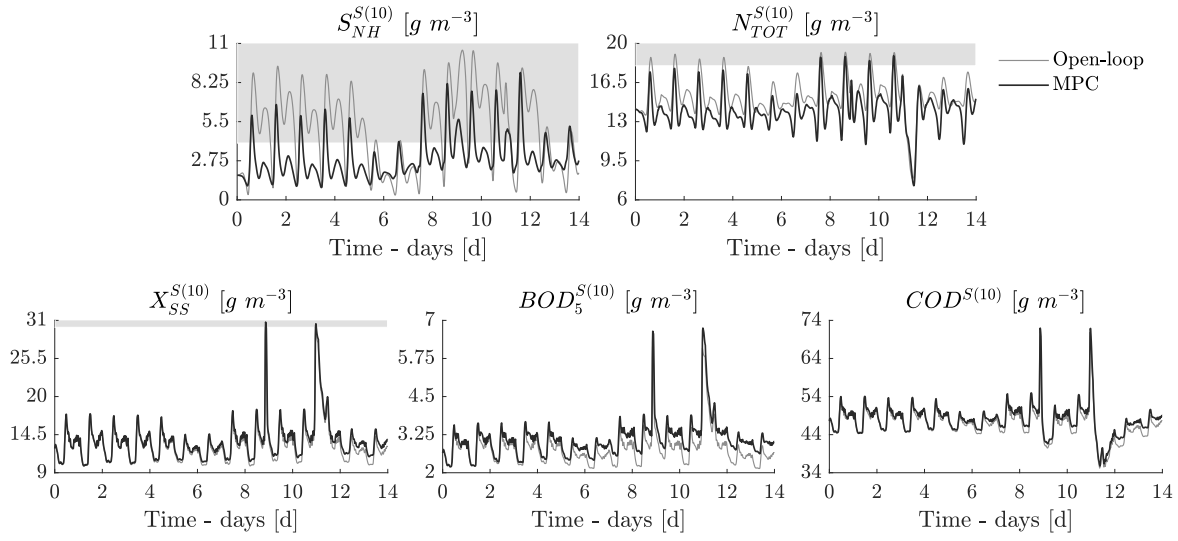
Finally, we summarise the estimation accuracy using the normalized mean square error (NMSE), $J_{\text{NMSE}}(y, \hat{y}) = \frac{1}{T} \sum_{k=0}^T (\|y_k - \hat{y}_k\|^2 / \|y_k\|^2)$, measuring, over the $T = (14/\Delta t_e)$ simulated measurements, the average deviation of the output estimates, \hat{y}_k , against the true outputs, y_k . The metrics $J_{\text{NMSE}}(w, \hat{w})$ and $J_{\text{NMSE}}(x, \hat{x})$ summarise the accuracy of the disturbance and state estimates (\hat{w}_k and \hat{x}_k) against the respective true values (w_k and x_k). The results, in Table 6, reflect a good performance in estimating the 145 state variables and the 14 disturbance variables using only the 15 available measurement variables, for all influent scenarios. The disturbance variables are those estimated with less precision, but still reflecting an overall good performance.

3.2.2 Model predictive control for conventional treatment

In this section, we present the configuration and results for the predictive control for wastewater treatment. For the activated sludge plant in Eq. (4), the linear models ($A^{(k)}, B^{(k)}, G^{(k)}, C^{(k)}$) are obtained from the benchmark's suggested operating point $P_k = (x^{SS}, u^{SS}, \hat{w}_k, y^{SS})$ with disturbance vector $\hat{w}_k = w(\lfloor \frac{k\Delta t_{sp}}{\Delta t_w} \rfloor \Delta t_w)$. This correspond to a zero-offset regulator control with $\Delta t_{sp} = \Delta t_w$, updating the linearised models once influent measurements are available. The discrete-time dynamics $f_{\Delta t}(\cdot | \theta_x)$ in Eq. (34) are evaluated from ($A^{(k)}, B^{(k)}, G^{(k)}, C^{(k)}$) with a sampling period of $\Delta t = (1/12)\text{d}$. The control horizon, Eq. (33), is set to one day, or $N = 12$. We assume weighting matrices $Q = C^{(k)\top} Q_y C^{(k)}$, with $Q_y = \text{diag}[0.01 \dots 0.01 \ 2 \ 30 \ 2 \ 1 \ 10]$, and $R = 10^{-4} I_{Nu}$. For the moment, the influent conditions are assumed to be measured once every $\Delta t_w = (1/2)$ days. Finally, all simulations consider initial state $x(0) = x^{SS}$.

The simulation results are shown in Figure 19 for the stormy influent conditions. The results show improved performance with respect to the open-loop operation (see Figure 15), despite the controller being unable to completely avoid violations of the quality constraints. Specifically,

Figure 19 – Treatment, MPC: Regulation of the effluent-based output variables.



Source: Prepared by the author.

the total number of crossings and time in violation was considerably decreased concerning the effluent nitrogen forms $S_{NH}^{S(10)}$ and $S_{NO}^{S(10)}$. The control also results in the undesirable effect of having two constraint violations for $X_{SS}^{S(10)}$. However, as this variable remains in violation for only 0.4% of the total period, this is not a concerning disadvantage of the controller.

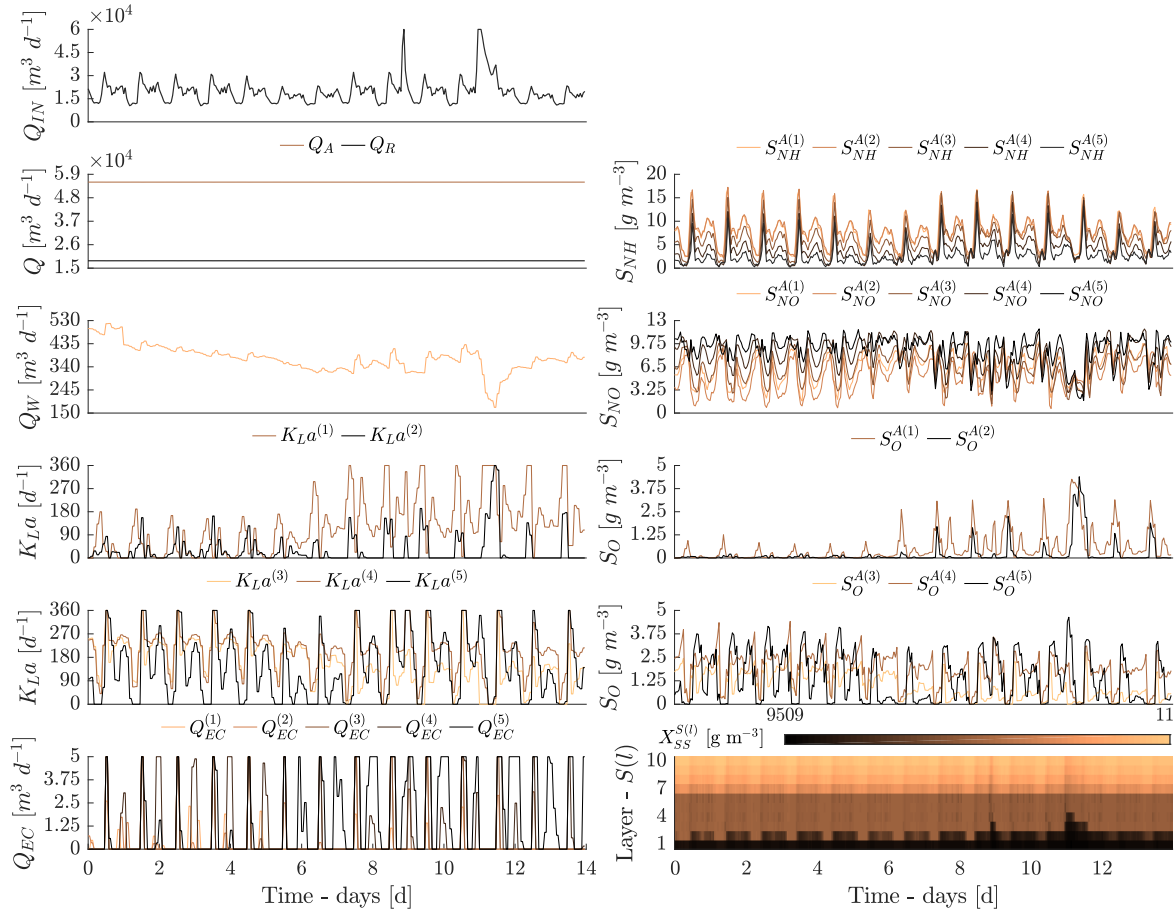
The control actions and a selection of responses are shown in Figure 20. During the first week ($t \in [0, 7]$), the controller mostly manipulates aeration in the last three reactors, $K_{La}^{(1\sim 3)}$, in order to reject the disturbances. Over the second week ($t \in [7, 14]$), more air is insufflated to the anoxic reactors $A(1,2)$, by increasing $K_{La}^{(1,2)}$. Despite dissolved oxygen in the second reactor, $S_O^{A(2)}$, remaining mostly at low levels, this action leads to an increase in oxygen content in the first reactor, $S_O^{A(1)}$. Moreover, the control reacts to the storm event occurring in $t \in [10, 12]$ by decreasing the wastage flow-rate, Q_W . This results in an accumulation of suspended solids in the bottom layer of the settler, $X_{SS}^{S(1)}$, such that more sludge can be provided to the first reactor by external recirculation. This action compensates the sudden decrease in nitrogen concentrations $S_{NO}^{A(r)}$ ($r = 1, \dots, 5$) by favouring the nitrification process in all reactors.

Finally, the overall performance of the treatment control is evaluated in terms of the effluent quality index (EQI, in kg Pollution Units), Figure 21. We compute this metric as a function of time by considering the term inside the integral in Eq. (7),

$$EQI(t) = Q_E(t)(2X_{SS}^{S(10)}(t) + COD^{S(10)}(t) + 2BOD_5^{S(10)}(t) + 30N_{TKN}^{S(10)}(t) + 10S_{NO}^{S(10)}(t)),$$

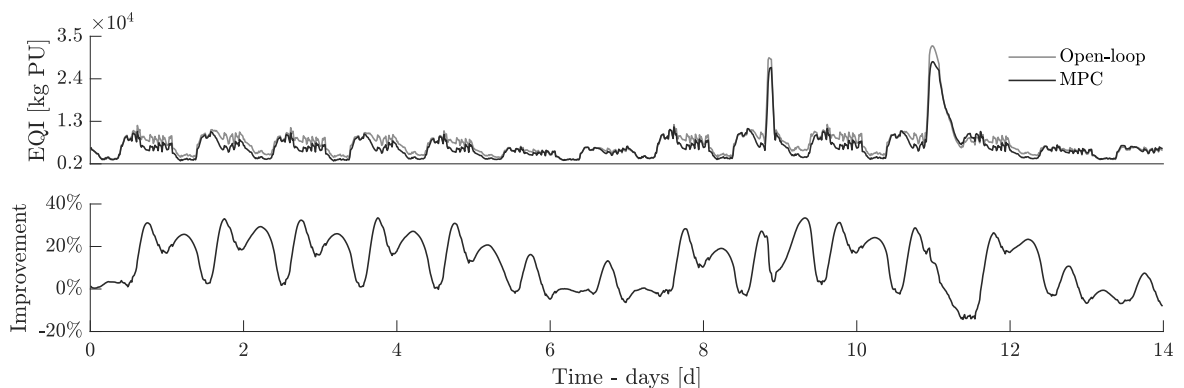
given effluent flow-rate $Q_E = Q_{IN} - Q_W$ and Kjeldahl nitrogen $N_{TKN}^{S(10)} = N_{TOT}^{S(10)} - S_{NO}^{S(10)}$. Moreover, the quality improvement is computed by the ratio $(EQI_{OP} - EQI_{MPC})/EQI_{OP}$, with EQI_{OP} and EQI_{MPC} the effluent quality under the open-loop and MPC operation, respectively. The

Figure 20 – Treatment control, MPC: Influent flow-rate Q_{IN} , flow-rates (Q_A, Q_R, Q_W), oxygen transfer coefficients $K_L a^{(1 \rightsquigarrow 5)}$, and extra carbon flow-rates $Q_{EC}^{(1 \rightsquigarrow 5)}$, left panels, together with nitrogen forms $S_{NH}^{A(1 \rightsquigarrow 5)}$ and $S_{NO}^{A(1 \rightsquigarrow 5)}$, soluble oxygen $S_O^{A(1 \rightsquigarrow 5)}$, and total suspended solids $X_{SS}^{S(1 \rightsquigarrow 10)}$, right panels.



Source: Prepared by the author.

Figure 21 – Treatment, MPC: Effluent quality index (EQI) under open-loop and closed-loop operation.



Source: Prepared by the author.

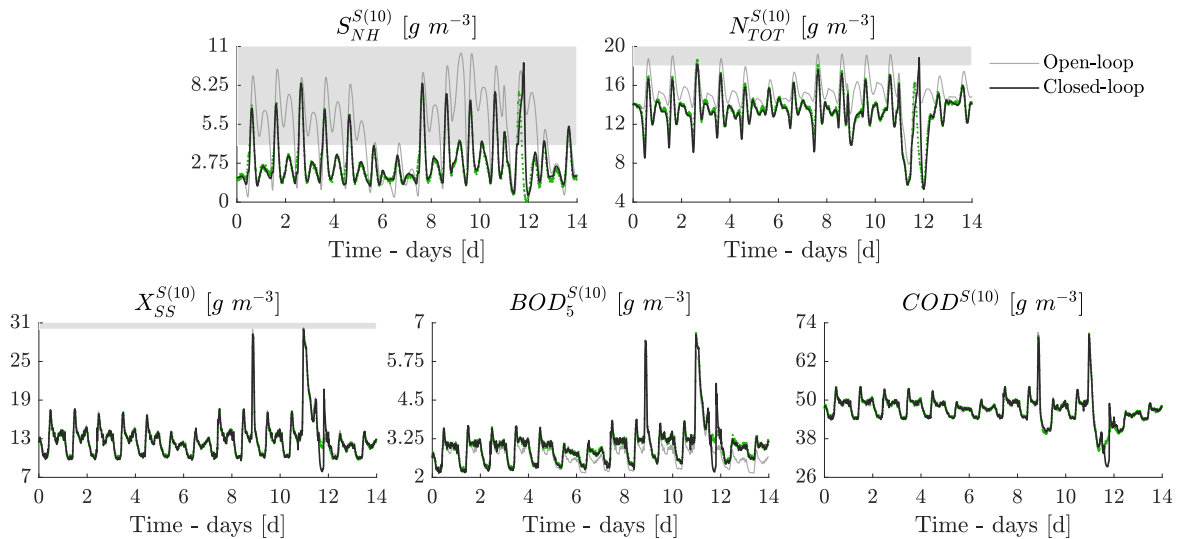
results demonstrate that the predictive controller was able to improve the quality of the water when compared to the open-loop operation. Specifically, the average EQI value decreases from $7233 \text{ kg PU } d^{-1}$, under open-loop operation, to $6355 \text{ kg PU } d^{-1}$, under closed-loop operation.

The results also show an average increase of 11.89% in the treated water quality.

Output model predictive control

We now present the simulation results obtained by the output predictive control of the activated sludge plant, when the process state is not assumed to be known. For the task, we design an output model predictive control based on a moving horizon estimator that estimates the state and disturbance variables under the model predictive control operation (Section 2.4). We consider the same estimator configuration setup from the MHE described in Section 3.2.1.

Figure 22 – Treatment, Output-MPC: Estimation and regulation of the effluent-based output variables.

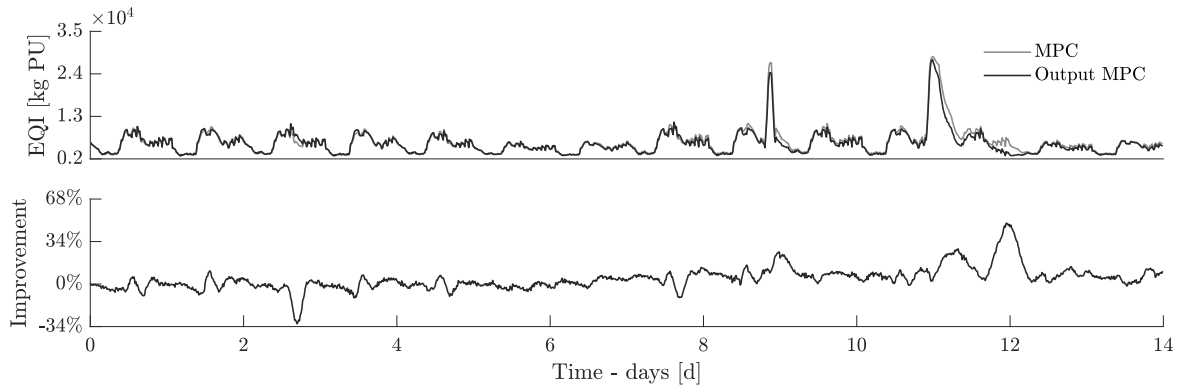


Source: Prepared by the author.

The results are shown in Figure 22 with respect to the usual effluent measurements of interest. As expected, the moving horizon estimator is able to provide accurate estimates for the model predictive controller. In this case, the overall performance of the control shows an improvement over the previous predictive controller. This reflects the advantageous feature of output model predictive controllers of having an estimate of the disturbance-vector available at each control horizon. As the high accuracy of the state estimates makes this setup comparable to assuming knowledge of the states, the estimation of disturbances allows for a better control strategy.

Moreover, we compare the performances of the Output-MPC controller and the MPC controller in terms of the effluent quality index (EQI), Figure 23. The results show a slight improvement over the previous controller, as expected. This increase in effluent quality is more noticeable in the second week period ($t \in [7, 14]$), especially during the storm events. In summary, the average EQI value decreases from 6355 kg PU d^{-1} , under the MPC operation, to 6028.4 kg PU d^{-1} , under the Output-MPC operation, with an average 5.14% increase in the effluent water quality.

Figure 23 – Treatment, Output-MPC: Effluent quality index (EQI) under closed-loop operations.



Source: Prepared by the author.

Summary and results comparison

The control performances are summarised in Table 7 under the different short-term disturbance regimes. The results show an overall improvement in the wastewater treatment performance under closed-loop, for all scenarios. This improvement is reflected in the reduction of EQI and a significant decrease of the percentage time in violation of quality limits, especially for $S_{NH}^{S(10)}$. The output model predictive controllers display the best performance. Specifically, the treated water quality is increased more than 13% under its operation, for all disturbance scenarios.

Table 7 – Results: Control performances in terms of effluent quality index (EQI, $\text{kg PU } d^{-1}$), number of quality limit crossings and percentage of time in violation (#Crossings and %Violation, respectively, for $S_{NH}^{S(10)}$ and $N_{TOT}^{S(10)}$), operation cost index (OCI), and energy costs (PE, AE and CAE).

	Dry weather			Storm event			Rain event		
	OL	MPC	O-MPC	OL	MPC	O-MPC	OL	MPC	O-MPC
EQI	6576.6	5833.8	5625.0	7233.0	6355.0	6028.4	7694.2	6929.9	6582.5
#Crossings (S_{NH})	14	14	17	14	15	17	14	15	22
%Violation (S_{NH})	61	17	15	62	19	18	62	19	26
#Crossings (N_{TOT})	9	5	1	8	4	2	7	3	2
%Violation (N_{TOT})	7	2	0	7	2	1	5	1	1
OCI	3729.6	7958.0	8994.4	3729.6	8154.4	10749.5	3729.6	7844.1	12236.9
PE	388.2	388.2	392.7	388.2	387.6	394.6	388.2	386.8	397.5
AE	3341.4	3622.3	4053.4	3341.4	3695.4	4363.3	3341.4	3673.8	4769.5
CAE	0.0	1315.8	1516.1	0.0	1357.1	1997.2	0.0	1261.1	2356.7

Source: Prepared by the author.

Moreover, we summarise the operational cost index (OCI, Section 1.3.3) associated with the control actions obtained for each controller, over each scenario. The results (also in Table 7) show

that the increase in performance is met with an increase in the energetic cost indices, highlighting the efficacy-efficiency trade-off. Despite the largest costs being associated with aeration energy, the carbon addition energy costs are mainly responsible for the significant increases in OCI. Conversely, the pumping energy costs remain low even in closed-loop conditions.

3.3 Wastewater reuse: set-point tracking

In this section, we present the simulation results obtained by the predictive control of the activated sludge plant when the process is requested to produce reclaimed water according to a specific reference trajectory. We first demonstrate the zero-offset control over a toy reference trajectory, and then we show the results when the plant is requested to produce effluent nitrogen for optimal crop growth. In all cases, we consider first a predictive control in which the process state is assumed to be known, then we consider the output predictive control strategy in which the state is estimated. We present the configuration settings that are common to both controllers, then we discuss the specific parameters and results. The performances are evaluated under constant and dynamic disturbance regimes in terms of tracking accuracy and operational costs.

3.3.1 Case study: toy effluent reference trajectory

In this section, we present the simulation results obtained by the predictive control of the activated sludge plant when the process is requested to produce water of specific quality. We consider a toy reference trajectory for effluent total nitrogen, $N_{TOT}^{S(10)}$, defined by the function

$$\tilde{y}^{SP}(t) = 22\chi_{[0,\Delta t_{sp})} + 18\chi_{[\Delta t_{sp},2\Delta t_{sp})} + 28\chi_{[2\Delta t_{sp},3\Delta t_{sp})} + 20\chi_{[3\Delta t_{sp},4\Delta t_{sp})} + 30\chi_{[4\Delta t_{sp},5\Delta t_{sp})},$$

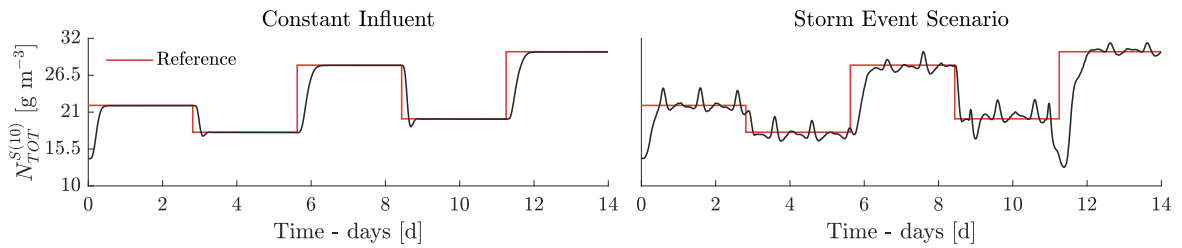
in which $\chi_{[0,\Delta t_{sp})}$ is the indicator function $\chi_{\mathcal{A}}(t) = 1$, if $t \in \mathcal{A}$, and $\chi_{\mathcal{A}}(t) = 0$, if $t \notin \mathcal{A}$.

Model predictive control for set-point tracking

This set-point tracking corresponds to considering $H = [0 \ \dots \ 0 \ 1]$ in Eq. (42). The sampling period of the reference is assumed $\Delta t_{sp} = 2.8$ days. For the activated sludge plant in Eq. (4), the linear models $(A^{(m)}, B^{(m)}, G^{(m)}, C^{(m)})$ around $P_m := (x_m^{SP}, u_m^{SP}, w_m^{SP}, y_m^{SP})$ are computed by solving the optimisation in Eq. (42) once every 2.8 days, when set-points $\tilde{y}_m^{SP} = \tilde{y}^{SP}((m+1)\Delta t_{sp})$ are available. We select weighting matrices $W_y = 10$ and $W_u = 0$. The dynamics $f_{\Delta t}(\cdot | \theta_x)$ in Eq. (34) are evaluated from $(A^{(m)}, B^{(m)}, G^{(m)}, C^{(m)})$ with a sampling period $\Delta t = (1/12)d$. The control horizon, Eq. (28), is set to be 1 day, or $N = 12$. We assume weighting matrices $Q = C^{(m)\top} Q_y C^{(m)}$ and $R = 10^{-4}$, with $Q_y = \text{diag}[0.01 \ \dots \ 0.01 \ 20]$. For the moment, the influent conditions are assumed to be measured once every $\Delta t_w = (1/2)$ days. The initial state is set $x(0) = x^{SS}$, the usual benchmark steady-state. This configuration is common under both dynamic and constant disturbances. For the latter, the influent conditions are set $w(t) = w^{SS}$.

The simulation results are shown in Figure 24 for constant and stormy influent conditions. In both cases, the controller was capable to drive the process towards the desired set-points. Under constant influent conditions, the predictive control perfectly stabilizes the plant around each reference value, with a settling time of 0.75d in the slowest transition. Under dynamic disturbances, the controller keeps the process close to the desired states despite complete disturbance rejection being not achieved. Interestingly, the zero-offset control is able to produce the desired output even when a set-point change occurs during a storm event ($t = 11.2$ d).

Figure 24 – Reuse, MPC: Reference tracking of effluent total nitrogen, $N_{TOT}^{S(10)}$.



Source: Prepared by the author.

The control actions and a selection of responses are shown in Figure 25. The controller serves the required effluent total nitrogen, $N_{TOT}^{S(10)}$, mainly by producing $S_{NO}^{S(10)}$ nitrogen through favouring nitrification in the aerobic section. This is achieved by manipulating $K_L a^{3 \rightsquigarrow 5}$ to increase (or decrease) the oxygen used in the production of $S_{NO}^{A(3 \rightsquigarrow 5)}$ in reactors $A(3,4,5)$. In the settler, the changes in the feed concentration $S_{NO}^{A(5)}$ are reflected in the effluent $S_{NO}^{S(10)}$; and consequently on $N_{TOT}^{S(10)}$. Moreover, we note how $K_L a^{A(1,2)}$ is manipulated in anoxic reactors $A(1,2)$ to increase the available oxygen whenever the production of $S_{NO}^{S(10)}$ is insufficient due to the dynamic disturbances. This effect is especially observed during the last storm event, at $t \in [10, 12]$.

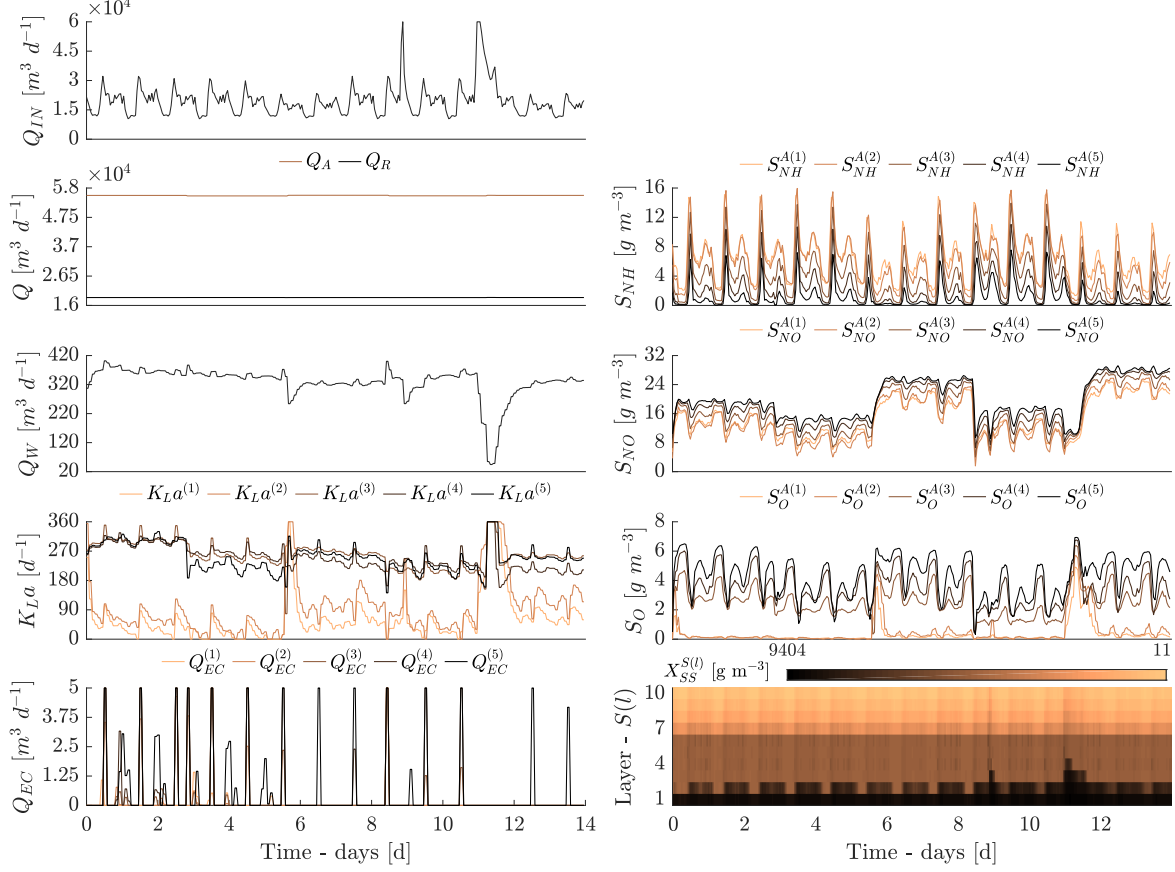
Output model predictive control

We now present the simulation results obtained by the zero-offset output predictive control of the activated sludge plant, when the process state is not assumed to be known. We consider the same estimator configuration setup from the MHE described in Section 3.2.2. Namely, we assume the measurement process with period of $\Delta t_e = (1/96)d = 15\text{min}$ between observations. The estimation horizon, Eq. (54), is set to 3 hours, or $N_e = 12$. The estimator assumes a stochastic representation of the plant, Eq. (45), with process disturbances $w_n \stackrel{i.i.d}{\sim} \mathcal{N}(\bar{w}_n, R_w)$ and measurement noise $v_n \stackrel{i.i.d}{\sim} \mathcal{N}(0, Q_v)$, given covariance matrices

$$R_w = \text{diag}[9 \cdot 10^7 \quad 5 \quad 50 \quad 10^3 \quad 75 \quad 10^3 \quad 10 \quad 2 \quad 9];$$

$$Q_v = \text{diag}[0.001I_5 \quad 0.006I_5 \quad 0.01 \quad 0.009 \quad 0.001 \quad 0.03 \quad 0.01].$$

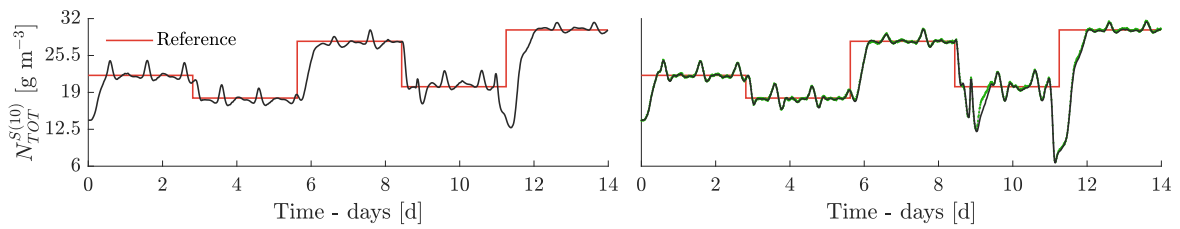
Figure 25 – Reuse, MPC: Influent flow-rate Q_{IN} , flow-rates (Q_A, Q_R, Q_W), oxygen transfer coefficients $K_La^{(1\rightsquigarrow 5)}$, and extra carbon flow-rates $Q_{EC}^{(1\rightsquigarrow 5)}$, left panels, together with nitrogen forms $S_{NH}^{A(1\rightsquigarrow 5)}$ and $S_{NO}^{A(1\rightsquigarrow 5)}$, soluble oxygen $S_O^{S(1\rightsquigarrow 5)}$, and total suspended solids $X_{SS}^{S(1\rightsquigarrow 10)}$, right panels.



Source: Prepared by the author.

We define the initial state uncertainty by assuming $x_{k-N_e+1} \sim \mathcal{N}(\bar{x}_{k-N_e+1}, Q_{x_0})$ with covariance matrix $Q_{x_0} = \text{diag}(0.01x^{SS})^2$, while the mean $\bar{x}_{k-N_e+1} \in \mathbb{R}^{N_x}$ is fixed at the state estimate from the previous iteration, or $\bar{x}_0 = x^{SS}$ for the first estimation horizon. In the Output MPC strategy, each k -th control horizon, Eq. 62, considers initial state, $x_k = \hat{x}_k$, and fixed disturbance $w_n = \hat{w}_k$ ($n = k, \dots, k+N$), with (\hat{x}_k, \hat{w}_k) the estimates from the moving horizon estimation.

The results are shown in Figure 26 with respect to effluent total nitrogen, $N_{TOT}^{S(10)}$, in comparison with the previous MPC result. The moving horizon estimator is able to provide accurate estimates for the model predictive controller, and the controller is able to reach the desired set-points. During most of the simulation, the tracking accuracy of the Output-MPC shows an improvement over the MPC as the effluent nitrogen produced is noticeably closer to the reference. Again, we attribute this to the benefit of having an estimate of the disturbance-vector available at each control horizon. During the storm events within $t \in [8, 12]$, however, the estimator performance deteriorates and the controller reacts poorly to the disturbances.

Figure 26 – Comparison, Output-MPC: Estimation and tracking of effluent total nitrogen, $N_{TOT}^{S(10)}$.

Source: Prepared by the author.

Summary and results comparison

The control performances are summarised in Table 8 under the different short-term disturbance regimes (*dry weather*, *storm event*, and *rain event*). The results show that the tracking accuracy is satisfactory, for all scenarios. Conversely from the results in Chapter 3.2, the Output-MPC strategy has the best overall performance only for the *rain event* scenario, despite having similar performance as the MPC in the remaining cases. Moreover, we summarise the operational cost index (OCI, Section 1.3.3) associated with the control actions obtained for each controller, over each scenario. The results (also in Table 8) show that this reference tracking task has operational costs similar to those obtained for the optimal wastewater treatment control. Again, despite the largest costs being associated with aeration energy, carbon addition energy costs dominate the OCI values. The pumping energy costs are generally low also for this application.

Table 8 – Results: Tracking accuracy in terms of normalised mean squared errors (NMSE), together with operation cost index (OCI) and energy costs (PE, AE and CAE).

	Dry weather		Storm event		Rain event	
	MPC	O-MPC	MPC	O-MPC	MPC	O-MPC
$J_{\text{NMSE}}(\hat{y}, \tilde{y}^{sp})$	0.00885	0.01012	0.01480	0.02356	0.01098	0.01094
OCI	7159.5	10499.7	7290.9	10868.6	7189.5	10539.4
PE	389.0	390.3	388.2	390.8	387.5	390.4
AE	5100.2	5882.6	5208.1	6053.9	5193.7	6430.7
CAE	556.8	1408.9	564.8	1474.6	536.1	1239.4

Source: Prepared by the author.

3.3.2 Case study: supply nitrogen for optimal crop growth

In this section, we present the simulation results obtained by the predictive control of the activated sludge plant when the process is requested to produce nitrogen for optimal crop growth (Section 1.3.3). We illustrate the results with two tuning configurations of the controller, one favouring the manipulation of $\text{NO}_2^- + \text{NO}_3^-$ nitrogen (S_{NO}) and another one favouring $\text{NH}_4^+ + \text{NH}_3$

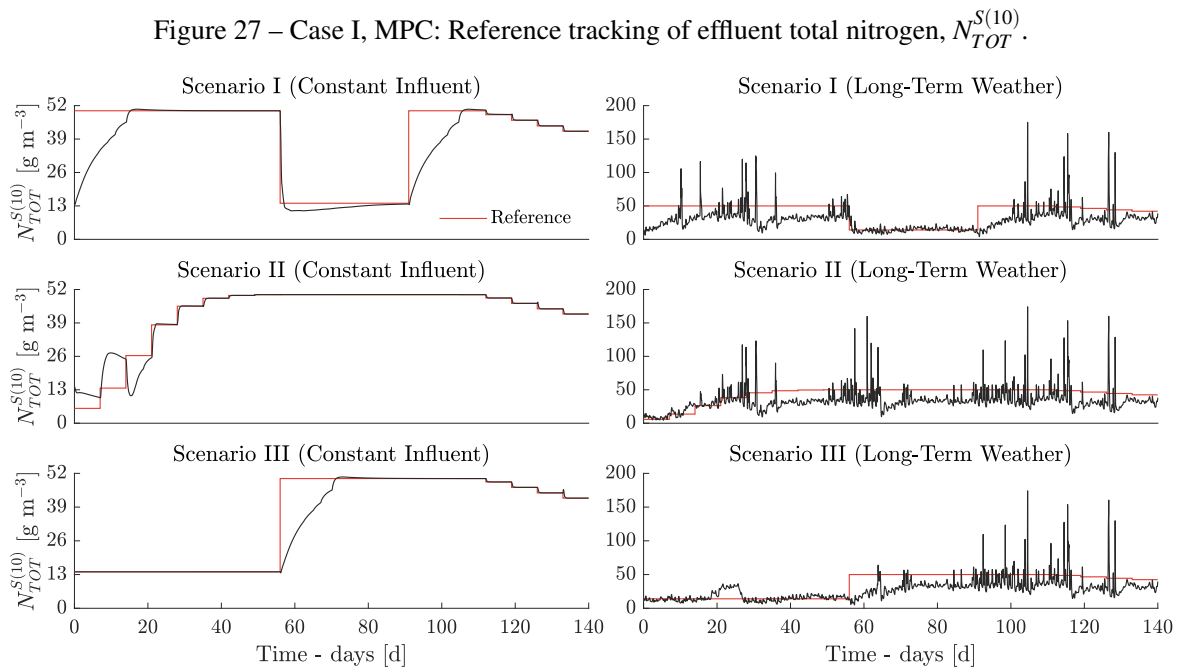
nitrogen (S_{NH}). We present the configuration settings that are common to both controllers, then we discuss the specific parameters and results separately.

Model predictive control for set-point tracking

We consider reference trajectories for effluent total nitrogen, $N_{TOT}^{S(10)}$, the nitrogen concentration of the irrigation water. This corresponds to considering $H = [0 \ \dots \ 1]$ in Eq. (42). The sampling period of the reference is $\Delta t_{sp} = 7d$. For the activated sludge plant in Eq. (4), the linear models $(A^{(m)}, B^{(m)}, G^{(m)}, C^{(m)})$ around $P_m := (x_m^{SP}, u_m^{SP}, w_m^{SP}, y_m^{SP})$ are computed by solving the optimisation in Eq. (42) once a week, when set-points $\tilde{y}_k^{SP} = \tilde{y}^{SP}((m+1)\Delta t_{sp})$ are available. The dynamics $f_{\Delta t}(\cdot | \theta_x)$ in Eq. (34) are evaluated from $(A^{(m)}, B^{(m)}, G^{(m)}, C^{(m)})$ with sampling period $\Delta t = (1/3)d$. The control horizon, Eq. (28), is set to be 7 days, or $N = 21$. We select weighting matrices $Q = C^{(m)T} C^{(m)}$ and $R = \text{diag}[10^{-4} \ 0.01 \ 0.01 \ 10^{-3} I_5 \ 10^4 I_5]$. The influent conditions are assumed to be measured once every $\Delta t_w = 1d$. We treat set-points $\tilde{y}^{SP}(t) = 0$ as corresponding to interrupted irrigation and control the plant for conventional treatment with $\tilde{y}_m^{SP} = Hg(x^{SS})$ whenever $\tilde{y}_m^{SP} = 0$. This setup is common to all cases, under both dynamic and constant influent. For the latter, we choose $w(t) = w^{SS}$. All simulations consider $x(0) = x^{SS}$.

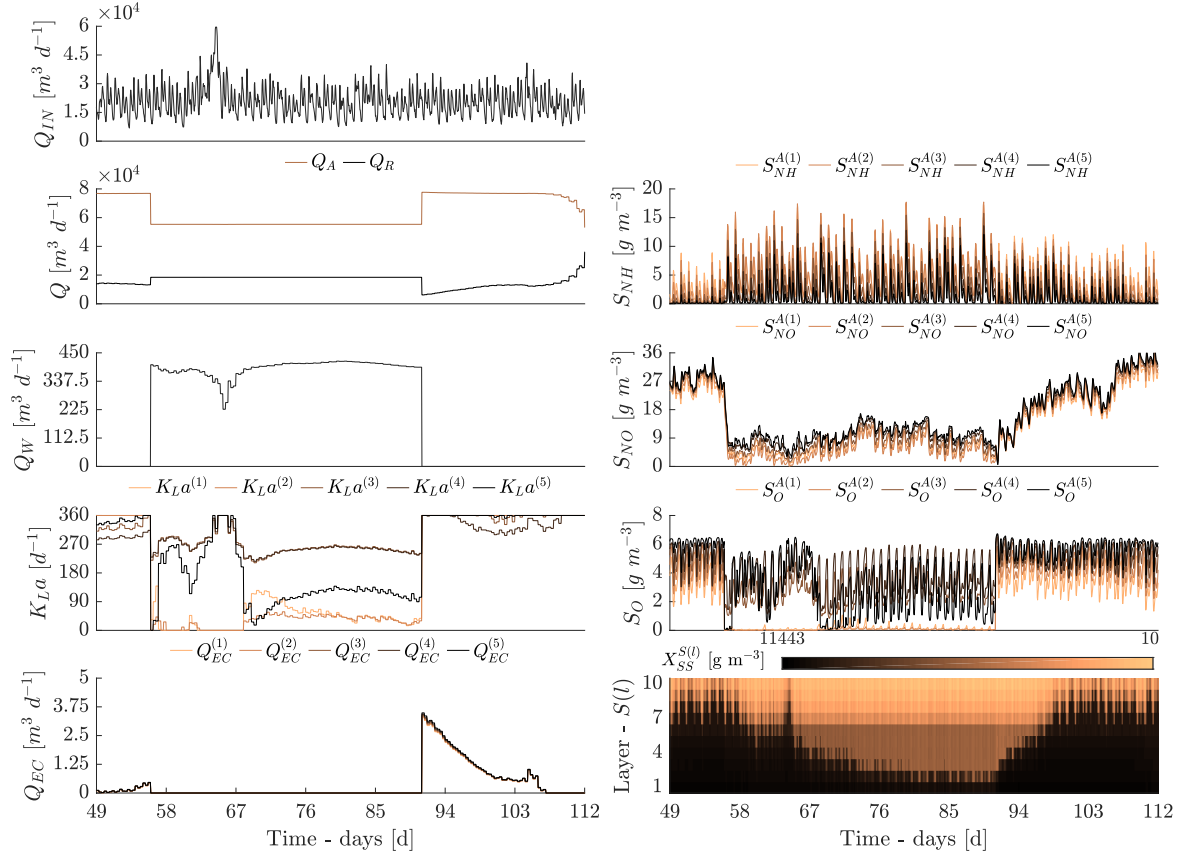
Case I: N_{TOT} control favouring $\text{NO}_2^- + \text{NO}_3^-$ nitrogen

To design a controller that favours the production of $\text{NO}_2^- + \text{NO}_3^-$ nitrogen when asked to track $\tilde{y}^{SP}(t) = N_{TOT}^{SP}(t)$, we set the steady-state optimisation parameters $W_y = 100$ and $W_u = 0$. The results (Figure 27) show that the controller is capable to drive the plant towards the reference values under constant influent conditions. However, performances deteriorate when the plant



Source: Prepared by the author.

Figure 28 – Case I, $t \in [49, 112]$: Influent flow-rate Q_{IN} , flow-rates (Q_A, Q_R, Q_W), oxygen transfer coefficients $K_{La}^{(1\sim 5)}$, and extra carbon flow-rates $Q_{EC}^{(1\sim 5)}$, left panels, together with nitrogen forms $S_{NH}^{A(1\sim 5)}$ and $S_{NO}^{A(1\sim 5)}$, soluble oxygen $S_O^{A(1\sim 5)}$, and total suspended solids $X_{SS}^{S(1\sim 10)}$, right panels.



Source: Prepared by the author.

is subject to dynamic influent conditions, specially when asked to track $y_m^{SP} \geq 40 \text{ g N m}^{-3}$. Specifically, the control is neither able to reject disturbances causing sudden peaks in the effluent concentrations, nor produce enough nitrogen when the influent content is insufficient.

The control actions and a selection of responses are depicted in Figure 28 when the controller serves the set-point changes at $t = \{56, 91\} \text{d}$ in Scenario I: The requested concentration changes are from 50 g N m^{-3} to 14.05 g N m^{-3} and back to 50 g N m^{-3} .

- In the first set-point change ($t = 56 \text{d}$), the controller decreases $N_{TOT}^{S(10)}$ mainly by producing $S_{NO}^{S(10)}$ nitrogen by explicitly acting on the denitrification-nitrification process: This solution is achieved by first reducing aeration in the first reactors $A^{(1,2)}$ through $K_{La}^{(1,2)}$, then, as the concentrations $S_{NO}^{A(1,2)}$ decrease noticeably, these concentrations are increased in the last reactors $A^{(3\sim 5)}$ by increasing aeration, through $K_{La}^{(3\sim 5)}$. As $S_{NO}^{A(5)}$ is the feed concentration to the settler, these changes are reflected at $S_{NO}^{A(1\sim 10)}$; and thus on $N_{TOT}^{S(10)}$. Moreover, wastage flow-rate Q_W is increased to reduce the accumulation of suspended solids $X_{SS}^{S(1\sim 10)}$ throughout the settler layers.

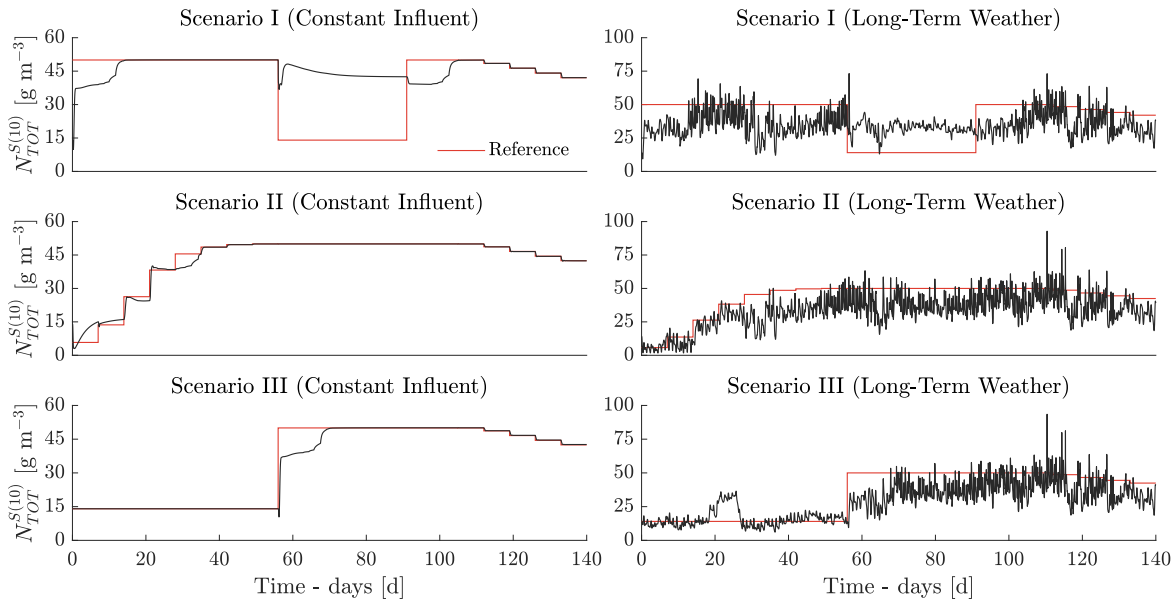
- In the second set-point change ($t = 91$ d), dissolved oxygen is added to all reactors $A^{(1\rightsquigarrow 5)}$ by increasing $K_{La}^{(1\rightsquigarrow 5)}$. As a result, nitrification is implemented throughout the entire process. Again, this effect is reflected at concentrations $S_{NO}^{S(1\rightsquigarrow 10)}$. As oxygen saturates, however, not enough nitrogen can be converted to reach the set-point. The controller thus attempts to complement the effluent total nitrogen using nitrogen entrapped in particulate matter. Wastage flow-rate Q_W is decreased in such way that suspended solids $X_{SS}^{S(1\rightsquigarrow 10)}$ accumulates in all settler layers $S^{(1\rightsquigarrow 10)}$. Thus, $N_{TOT}^{S(10)}$ increases due to nitrogen taken from effluent concentrations of biomass ($X_{BH}^{S(10)}, X_{BA}^{S(10)}$) and organic matter ($X_I^{S(10)}, X_P^{S(10)}$).

Case II: N_{TOT} control favouring $\text{NH}_4^+ + \text{NH}_3$ nitrogen

To favour $\text{NH}_4^+ + \text{NH}_3$ nitrogen when asked to track $\tilde{y}^{SP}(t) = N_{TOT}^{SP}(t)$, we consider a controller that is based on linearisations ($A^{(m)}, B^{(m)}, G^{(m)}, C^{(m)}$) around points $P_m := (x_m^{SP}, u_m^{SP}, w_m^{SP}, y_m^{SP})$ that solve problem Eq. (42) with weighting matrices configured to be $W_y = 100$ and $W_u = 0.01I_{N_u}$.

The results, Fig. 29, show that also this controller can drive the plant towards the set-points when operated against constant influent conditions. More importantly, the overall performance with dynamic influent conditions is improved. However, this control is not able to drive the plant back to the wastewater treatment operation corresponding to set-points $\tilde{y}_m^{SP} = 14.05 \text{ g N m}^{-3}$.

Figure 29 – Case II, MPC: Reference tracking of effluent total nitrogen, $N_{TOT}^{S(10)}$.

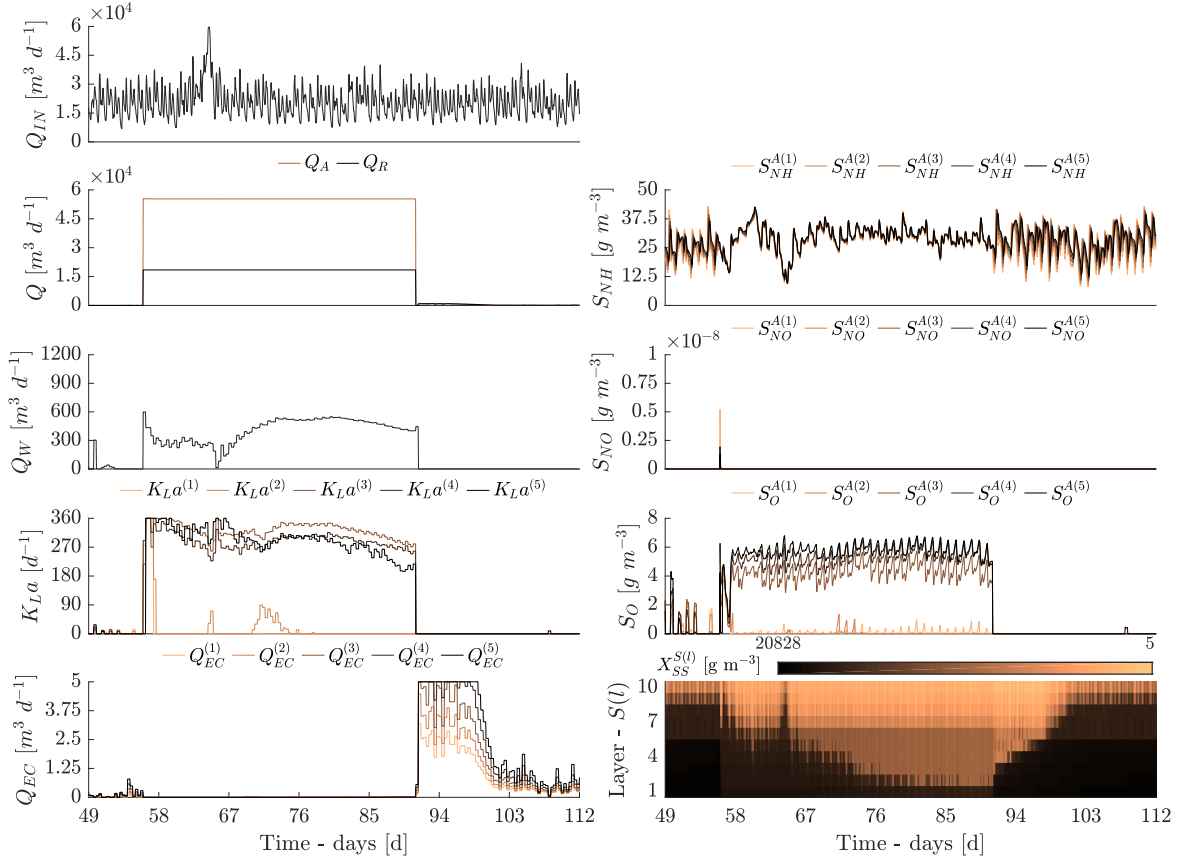


Source: Prepared by the author.

The control actions and a selection of responses are depicted in Figure 30 when the controller serves the set-point changes at $t = \{56, 91\}$ d in Scenario I. The requested concentration changes are from 50 g N m^{-3} to 14.05 g N m^{-3} and back to 50 g N m^{-3} .

- In the first change ($t = 56$ d), the controller attempts to decrease the effluent $N_{TOT}^{S(10)}$ mostly

Figure 30 – Case II, $t \in [49, 112]$: Influent flow-rate Q_{IN} , flow-rates (Q_A, Q_R, Q_W), oxygen transfer coefficients $K_La^{(1\sim 5)}$, and extra carbon flow-rates $Q_{EC}^{(1\sim 5)}$, left panels, together with nitrogen forms $S_{NH}^{A(1\sim 5)}$ and $S_{NO}^{A(1\sim 5)}$, soluble oxygen $S_O^{A(1\sim 5)}$, and total suspended solids $X_{SS}^{S(1\sim 10)}$, right panels.



Source: Prepared by the author.

by converting nitrogen from S_{NH} back to S_{NO} through nitrification: Air is added to all reactors, specially for the conventional aerobic section $A^{(3\sim 5)}$, by directly increasing $K_La^{(1\sim 5)}$. As the concentrations of $S_{NO}^{A(1\sim 5)}$ are virtually reduced to zero during the initial interval, not enough nitrogen can be converted in time to reach the set-point. Moreover, wastage flow-rate, Q_W , is still increased over same interval to reduce the total suspended solids, $X_{SS}^{S(l)}$ ($l = 1, \dots, 10$), accumulated in the settler.

- In the second change ($t = 91d$), the controller attempts to increase the effluent $N_{TOT}^{S(10)}$ by producing $S_{NH}^{S(10)}$ mostly by interrupting the nitrification–denitrification process: The controls are immediately shut down, including recirculation flow-rates. All reactors are set under anoxic conditions by reducing aeration with $K_La^{(r)}$ ($r = 1, \dots, 5$). Thus, influent $NH_4^+ + NH_3$ nitrogen, S_{NH}^I , is not consumed by autotrophic bacteria throughout the reactors, being then emitted in the effluent $S_{NH}^{S(10)}$. As in Case I, the controller complements the remaining $N_{TOT}^{S(10)}$ using nitrogen entrapped in particulate matter whenever influent ammonia is insufficient. Flow-rate Q_W is thus decreased to allow $X_{SS}^{S(l)}$ to accumulate.

This control strategy has one undesirable effect: When recirculation is not applied, chemical concentrations which are absent in the influent wastewater (namely, X_{BA}^{IN} , X_P^{IN} , S_O^{IN} , and S_{NO}^{IN}), are removed from the process through the effluent water. As a consequence, the denitrification-nitrification process can never be re-implemented without “restarting” the plant by explicitly adding $\text{NO}_2^- + \text{NO}_3^-$ nitrogen (S_{NO}) and active autotrophic biomass (X_{BA}) to the reactors. This is due to the fact that the dynamics of both variables are interdependent (see Appendix 4).

Case I and Case II: Comparison

We first discuss the effects of disturbances on the control with respect to Scenario I, Figure 31. We condense the disturbances as influent total nitrogen, N_{TOT}^{IN} , defined as

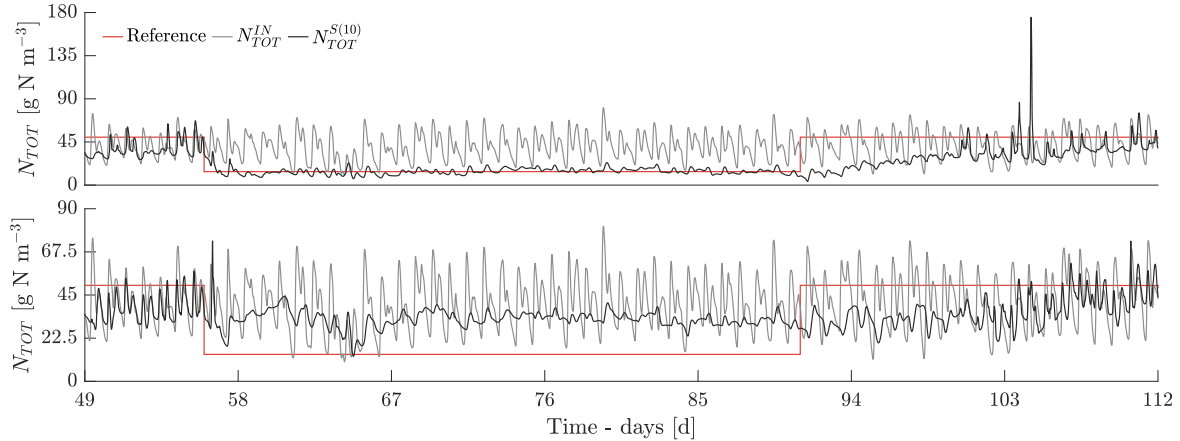
$$N_{TOT}^{IN} = S_{NO}^{IN} + S_{NH}^{IN} + S_{ND}^{IN} + X_{ND}^{IN} + i_{XB}(X_{BH}^{IN} + X_{BA}^{IN}) + i_{XP}(X_P^{IN} + X_I^{IN}).$$

We then summarise these effects in terms of average nitrogen removal efficiency,

$$\eta_{N_{TOT}}(t_0, t_f) = \frac{1}{t_f - t_0} \int_{t_0}^{t_f} \left(1 - \frac{Q_E(t) N_{TOT}^{S(10)}(t)}{Q_{IN}(t) N_{TOT}^{IN}(t)} \right) dt,$$

for a specific time interval $T = t_f - t_0$, with effluent flow-rate $Q_E = Q_{IN} - Q_W$.

Figure 31 – Comparison, $t \in [49, 112]$: Nitrogen removal shown by the difference between influent N_{TOT}^{IN} and effluent N_{TOT}^{IN} total nitrogen for the predictive control in Case I (left) and Case II (right).



Source: Prepared by the author.

- Case I: The average $\eta_{N_{TOT}}(56, 91) = 0.60$ indicates that 60% of influent nitrogen is removed in $t \in [56, 91]$. Conversely, $\eta_{N_{TOT}}(49, 56) = 0.06$ shows that roughly 94% of the influent total nitrogen is still preserved in the effluent during $t \in [49, 56]$. $\eta_{N_{TOT}}(91, 112) = 0.18$ for $t \in [91, 112]$ indicates that 82% of influent total nitrogen is still preserved in the effluent.
- Case II: The average $\eta_{N_{TOT}}(56, 91) = 0.10$ for $t \in [56, 91]$ indicates that only 10% of the in-

fluent nitrogen is removed during this time interval. Conversely, averages $\eta_{N_{TOT}}(49, 56) = 0.04$ for $t \in [49, 56]$ and $\eta_{N_{TOT}}(91, 112) = 0.03$ for $t \in [91, 112]$ indicates respectively that 96% and 97% of influent total nitrogen is still preserved in the effluent during these interval.

We evaluate the controllers overall performance by the usual normalised mean squared error (NMSE) metric (Section 1.3.3). The results (Table 9) show generally good performance for the control simulations under constant influent conditions. We note that Scenario I as an exception, as accuracy lowers during set-point changes in both cases. Moreover, the results show that performance worsens with dynamic disturbances, being Case II controllers generally less affected.

Table 9 – Results: Tracking accuracy, $J_{NMSE}(\tilde{y}, \tilde{y}^{sp})$, with respect to each reference trajectories.

	Case I		Case II	
	$w(t)$ constant	$w(t)$ dynamic	$w(t)$ constant	$w(t)$ dynamic
Scenario I	0.0418	0.1619	1.1360	0.5408
Scenario II	0.0903	0.1806	0.0521	0.1085
Scenario III	0.0147	0.1911	0.0057	0.1469

Source: Prepared by the author.

Finally, we evaluate the overall cost index, (OCI, Section 1.3.3), considering the predictive control operating under dynamic influent conditions. As expected, the results (Table 10) show that a solution favouring nitrogen in the form of S_{NH} costs significantly less than favouring S_{NO} . Despite the pumping costs being generally low in all cases, aeration and carbon addition costs are significantly smaller in Case II.

Table 10 – Results: Energy costs (PE, AE, and CAE) and operational cost indices (OCI, in kWh d⁻¹).

	Case I				Case II			
	PE	AE	CAE	OCI	PE	AE	CAE	OCI
Scenario I	409.3	7858.8	793.2	10647.9	101.2	1459.1	1525.8	6137.7
Scenario II	426.7	8389.5	513.7	10357.4	48.2	535.5	2031.7	6678.7
Scenario III	404.7	7330.7	499.7	9234.5	158.0	1525.2	842.0	4209.1

Source: Prepared by the author.

Output model predictive control

We now present the simulation results obtained by the zero-offset output predictive control of the activated sludge plant, when the process state is not assumed to be known. For the task, we design an output model predictive control based on a moving horizon estimator that estimates the

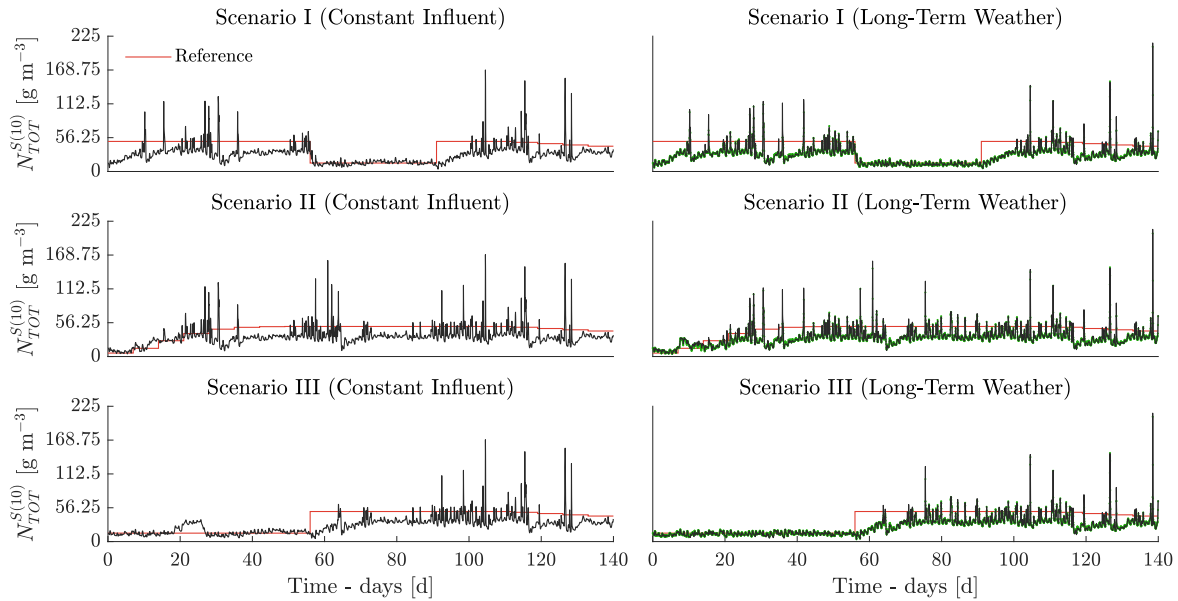
state and disturbance variables under the model predictive control operation (Chapter 2.4). In this case, we assume that the influent flow-rate, Q_{IN} , is known. A measurement process with period of $\Delta t_e = (1/96)d = 15\text{min}$ between observations is considered. The estimation horizon, Eq. (54), is set to 3 hours, or $N_e = 12$. The estimator assumes a stochastic representation of the plant, Eq. (45), with process disturbances $w_n \stackrel{i.i.d}{\sim} \mathcal{N}(\bar{w}_n, R_w)$ and measurement noise $v_n \stackrel{i.i.d}{\sim} \mathcal{N}(0, Q_v)$, given covariance matrices

$$R_w = \text{diag}[0.2 \ 3 \ 0.1 \ 0.5 \ 0.1 \ 0.6 \ 0.075 \ 0.125];$$

$$Q_v = \text{diag}[0.001I_5 \ 0.006I_5 \ 0.01 \ 0.009 \ 0.001 \ 0.03 \ 0.01].$$

We define the initial state uncertainty by assuming $x_{k-N_e+1} \sim \mathcal{N}(\bar{x}_{k-N_e+1}, Q_{x_0})$ with covariance matrix is set $Q_{x_0} = \text{diag}(0.01x^{SS})^2$, while the mean $\bar{x}_{k-N_e} \in \mathbb{R}^{N_x}$ is fixed at the state estimate from the previous iteration, or $\bar{x}_0 = x^{SS}$ for the first estimation horizon. In the Output MPC strategy, each k -th control horizon, Eq. 33, consider initial state, $x_k = \hat{x}_k$, and fixed disturbance $w_n = \hat{w}_k$ ($n = k, \dots, k+N$), with (\hat{x}_k, \hat{w}_k) the estimates from the moving horizon estimation.

Figure 32 – Comparison, Output-MPC: Estimation and tracking of effluent total nitrogen, $N_{TOT}^{S(10)}$.



Source: Prepared by the author.

The results are shown in Figure 32 with respect to effluent total nitrogen, $N_{TOT}^{S(10)}$, in comparison with the previous MPC result. Again, the moving horizon estimator is able to provide accurate estimates and the output predictive controller is also able to partially reach the desired set-points. Moreover, the effluent total nitrogen produced by the Output MPC is seemingly closer to the reference for the time periods in which the MPC controller was unable to produce enough nitrogen. Again, this is due to the availability of disturbance estimates.

The control performances are summarised in Table 11 under the different reference scenarios.

The results show that the output predictive controller has similar tracking accuracy and operational cost index when compared to the predictive controller when the state and disturbances were measured. Specifically, the pumping and aeration energies (PE and AE) are lower for the Output MPC operation, while the carbon addition energy (CAE) are higher for this controller. Again, despite the largest costs being associated with aeration energy, carbon addition energy costs dominate the OCI values. The pumping energy costs are generally low also for this application.

Table 11 – Results: Tracking accuracy in terms of normalised mean squared errors (NMSE), together with operation cost index (OCI) and energy costs (PE, AE and CAE).

	Scenario I		Scenario II		Scenario III	
	MPC	O-MPC	MPC	O-MPC	MPC	O-MPC
$J_{NMSE}(\tilde{y}, \tilde{y}^{sp})$	0.1619	0.1691	0.1806	0.1876	0.1911	0.1241
OCI	10647.9	10936.4	10357.4	10509.8	9234.5	8994.9
PE	409.3	405.2	426.7	424.5	404.7	403.9
AE	7858.8	7338.5	8389.5	7578.7	7330.7	6557.1
CAE	793.2	1064.2	513.7	835.5	499.7	677.9

Source: Prepared by the author.

4 CONCLUSION

This work has presented an analysis of the dynamical properties of activated sludge plants and the simulation results for the predictive control operating these plants for wastewater treatment and water reuse tasks. Regarding the dynamical analysis (Chapter 3.1), the results show that:

- BSM1-like plants are controllable but not observable in the structural sense.
- With respect to the default linearisation, BSM1-plants are stable but uncontrollable and unobservable in the conventional sense. However, a large portion of the state-space is still controllable and observable. Due to stability, the plant is both stabilizable and detectable.
- Controlling and observing BSM1-plants are energy demanding tasks even for minimal realisations of the conventional linearisation suggested by the benchmark.
- The controllability and observability energies are comprised in a small number of state-space directions. Moreover, the efforts required to control or reconstruct the entire state-space is the lowest if we were to observe and actuate directly on organic matter in the reactors.

According to the simulation results for the wastewater treatment control (Chapter 3.2), the predictive controller is able to improve the effluent wastewater quality, mainly by reducing the time in violation of the quality requirements of nitrogen concentrations. However, the closed-loop operation leads to a significantly higher operational cost index. A moving horizon estimation under the open-loop operation of the plant is also discussed. The results show that it is possible to estimate the trajectories of the 145 state and 14 disturbance variables through only 15 noisy measurement variables. Finally, the results also show that the output model predictive control strategy performs better than the strategy of assuming knowledge about the states.

The simulation results in Chapter 3.3 concerns the zero-offset predictive control that operates the plant to produce nitrogen according to specific reference trajectories. The results show that the controller is capable to drive the plant to the desired set-points from the piecewise linear toy reference trajectory of Section 3.3.1, under both constant and dynamic influent conditions. Regarding the control task of supplying nitrogen for optimal crop growth (3.3.2), the results show that, also for this difficult reference, the zero-offset controller is able to drive the plant to the desired set-points when influent conditions are constant. However, performance deteriorates when the plant is subject to dynamic influent conditions, as the controller is not capable to perfectly reject disturbances in general. Moreover, the experiments show that two distinct control strategies exist according to two tuning configurations of the controller:

- When the steady-inputs used for linearisations are let free, the resulting control strategy favours the manipulation of $\text{NO}_2^- + \text{NO}_3^-$ nitrogen. Control actions are applied in order to favour the nitrification process within the reactors, and also to allow accumulation of suspended solids in the settler to supplement the effluent nitrogen using organic matter.

- When the steady-inputs used for linearisations are minimized, the resulting control strategy favours the manipulation of $\text{NH}_4^+ + \text{NH}_3$ nitrogen. Control actions are shut down in order to allow the influent ammonia to be emitted in the effluent, and also to allow accumulation of suspended solids in the settler to supplement the effluent nitrogen using organic matter. The results also show that this strategy has the undesirable effect of removing all nitrates and autotrophic bacteria from the process, such that the controller is unable to return to conventional wastewater treatment operation.

REFERENCES

- AIT MOUHEB, N.; BOURRIÉ, G.; THAYER, B. B.; BENYAHIA, B.; CHERKI, B.; CONDOM, N.; DECLERCQ, R.; HÉLAN, M.; KHALIFA, R.; MOLLE, B.; PATUREAU, D.; RENAULT, P.; ROMAGNY, B.; SINFORT, C.; STEYER, J. P.; SARI, T.; WERY, N.; HARMAND, J. The reuse of reclaimed water for irrigation around the Mediterranean Rim: a step towards a more virtuous cycle? **Regional Environmental Change**, v. 18, n. 3, p. 693–705, 2018. DOI: 10.1007/s10113-018-1292-z.
- ALEX, J.; TSCHEPETZKI, R.; JUMAR, U. Predictive control of nitrogen removal in WWTP using parsimonious models. In: PROCEEDINGS of the Fifteenth IFAC World Congress on Automatic Control. Barcelona, Spain, 2002. p. 1458–1458. DOI: 10.3182/20020721-6-ES-1901.01460.
- ÅMAND, L.; OLSSON, G.; CARLSSON, B. Aeration control - A review. **Water Science & Technology**, v. 67, n. 1, p. 2374–2398, 2013. DOI: 10.2166/wst.2013.139.
- ARNOLD, E.; DIETZE, S. Nonlinear Moving Horizon State Estimation of an Activated Sludge Model. **IFAC Proceedings Volumes**, v. 34, n. 8, p. 545–550, 2001. 9th IFAC Symposium on Large Scale Systems: Theory and Applications 2001, Bucharest, Romania, 18-20 July 2001. DOI: 10.1016/S1474-6670(17)40871-8.
- BENNER, P.; LI, J.-R.; PENZL, T. Numerical solution of large-scale Lyapunov equations, Riccati equations, and linear-quadratic optimal control problems. **Numerical Linear Algebra with Applications**, v. 15, n. 9, p. 755–777, 2008. DOI: 10.1002/nla.622.
- BETTS, J. T. **Practical methods for optimal control and estimation using nonlinear programming**. SIAM, 2010. (Advances in Design and Control). ISBN 978-0-89871-688-7.
- BISHOP, C. M. **Pattern recognition and machine learning**. Springer, 2006. ISBN 978-0-387-31073-2.
- BONNANS, F. J.; GIORGI, D.; GRELARD, V.; HEYMANN, B.; MAINDRAULT, S.; MARTINON, P.; TISSOT, O.; LIU, J. **Bocop – A collection of examples**. 2017. Available from: <<http://www.bocop.org>>.
- BORRELLI, F.; BEMPORAD, A.; MORARI, M. **Predictive Control for Linear and Hybrid Systems**. Cambridge University Press, 2017. ISBN 978-1-13-906175-9.
- BOYD, S. P.; VANDENBERGHE, L. **Convex optimization**. Cambridge University Press, 2004. ISBN 978-0-52-183378-3.
- BUSCH, J.; ELIXMANN, D.; KÜHL, P.; GERKENS, C.; SCHLÖDER, J. P.; BOCK, H. G.; MARQUARDT, W. State estimation for large-scale wastewater treatment plants. **Water Research**, v. 47, n. 13, p. 4774–4787, 2013. DOI: 10.1016/j.watres.2013.04.007.

CALLIER, F. M.; DESOER, C. A. **Linear System Theory**. Springer Science & Business Media, 1991. (Springer Texts in Electrical Engineering). ISBN 978-1-4612-0957-7.

CHEN, C.-T. **Linear System Theory and Design**. 3. ed.: Oxford University Press, 1998. (The Oxford Series in Electrical and Computer Engineering). ISBN 978-0-19-511777-6.

CORMEN, T. H.; LEISERSON, C. E.; RIVEST, R. L.; STEIN, C. **Introduction to Algorithms**. 3. ed.: MIT Press, 2009. ISBN 978-0-26-253305-8.

CORRIOU, J.-P.; PONS, M.-N. Model predictive control of wastewater treatment plants: Application to the BSM1 benchmark. In: BARBOSA-POVOA, A.; MATOS, H. (Eds.). **European Symposium on Computer-Aided Process Engineering-14, Thirty-seventh European Symposium of the Working Party on Computer-Aided Process Engineering**. Elsevier, 2004. v. 18. (Computer Aided Chemical Engineering). p. 625–630. DOI: 10.1016/S1570-7946(04)80170-6.

EKMAN, M. Bilinear black-box identification and MPC of the activated sludge process. **Journal of Process Control**, v. 18, n. 7–8, p. 643–653, 2008. DOI: 10.1016/j.jprocont.2007.12.006.

FALCONE, P.; BORRELLI, F.; ASGARI, J.; TSENG, H. E.; HROVAT, D. Predictive Active Steering Control for Autonomous Vehicle Systems. **IEEE Transactions on Control Systems Technology**, v. 15, n. 3, p. 566–580, 2007. DOI: 10.1109/TCST.2007.894653.

FORBES, M. G.; PATWARDHAN, R. S.; HAMADAH, H.; GOPALUNI, R. B. Model Predictive Control in Industry: Challenges and Opportunities. **IFAC-PapersOnLine**, v. 48, n. 8, p. 531–538, 2015. 9th IFAC Symposium on Advanced Control of Chemical Processes ADCHEM 2015. DOI: 10.1016/j.ifacol.2015.09.022.

FRANCISCO, M.; SKOGESTAD, S.; VEGA, P. Model predictive control for the self-optimized operation in wastewater treatment plants: Analysis of dynamic issues. **Computers & Chemical Engineering**, v. 82, p. 259–272, 2015. DOI: 10.1016/j.compchemeng.2015.07.003.

GERNAEY, K.; JEPSSON, U.; VANROLLEGHEM, P.; COPP, J. **Benchmarking of Control Strategies for Wastewater Treatment Plants**. IWA Publishing, 2014. (Scientific and Technical Report Series No. 23). DOI: 978-1-84-339146-3.

GRADY JR, C. L.; DAIGGER, G. T.; LOVE, N. G.; FILIPE, C. D. **Biological wastewater treatment**. 3. ed.: CRC press, 2011. DOI: 978-0-84-939679-3.

GRIEWANK, A.; TOINT, P. L. Partitioned variable metric updates for large structured optimization problems. **Numerische Mathematik**, v. 39, n. 1, p. 119–137, 1982. DOI: 10.1007/BF01399316.

GROS, S.; ZANON, M.; QUIRYNEN, R.; BEMPORAD, A.; DIEHL, M. From linear to nonlinear MPC: bridging the gap via the real-time iteration. **International Journal of Control**, v. 93, n. 1, p. 62–80, 2020. DOI: 10.1080/00207179.2016.1222553.

HALL, P. On Representatives of Subsets. **Journal of the London Mathematical Society**, s1-10, n. 1, p. 26–30, 1935. DOI: 10.1112/jlms/s1-10.37.26.

HAN, H.-G.; QIAN, H.-H.; QIAO, J.-F. Nonlinear multiobjective model-predictive control scheme for wastewater treatment process. **Journal of Process Control**, v. 24, n. 3, p. 47–59, 2014. DOI: 10.1016/j.jprocont.2013.12.010.

HAUTUS, M. L. J. Stabilization, controllability and observability of linear autonomous systems. **Indagationes Mathematicae (Proceedings)**, v. 73, p. 448–455, 1970. DOI: 10.1016/S1385-7258(70)80049-X.

HENZE, M.; GUJER, W.; MINO, T.; LOOSDRECHT, M. C. M. van. **Activated Sludge Models ASM1, ASM2, ASM2d and ASM3**. IWA Publishing, 2000. (Scientific and Technical Report Series No. 9).

HOLENDA, B.; DOKOMOSA, E.; RÈDEY, Á.; FAZAKAS, J. Dissolved oxygen control of the activated sludge wastewater treatment process using model predictive control. **Computers & Chemical Engineering**, v. 33, n. 6, p. 1270–1278, 2008. DOI: 10.1016/j.compchemeng.2007.06.008.

KALMAN, R. E. Mathematical Description of Linear Dynamical Systems. **Journal of the Society for Industrial and Applied Mathematics Series A Control**, v. 1, n. 2, p. 152–192, 1963. DOI: 10.1137/0301010.

KALMAN, R. On the general theory of control systems. In: 1ST INTERNATIONAL IFAC CONGRESS ON AUTOMATIC AND REMOTE CONTROL, 1., Moscow, USSR. **IFAC Proceedings Volumes**. 1960. v. 1, p. 491–502. DOI: 10.1016/S1474-6670(17)70094-8.

KEVICZKY, T.; BALAS, G. J. Software-Enabled Receding Horizon Control for Autonomous Unmanned Aerial Vehicle Guidance. **Journal of Guidance, Control, and Dynamics**, v. 29, n. 3, p. 680–694, 2006. DOI: 10.2514/1.15562.

KIRK, D. E. **Optimal control theory: an introduction**. Courier Corporation, 2004. ISBN 978-0-48-643484-1.

LIN, C.-T. Structural controllability. **IEEE Transactions on Automatic Control**, v. 19, n. 3, p. 201–208, 1974. DOI: 10.1109/TAC.1974.1100557.

LIU, Y.-Y.; SLOTINE, J.-J.; BARABÁSI, A.-L. Controllability of complex networks. **Nature**, v. 473, n. 7346, p. 167–173, 2011. DOI: 10.1038/nature10011.

LIU, Y.-Y.; SLOTINE, J.-J.; BARABÁSI, A.-L. Observability of complex systems. **Proceedings of the National Academy of Sciences**, National Academy of Sciences, v. 110, n. 7, p. 2460–2465, 2013. DOI: 10.1073/pnas.1215508110.

MAYBECK, P. S. **Stochastic models, estimation, and control**. Academic Press, 1979. v. 1. ISBN 978-0-12-411042-7.

MAYNE, D.; RAWLINGS, J.; RAO, C.; SCOKAERT, P. Constrained model predictive control: Stability and optimality. **Automatica**, v. 36, n. 6, p. 789–814, 2000. DOI: 10.1016/S0005-1098(99)00214-9.

MOLINER-HEREDIA, R.; PENARROCHA-ALOS, I.; SANCHIS-LLOPIS, R. Economic model predictive control of wastewater treatment plants based on BSM1 using linear prediction models. In: IEEE 15th International Conference on Control and Automation (ICCA). 2019. p. 73–78. DOI: 10.1109/ICCA.2019.8899974.

MÜLLER, P. C.; WEBER, H. I. Analysis and Optimization of Certain Qualities of Controllability and Observability for Linear Dynamical Systems. **Automatica**, USA, v. 8, n. 3, p. 237–246, 1972. DOI: 10.1016/0005-1098(72)90044-1.

NETO, O. B. L.; HADDON, A.; AICHOUCHE, F.; HARMAND, J.; MULAS, M.; CORONA, F. Predictive control of activated sludge plants to supply nitrogen for optimal crop growth. In: 11TH IFAC SYMPOSIUM ON ADVANCED CONTROL OF CHEMICAL PROCESSES. **Proceedings of the 11th IFAC Symposium on Advanced Control of Chemical Processes**. IFAC, 2021. (to appear).

NETO, O. B. L.; MULAS, M.; CORONA, F. On the controllability of activated sludge plants. In: 2020 EUROPEAN CONTROL CONFERENCE (ECC). **Proceedings of the 2020 European Control Conference**. IEEE, 2020. p. 581–586. DOI: 10.23919/ECC51009.2020.9143863.

NETO, O. B. L.; MULAS, M.; CORONA, F. On the observability of activated sludge plants. **IFAC-PapersOnLine**, v. 53, n. 2, p. 16802–16807, 2020. 21th IFAC World Congress. DOI: 10.1016/j.ifacol.2020.12.1151.

OLSSON, G.; ANDREWS, J. The dissolved oxygen profile - a valuable tool for control of the activated sludge process. **Water Research**, v. 12, n. 11, p. 985–1004, 1978. DOI: 10.1016/0043-1354(78)90082-9.

OLSSON, G.; CARLSSON, B.; COMAS, J.; COPP, J.; GERNAEY, K.; INGILDSEN, P.; JEPPSSON, U.; KIM, C.; RIEGER, L.; RODRÌGUEZ-RODA, I.; STEYER, J.; TAKÁCS, I.; VANROLLEGHEM, P.; VARGAS, A.; YUAN, Z.; ÅMAND, L. Instrumentation, control and automation in wastewater - from London 1973 to Narbonne 2013. **Water Science & Technology**, v. 69, n. 7, p. 1372–1385, 2014. DOI: 10.2166/wst.2014.057.

OLSSON, G.; NIELSEN, M.; YUAN, Z.; LYNGGAARD-JENSEN, A.; STEYER, J. **Instrumentation, Control and Automation in Wastewater Systems**. IWA Publishing, London, 2005. ISBN 978-1-90-022283-9.

OLSSON, G.; EKLUND, K.; DAHLQVIST, K.; ULMGREN, L. **Control Problems in Wastewater Treatment Plants**. Department of Automatic Control, Lund Institute of Technology (LTH), 1973. (Research Reports TFRT-3064). ISBN 0346-5500.

OSTACE, G.; CRISTEA, V.; AGACHI, P. Cost reduction of the wastewater treatment plant operation by MPC based on modified ASM1 with two-step nitrification/denitrification model. **Computers & Chemical Engineering**, v. 35, n. 11, p. 2469–2479, 2011. DOI: 10.1016/j.compchemeng.2011.03.031.

PASQUALETTI, F.; ZAMPIERI, S.; BULLO, F. Controllability Metrics, Limitations and Algorithms for Complex Networks. **IEEE Transactions on Control of Network Systems**, v. 1, n. 1, p. 40–52, 2014. DOI: 10.1109/TCNS.2014.2310254.

PELAK, N.; REVELLI, R.; PORPORATO, A. A dynamical systems framework for crop models: Toward optimal fertilization and irrigation strategies under climatic variability. **Ecological Modelling**, v. 365, p. 80–92, 2017. ISSN 0304-3800. DOI: 10.1016/j.ecolmodel.2017.10.003.

RAO, C. V.; RAWLINGS, J. B.; MAYNE, D. Q. Constrained state estimation for nonlinear discrete-time systems: stability and moving horizon approximations. **IEEE Transactions on Automatic Control**, v. 48, n. 2, p. 246–258, 2003. DOI: 10.1109/TAC.2002.808470.

RAWLINGS, J. B.; BAKSHI, B. R. Particle filtering and moving horizon estimation. **Computers & Chemical Engineering**, v. 30, n. 10, p. 1529–1541, 2006. DOI: 10.1016/j.compchemeng.2006.05.031.

RAWLINGS, J. B.; MAYNE, D. Q.; DIEHL, M. M. **Model Predictive Control: Theory, Computation and Design**. 2. ed.: Nob Hill Publishing, LLC., 2020. ISBN 978-0-9759377-5-4.

REINSCHKE, K. J. **Multivariable Control: a Graph-theoretic Approach**. Springer, 1988. ISBN 978-3-540-18899-5.

RICART, S.; RICO, A. M. Assessing technical and social driving factors of water reuse in agriculture: A review on risks, regulation and the yuck factor. **Agricultural Water Management**, v. 217, p. 426–439, 2019. ISSN 0378-3774. DOI: 10.1016/j.agwat.2019.03.017.

ROSEN, C.; LARSSON, M.; JEPSSON, U.; YUAN, Z. A Framework for extreme-event control in wastewater treatment. **Water Science & Technology**, v. 45, n. 4–5, p. 299–308, 2002. DOI: 10.2166/wst.2002.0610.

SHEN, W.; CHEN, X.; CORRIOU, J. Application of model predictive control to the BSM1 benchmark of wastewater treatment process. **Computers & Chemical Engineering**, v. 22, n. 12, p. 2849–2856, 2008. DOI: 10.1016/j.compchemeng.2008.01.009.

SOTOMAYOR, O.; GARCIA, C. Model-based predictive control of a pre-denitrification plant: linear state-space model approach. In: PROCEEDINGS of the Fifteenth IFAC World Congress on Automatic Control. Barcelona, Spain, 2002. p. 1462–1462. DOI: 10.3182/20020721-6-ES-1901.01464.

STARE, A.; VREČKO, D.; HVALA, N.; STRMČNIK, S. Comparison of control strategies for nitrogen removal in an activated sludge process in terms of operating costs: A simulation study. **Water Research**, v. 41, n. 9, p. 2004–2014, 2007. DOI: 10.1016/j.watres.2007.01.029.

SUMMERS, T. H.; CORTESI, F. L.; LYGEROS, J. On Submodularity and Controllability in Complex Dynamical Networks. **IEEE Transactions on Control of Network Systems**, v. 3, n. 1, p. 91–101, 2016. DOI: 10.1109/TCNS.2015.2453711.

TAKÁCS, I.; PATRY, G.; NOLASCO, D. A dynamic model of the clarification-thickening process. **Water Research**, v. 25, n. 10, p. 1263–1271, 1991. DOI: 10.1016/0043-1354(91)90066-Y.

THWAITES, B. J.; SHORT, M. D.; STUETZ, R. M.; REEVE, P. J.; ALVAREZ GAITAN, J.-P.; DINESH, N.; VAN DEN AKKER, B. Comparing the performance of aerobic granular sludge versus conventional activated sludge for microbial log removal and effluent quality: Implications for water reuse. **Water Research**, v. 145, p. 442–452, 2018. ISSN 0043-1354. DOI: 10.1016/j.watres.2018.08.038.

VAN DOOREN, P. The generalized eigenstructure problem in linear system theory. **IEEE Transactions on Automatic Control**, v. 26, n. 1, p. 111–129, 1981. DOI: 10.1109/TAC.1981.1102559.

YIN, X.; DECARDI-NELSON, B.; LIU, J. Subsystem decomposition and distributed moving horizon estimation of wastewater treatment plants. **Chemical Engineering Research and Design**, v. 134, p. 405–419, 2018. DOI: 10.1016/j.cherd.2018.04.032.

YIN, X.; LIU, J. State estimation of wastewater treatment plants based on model approximation. **Computers & Chemical Engineering**, v. 111, p. 79–91, 2018. DOI: 10.1016/j.compchemeng.2018.01.003.

YIN, X.; LIU, J. Subsystem decomposition of process networks for simultaneous distributed state estimation and control. **AIChE Journal**, v. 65, n. 3, p. 904–914, 2019. DOI: 10.1002/aic.16426.

ZENG, J.; LIU, J. Economic Model Predictive Control of Wastewater Treatment Processes. **Industrial & Engineering Chemistry Research**, v. 54, n. 21, p. 5710–5721, 2015. DOI: 10.1021/ie504995n.

ZENG, J.; LIU, J.; ZOU, T.; YUAN, D. Distributed Extended Kalman Filtering for Wastewater Treatment Processes. **Industrial & Engineering Chemistry Research**, v. 55, n. 28, p. 7720–7729, 2016. DOI: 10.1021/acs.iecr.6b00529.

ZHANG, A.; LIU, J. Economic MPC of Wastewater Treatment Plants Based on Model Reduction. **Processes**, v. 7, p. 682, 2019. DOI: 10.3390/pr7100682.

ZHAO, C.; WANG, W.-X.; LIU, Y.-Y.; SLOTINE, J.-J. Intrinsic dynamics induce global symmetry in network controllability. **Scientific Reports**, v. 5, n. 8422, 2015. DOI: 10.1038/srep08422.

Appendix A – Model equations and parameters

In this appendix, the state-space model equations, alongside model parameters and complementary information, are provided for the systems discussed in this work. The explicit state equations of the Benchmark Simulation Model No. 1 are presented, then the default model parameters and steady-state operating point are given. Finally, the description of the crop growth model used to generate optimal nitrogen trajectories is discussed, together with the optimal control problem from which these trajectories are computed.

Benchmark Model No. 1 (BSM1)

We start by describing the dynamics of concentrations within each r -th reactor, represented by the set of state variables $x^{A(r)}$ given in Section 1.3.1. For any component $Z^{A(r)} \in x^{A(r)}$,

$$\dot{Z}^{A(r)} = \begin{cases} \frac{Q^{(r)}}{V^{A(r)}} [Z^{A(r-1)} - Z^{A(r)}] - \frac{Q_{EC}^{(r)}}{V^{A(r)}} Z^{A(r)} + R_{Z^{A(r)}} & (r = 2, \dots, 5) \\ \frac{1}{V^{A(1)}} [Q_{IN} Z^{A(IN)} + Q_A Z^{A(5)} + Q_R Z^{S(1)}] - \frac{Q^{(1)} + Q_{EC}^{(1)}}{V^{A(1)}} Z^{A(1)} + R_{Z^{A(1)}} & (r = 1) \end{cases}, \quad (66)$$

where $Q^{(r)} = (Q_{IN} + Q_A + Q_R + \sum_{j=1}^{r-1} Q_{EC}^{(j)})$, for all $r = 1, \dots, 5$, and $R_{Z^{A(r)}}$ is the contribution from process reactions associated to component $Z^{A(r)}$, as presented in Henze et al. (2000). Whenever $Z^{A(r)} = S_O^{A(r)}$ we add the term $K_{La}^{(r)} [S_O^{sat} - S_O^{A(r)}]$ for both cases in (66). When $Z^{A(r)} = S_S^{A(r)}$ we add $(Q_{EC}^{(r)}/V^{A(r)}) S_S^{EC}$, for both cases in (66).

Specifically, the dynamics the concentrations in reactors $r = 2, \dots, 5$ are given as

$$\dot{S}_I^{A(r)} = \frac{Q^{(r)}}{V^{A(r)}} [S_I^{A(r-1)} - S_I^{A(r)}] - \frac{Q_{EC}^{(r)}}{V^{A(r)}} S_I^{A(r)} \quad (67)$$

$$\begin{aligned} \dot{S}_S^{A(r)} = & \frac{Q^{(r)}}{V^{A(r)}} [S_S^{A(r-1)} - S_S^{A(r)}] + \frac{Q_{EC}^{(r)}}{V^{A(r)}} [S_S^{EC} - S_S^{A(r)}] \\ & - \frac{\mu_H}{Y_H} \frac{S_S^{A(r)}}{K_S + S_S^{A(r)}} \left[\frac{S_O^{A(r)}}{K_{OH} + S_O^{A(r)}} + \eta_g \frac{K_{OH}}{K_{OH} + S_O^{A(r)}} \frac{S_{NO}^{A(r)}}{K_{NO} + S_{NO}^{A(r)}} \right] X_{BH}^{A(r)} \\ & + k_h \frac{X_S^{A(r)}}{K_X X_{BH}^{A(r)} + X_S^{A(r)}} \left[\frac{S_O^{A(r)}}{K_{OH} + S_O^{A(r)}} + \eta_h \frac{K_{OH}}{K_{OH} + S_O^{A(r)}} \frac{S_{NO}^{A(r)}}{K_{NO} + S_{NO}^{A(r)}} \right] X_{BH}^{A(r)} \end{aligned} \quad (68)$$

$$\dot{X}_I^{A(r)} = \frac{Q^{(r)}}{V^{A(r)}} [X_I^{A(r-1)} - X_I^{A(r)}] - \frac{Q_{EC}^{(r)}}{V^{A(r)}} X_I^{A(r)} \quad (69)$$

$$\begin{aligned} \dot{X}_S^{A(r)} = & \frac{Q^{(r)}}{V^{A(r)}} [X_S^{A(r-1)} - X_S^{A(r)}] - \frac{Q_{EC}^{(r)}}{V^{A(r)}} X_S^{A(r)} \\ & - k_h \frac{X_S^{A(r)}}{K_X X_{BH}^{A(r)} + X_S^{A(r)}} \left[\frac{S_O^{A(r)}}{K_{OH} + S_O^{A(r)}} + \eta_h \frac{K_{OH}}{K_{OH} + S_O^{A(r)}} \frac{S_{NO}^{A(r)}}{K_{NO} + S_{NO}^{A(r)}} \right] X_{BH}^{A(r)} \\ & + [1 - f_p] b_H X_{BH}^{A(r)} + [1 - f_p] b_A X_{BA}^{A(r)} \end{aligned} \quad (70)$$

$$\dot{X}_{BH}^{A(r)} = \frac{Q^{(r)}}{VA^{(r)}} \left[X_{BH}^{A(r-1)} - X_{BH}^{A(r)} \right] - \frac{Q_{EC}^{(r)}}{VA^{(r)}} X_{BH}^{A(r)} \quad (71)$$

$$+ \mu_H \frac{S_S^{A(r)}}{K_S + S_S^{A(r)}} \left[\frac{S_O^{A(r)}}{K_{OH} + S_O^{A(r)}} + \eta_g \frac{K_{OH}}{K_{OH} + S_O^{A(r)}} \frac{S_{NO}^{A(r)}}{K_{NO} + S_{NO}^{A(r)}} \right] X_{BH}^{A(r)} - b_H X_{BH}^{A(r)}$$

$$\dot{X}_{BA}^{A(r)} = \frac{Q^{(r)}}{VA^{(r)}} \left[X_{BA}^{A(r-1)} - X_{BA}^{A(r)} \right] - \frac{Q_{EC}^{(r)}}{VA^{(r)}} X_{BA}^{A(r)} + \mu_A \frac{S_{NH}^{A(r)}}{K_{NH} + S_{NH}^{A(r)}} \frac{S_O^{A(r)}}{K_{OA} + S_O^{A(r)}} X_{BA}^{A(r)} - b_A X_{BA}^{A(r)} \quad (72)$$

$$\dot{X}_P^{A(r)} = \frac{Q^{(r)}}{VA^{(r)}} \left[X_P^{A(r-1)} - X_P^{A(r)} \right] - \frac{Q_{EC}^{(r)}}{VA^{(r)}} X_P^{A(r)} + f_P \left[b_H X_{BH}^{A(r)} + b_A X_{BA}^{A(r)} \right] \quad (73)$$

$$\dot{S}_O^{A(r)} = \frac{Q^{(r)}}{VA^{(r)}} \left[S_O^{A(r-1)} - S_O^{A(r)} \right] - \frac{Q_{EC}^{(r)}}{VA^{(r)}} S_O^{A(r)} + K_{Ld}^{(r)} \left[S_O^{sat} - S_O^{A(r)} \right] \quad (74)$$

$$- \frac{1 - Y_H}{Y_H} \mu_H \frac{S_S^{A(r)}}{K_S + S_S^{A(r)}} \frac{S_O^{A(r)}}{K_{OH} + S_O^{A(r)}} X_{BH}^{A(r)} - \frac{4.57 - Y_A}{Y_A} \mu_A \frac{S_{NH}^{A(r)}}{K_{NH} + S_{NH}^{A(r)}} \frac{S_O^{A(r)}}{K_{OA} + S_O^{A(r)}} X_{BA}^{A(r)}$$

$$\dot{S}_{NO}^{A(r)} = \frac{Q^{(r)}}{VA^{(r)}} \left[S_{NO}^{A(r-1)} - S_{NO}^{A(r)} \right] - \frac{Q_{EC}^{(r)}}{VA^{(r)}} S_{NO}^{A(r)} \quad (75)$$

$$- \frac{1 - Y_H}{2.86 Y_H} \mu_H \frac{S_S^{A(r)}}{K_S + S_S^{A(r)}} \frac{K_{OH}}{K_{OH} + S_O^{A(r)}} \frac{S_{NO}^{A(r)}}{K_{NO} + S_{NO}^{A(r)}} \eta_g X_{BH}^{A(r)} + \frac{\mu_A}{Y_A} \frac{S_{NH}^{A(r)}}{K_{NH} + S_{NH}^{A(r)}} \frac{S_O}{K_{OA} + S_O^{A(r)}} X_{BA}^{A(r)}$$

$$\dot{S}_{NH}^{A(r)} = \frac{Q^{(r)}}{VA^{(r)}} \left[S_{NH}^{A(r-1)} - S_{NH}^{A(r)} \right] - \frac{Q_{EC}^{(r)}}{VA^{(r)}} S_{NH}^{A(r)} \quad (76)$$

$$- \mu_H \frac{S_S}{K_S + S_S^{A(r)}} \left[\frac{S_O^{A(r)}}{K_{OH} + S_O^{A(r)}} + \eta_g \frac{K_{OH}}{K_{OH} + S_O^{A(r)}} \frac{S_{NO}^{A(r)}}{K_{NO} + S_{NO}^{A(r)}} \right] i_{XB} X_{BH}^{A(r)}$$

$$- \mu_A \left(i_{XB} + \frac{1}{Y_A} \right) \frac{S_{NH}^{A(r)}}{K_{NH} + S_{NH}^{A(r)}} \frac{S_O^{A(r)}}{K_{OA} + S_O^{A(r)}} X_{BA}^{A(r)} + k_a S_{ND}^{A(r)} X_{BH}^{A(r)}$$

$$\dot{S}_{ND}^{A(r)} = \frac{Q^{(r)}}{VA^{(r)}} \left[S_{ND}^{A(r-1)} - S_{ND}^{A(r)} \right] - \frac{Q_{EC}^{(r)}}{VA^{(r)}} S_{ND}^{A(r)} \quad (77)$$

$$- k_a S_{ND}^{A(r)} X_{BH}^{A(r)} + k_h \frac{X_{ND}^{A(r)} X_{BH}^{A(r)}}{K_X X_{BH}^{A(r)} + X_S^{A(r)}} \left[\frac{S_O^{A(r)}}{K_{OH} + S_O^{A(r)}} + \eta_h \frac{K_{OH}}{K_{OH} + S_O^{A(r)}} \frac{S_{NO}^{A(r)}}{K_{NO} + S_{NO}^{A(r)}} \right]$$

$$\dot{X}_{ND}^{A(r)} = \frac{Q^{(r)}}{VA^{(r)}} \left[X_{ND}^{A(r-1)} - X_{ND}^{A(r)} \right] - \frac{Q_{EC}^{(r)}}{VA^{(r)}} X_{ND}^{A(r)} \quad (78)$$

$$- k_h \frac{X_{ND}^{A(r)}}{K_X X_{BH}^{A(r)} + X_S^{A(r)}} \left[\frac{S_O^{A(r)}}{K_{OH} + S_O^{A(r)}} + \eta_h \frac{K_{OH}}{K_{OH} + S_O^{A(r)}} \frac{S_{NO}^{A(r)}}{K_{NO} + S_{NO}^{A(r)}} \right] X_{BH}^{A(r)}$$

$$+ b_H \left(i_{XB} - f_{PiXP} \right) X_{BH}^{A(r)} + b_A \left(i_{XB} - f_{PiXP} \right) X_{BA}^{A(r)}$$

$$\begin{aligned}
\dot{S}_{ALK}^{A(r)} &= \frac{Q^{(r)}}{VA^{(r)}} \left[S_{ALK}^{A(r-1)} - S_{ALK}^{A(r)} \right] - \frac{Q_{EC}^{(r)}}{VA^{(r)}} S_{ALK}^{A(r)} \\
&- \frac{i_{XB}}{14} \mu_H \frac{S_S^{A(r)}}{K_S + S_S^{A(r)}} \frac{S_O^{A(r)}}{K_{OH} + S_O^{A(r)}} X_{BH}^{A(r)} + \frac{1}{14} k_a S_{ND}^{A(r)} X_{BH}^{A(r)} \\
&+ \left(\frac{1 - Y_H}{14 \times 2.86 Y_H} - \frac{i_{XB}}{14} \right) \mu_H \frac{S_S^{A(r)}}{K_S + S_S^{A(r)}} \frac{K_{OH}}{K_{OH} + S_O^{A(r)}} \frac{S_{NO}^{A(r)}}{K_{NO} + S_{NO}^{A(r)}} \eta_g X_{BH}^{A(r)} \\
&- \left(\frac{i_{XB}}{14} + \frac{1}{7 Y_A} \right) \mu_A \frac{S_{NH}^{A(r)}}{K_{NH} + S_{NH}^{A(r)}} \frac{S_O^{A(r)}}{K_{OA} + S_O^{A(r)}} X_{BA}^{A(r)}.
\end{aligned} \tag{79}$$

The dynamics for suspended solids in each l -th settler's layer, $X_{SS}^{S(l)}$, are described by

$$\dot{X}_{SS}^{S(l)} = \begin{cases} \frac{Q_e}{VS^{(l)}} \left[X_{SS}^{S(l-1)} - X_{SS}^{S(l)} \right] - \frac{1}{h^{S(l)}} J_{cla} \left(X_{SS}^{S(l)}, X_{SS}^{S(l-1)} \right) & (l = 10) \\ \frac{Q_e}{VS^{(l)}} \left[X_{SS}^{S(l-1)} - X_{SS}^{S(l)} \right] + \frac{1}{h^{S(l)}} \left[J_{cla} \left(X_{SS}^{S(l+1)}, X_{SS}^{S(l)} \right) - J_{cla} \left(X_{SS}^{S(l)}, X_{SS}^{S(l-1)} \right) \right] & (l = 7, \dots, 9) \\ \frac{Q_f}{VS^{(l)}} \left[X_f - X_{SS}^{S(l)} \right] + \frac{1}{h^{S(l)}} \left[J_{cla} \left(X_{SS}^{S(l+1)}, X_{SS}^{S(l)} \right) - J_{st} \left(X_{SS}^{S(l)}, X_{SS}^{S(l-1)} \right) \right] & (l = 6) \\ \frac{Q_u}{VS^{(l)}} \left[X_{SS}^{S(l+1)} - X_{SS}^{S(l)} \right] + \frac{1}{h^{S(l)}} \left[J_{st} \left(X_{SS}^{S(l+1)}, X_{SS}^{S(l)} \right) - J_{st} \left(X_{SS}^{S(l)}, X_{SS}^{S(l-1)} \right) \right] & (l = 2, \dots, 5) \\ \frac{Q_u}{VS^{(l)}} \left[X_{SS}^{S(l+1)} - X_{SS}^{S(l)} \right] + \frac{1}{h^{S(l)}} J_{st} \left(X_{SS}^{S(l+1)}, X_{SS}^{S(l)} \right) & (l = 1) \end{cases}$$

Moreover, the time evolution of any soluble matter $S_{(\cdot)}^{S(l)}$ within each l -th layer is

$$\dot{S}_{(\cdot)}^{S(l)} = \begin{cases} \frac{Q_e}{VS^{(l)}} \left[S_{(\cdot)}^{S(l-1)} - S_{(\cdot)}^{S(l)} \right] & (l = 7, \dots, 10); \\ \frac{Q_f}{VS^{(l)}} \left[S_{(\cdot)}^{A(5)} - S_{(\cdot)}^{S(l)} \right] & (l = 6); \\ \frac{Q_u}{VS^{(l)}} \left[S_{(\cdot)}^{S(l+1)} - S_{(\cdot)}^{S(l)} \right] & (l = 1, \dots, 5), \end{cases} \tag{80}$$

with $X_f = 0.75 \left(X_I^{A(5)} + X_S^{A(5)} + X_{BH}^{A(5)} + X_{BA}^{A(5)} + X_P^{A(5)} \right)$, $Q_f = (Q_{IN} + Q_R)$, $Q_u = (Q_R + Q_W)$, and $Q_e = (Q_{IN} - Q_W)$. The downward and upward flux of solids are respectively given by

$$J_{st} \left(X_{SS}^{S(l)}, X_{SS}^{S(l-1)} \right) = \min \left[v_s \left(X_{SS}^{S(l-1)} \right) X_{SS}^{S(l-1)}, v_s \left(X_{SS}^{S(l)} \right) X_{SS}^{S(l)} \right]; \tag{81}$$

$$J_{cla} \left(X_{SS}^{S(l)}, X_{SS}^{S(l-1)} \right) = \begin{cases} \min \left[v_s \left(X_{SS}^{S(l-1)} \right) X_{SS}^{S(l-1)}, v_s \left(X_{SS}^{S(l)} \right) X_{SS}^{S(l)} \right] & \text{if } X_{SS}^{S(l-1)} > X_f; \\ v_s \left(X_{SS}^{S(l)} \right) X_{SS}^{S(l)} & \text{otherwise,} \end{cases} \tag{82}$$

in which

$$v_s \left(X_{SS}^{S(l)} \right) = \max \left\{ 0, \min \left[v_0^{max}, v_0 \left(e^{-r_h \left(X_{SS}^{S(l)} - f_{ns} X_f \right)} - e^{-r_p \left(X_{SS}^{S(l)} - f_{ns} X_f \right)} \right) \right] \right\}. \tag{83}$$

To compute Jacobian linearisations, the vector-valued functions $f(\cdot)$ and $g(\cdot)$ must be differentiable. Due to the discontinuous functions in the model of the settler, this is not true for the formulation above. A smooth approximation of the original model was obtained by replacing the many terms corresponding to minimum and maximum functions between two terms with a log-sum-exp or softmax function, whereas an hyperbolic tangent function was used for approximating conditional statements. Specifically, we rewrite the condition for the downward flux of solids, $J_{cla}(\cdot)$ from Eq. (82), as

$$J_{cla}(\cdot) = \varphi(X_{SS}^{S(l-1)}) \min \left[v_s(X_{SS}^{S(l-1)})X_{SS}^{S(l-1)}, v_s(X_{SS}^{S(l)})X_{SS}^{S(l)} \right] + [1 - \varphi(X_{SS}^{S(l-1)})] v_s(X_{SS}^{S(l)})X_{SS}^{S(l)}$$

with $\varphi(X_{SS}^{S(l-1)}) = 1$ when $X_{SS}^{S(l-1)} - X_t > 0$ and $\varphi(X_{SS}^{S(l-1)}) = 0$ otherwise. We approximate the step function $\varphi(X_{SS}^{S(l-1)})$ with an hyperbolic tangent function

$$\varphi(X_{SS}^{S(l-1)}) \approx 0.5 + 0.5 \tanh \left(50(X_{SS}^{S(l-1)} - X_t) \right).$$

The differential equations depend on the set of stoichiometric, kinetic and general parameters described at Table 12. Finally, the conventional operation of the plant corresponding to the steady-state point $SS := (x^{SS}, u^{SS}, w^{SS}, y^{SS})$ is presented at Table 13.

The control variables of this process are constrained by operational limits. Specifically, the recirculation flow-rates are constrained as $Q_A \leq 5Q_{IN}^{SS} = 92230 \text{ m}^3 \text{ d}^{-1}$ and $Q_R \leq 3Q_{IN}^{SS} = 36892 \text{ m}^3 \text{ d}^{-1}$, and the wastage flow-rate is limited by $Q_W \leq 0.1Q_{IN}^{SS} = 1844.6 \text{ m}^3 \text{ d}^{-1}$. Moreover, the oxygen transfer coefficient and external carbon flow-rate are constrained by $K_L a^{(r)} \leq 360 \text{ d}^{-1}$ and $Q_{EC}^{(r)} \leq 5 \text{ m}^3 \text{ d}^{-1}$, respectively, in all reactors ($r = 1, \dots, 5$).

Table 12 – Benchmark Model No. 1: Model constant parameters.

	Stoichiometric parameter	Value	Units
Y_A	Autotrophic yield	0.24	$\text{g } X_{BA} \text{ COD formed} \cdot (\text{g N oxidised})^{-1}$
Y_H	Heterotrophic yield	0.67	$\text{g } X_{BH} \text{ COD formed} \cdot (\text{g COD utilised})^{-1}$
f_P	Fraction of biomass to particulate products	0.08	$\text{g } X_P \text{ COD formed} \cdot (\text{g } X_{BH} \text{ decayed})^{-1}$
i_{XB}	Fraction nitrogen in biomass	0.08	g N (g COD)^{-1} in biomass
i_{XP}	Fraction nitrogen in particulate products	0.06	g N (g COD)^{-1} in X_P
	Kinetic parameter	Value	Units
μ_H	Maximum heterotrophic growth rate	4.00	d^{-1}
K_S	Half-saturation (heterotrophic growth)	10.0	g COD m^{-3}
K_{OH}	Half-saturation (heterotrophic oxygen)	0.20	$\text{g O}_2 \text{ m}^{-3}$
K_{NO}	Half-saturation (nitrate)	0.50	$\text{g NO}_3\text{-N m}^{-3}$
b_H	Heterotrophic decay rate	0.30	d^{-1}
v_g	Anoxic growth rate correction factor	0.80	dimensionless
v_h	Anoxic hydrolysis rate correction factor	0.80	dimensionless
k_h	Maximum specific hydrolysis rate	3.00	$\text{g } X_S (\text{g } X_{BH} \text{ COD d})^{-1}$
K_X	Half-saturation (hydrolysis)	0.10	$\text{g } X_S (\text{g } X_{BH} \text{ COD})^{-1}$
μ_A	Maximum autotrophic growth rate	0.50	d^{-1}
K_{NH}	Half-saturation (autotrophic growth)	1.00	$\text{g NH}_4\text{-N m}^{-3}$
b_A	Autotrophic decay rate	0.05	d^{-1}
K_{OA}	Half-saturation (autotrophic oxygen)	0.40	$\text{g O}_2 \text{ m}^{-3}$
k_a	Ammonification rate	0.05	$\text{m}^3 (\text{g COD d})^{-1}$
	Secondary settler parameter	Value	Units
v_0^{max}	Maximum settling velocity	250.0	m d^{-1}
v_0	Maximum Vesilind settling velocity	474.0	m d^{-1}
r_h	Hindered zone settling parameter	0.000576	$\text{m}^3 (\text{g SS})^{-1}$
r_p	Flocculant zone settling parameter	0.00286	$\text{m}^3 (\text{g SS})^{-1}$
f_{ns}	Non-settleable fraction	0.00228	dimensionless
	General parameter	Value	Units
$V^{A(1\sim 2)}$	Reactor volume (anoxic section)	1000	m^3
$V^{A(3\sim 5)}$	Reactor volume (aerobic section)	1333	m^3
$V^{S(l)}$	Settler layer volume	600	m^3
$h^{S(l)}$	Settler layer height	0.4	m
S_S^{EC}	External carbon source concentration	$4 \cdot 10^5$	g COD m^{-3}
S_O^{sat}	Oxygen saturation concentration	8.0	$\text{g O}_2 \text{ m}^{-3}$
X_t	Settling threshold concentration	3000	g m^{-3}

Source: Prepared by the author.

Table 13 – Benchmark Model No. 1: Steady-state point $SS := (x^{SS}, u^{SS}, w^{SS}, y^{SS})$.

	Influent		Reactor					Units
	IN	A(1)	A(2)	A(3)	A(4)	A(5)		
S_I	30	30	30	30	30	30	g COD m ⁻³	
S_S	69.5	2.81	1.46	1.15	0.995	0.889	g COD m ⁻³	
X_I	51.2	1149	1149	1149	1149	1149	g COD m ⁻³	
X_S	202.32	82.1	76.4	64.9	55.7	49.3	g COD m ⁻³	
X_{BH}	28.17	2552	2553	2557	2559	2559	g COD m ⁻³	
X_{BA}	0	148	148	149	150	150	g COD m ⁻³	
X_P	0	449	450	450	451	452	g COD m ⁻³	
S_O	0	0.0043	6.31E-5	1.72	2.43	0.491	g O ₂ m ⁻³	
S_{NO}	0	5.37	3.66	6.54	9.30	10.4	g N m ⁻³	
S_{NH}	31.56	7.92	8.34	5.55	2.97	1.73	g N m ⁻³	
S_{ND}	6.95	1.22	0.882	0.829	0.767	0.688	g N m ⁻³	
X_{ND}	10.59	5.28	5.03	4.39	3.88	3.53	g N m ⁻³	
S_{ALK}	7	4.93	5.08	4.67	4.29	4.13	mol HCO ₃ ⁻ m ⁻³	

	Settler Layer										Units
	S(1)	S(2)	S(3)	S(4)	S(5)	S(6)	S(7)	S(8)	S(9)	S(10)	
X_{SS}	6394	356.07	356.07	356.07	356.07	356.07	68.98	29.54	18.11	12.5	g COD m ⁻³
S_I	30	30	30	30	30	30	30	30	30	30	g COD m ⁻³
S_S	0.89	0.89	0.89	0.89	0.89	0.89	0.89	0.89	0.89	0.89	g COD m ⁻³
S_O	0.49	0.49	0.49	0.49	0.49	0.49	0.49	0.49	0.49	0.49	g O ₂ m ⁻³
S_{NO}	10.42	10.42	10.42	10.42	10.42	10.42	10.42	10.42	10.42	10.42	g N m ⁻³
S_{NH}	1.73	1.73	1.73	1.73	1.73	1.73	1.73	1.73	1.73	1.73	g N m ⁻³
S_{ND}	0.69	0.69	0.69	0.69	0.69	0.69	0.69	0.69	0.69	0.69	g N m ⁻³
S_{ALK}	4.13	4.13	4.13	4.13	4.13	4.13	4.13	4.13	4.13	4.13	mol HCO ₃ ⁻ m ⁻³

	Input	Units
Q_{IN}	18846	m ³ d ⁻¹
Q_A	55338	m ³ d ⁻¹
Q_R	18446	m ³ d ⁻¹
Q_W	385	m ³
$K_L a^{(1)}$	0	d ⁻¹
$K_L a^{(2)}$	0	d ⁻¹
$K_L a^{(3)}$	240	d ⁻¹
$K_L a^{(4)}$	240	d ⁻¹
$K_L a^{(5)}$	84	d ⁻¹
$Q_{EC}^{(1)}$	0	m ³ d ⁻¹
$Q_{EC}^{(2)}$	0	m ³ d ⁻¹
$Q_{EC}^{(3)}$	0	m ³ d ⁻¹
$Q_{EC}^{(4)}$	0	m ³ d ⁻¹
$Q_{EC}^{(5)}$	0	m ³ d ⁻¹

Source: Prepared by the author.

Agricultural Crop System

We consider the model of a crop grown in monoculture that is irrigated continuously with treated wastewater over the course of a growing season on a uniform area of land at field-scale. As a first approach, we assume the idealized model of (PELAK et al., 2017) describing a simplified crop development process focused on the water and nitrogen dynamics of the crop and soil.

From a system perspective, the crop dynamics are described using its canopy cover (C) and plant biomass per unit area (B). The soil dynamics are described by the vertically averaged relative soil moisture (S) and nitrogen content per unit area of soil (N). The crop is controlled by manipulating the continuous irrigation described by its flow-rate per unit area (I) and its nitrogen concentration (F_N). Table 14 provides a description of each variable.

Table 14 – Crop system: State and input variables.

	Description	Units
C	Canopy cover	$\text{m}^2 \text{m}^{-2}$
B	Crop biomass per unit area	kg m^{-2}
S	Relative Soil moisture	$\text{m}^3 \text{m}^{-3}$
N	Nitrogen content per unit area of soil	g m^{-2}
I	Irrigation flow-rate per unit area	mm d^{-1}
F_N	Nitrogen concentration of irrigation water	g m^{-3}

Source: Prepared by the author.

The state-space model for the crop system is given by

$$\dot{x}(t) = f(x(t), u(t) | \theta_C), \quad (84)$$

with state $x = [C \ B \ S \ N]^T \in \mathbb{R}_{\geq 0}^4$ and input $u = [I \ F_N] \in \mathbb{R}_{\geq 0}^2$. The time-invariant dynamics $f(\cdot | \theta_C)$ depend on a set of parameters denoted by θ_C . We consider the parameters referring to the dynamics of a modern corn cultivar grown on a silty loam type soil. The state equations are

$$\dot{C} = (r_G f_\eta(N) K_s(S) K_{cb} E T_0) C - (r_M + \gamma(t - t_{sen}) \Theta(t - t_{sen})) C^2; \quad (85)$$

$$\dot{B} = \frac{W^*}{\eta_C} (K_s(S) K_{cb} f_\eta(N)) C; \quad (86)$$

$$\dot{S} = \frac{1}{\phi Z} \left(R + I - (K_s(S) K_{cb} E T_0) C - (K_r(S) K_{ec} E T_0) (1 - C) - \frac{aN}{S \phi Z} k_{sat} S^d \right); \quad (87)$$

$$\dot{N} = D + F - \frac{aN}{S \phi Z} k_{sat} S^d - (f_\eta(N) K_s(S) K_{cb} E T_0) C, \quad (88)$$

where $\Theta(x)$ is the Heaviside function which is $\Theta(x) = 1$ if $x > 0$ and $\Theta(x) = 0$ otherwise. The

water stress coefficient $K_s(S)$ and evaporation reduction coefficient $f_\eta(N)$ are defined as

$$K_s(S) = \begin{cases} 0 & S \leq S_w \\ \frac{S-S_w}{S^*-S_w} & S_w < S \leq S^* ; \\ 1 & S \geq S^* \end{cases} ; \quad K_r(S) = \begin{cases} 0 & \text{if } S \leq S_h \\ \frac{S-S_h}{1-S_h} & \text{otherwise} \end{cases} . \quad (89)$$

The nitrogen uptake is saturated to a given critical concentration η_c according to the function

$$f_\eta(N) = \begin{cases} \frac{aN}{S\phi Z} & \text{if } \frac{aN}{S\phi Z} < \eta_c \\ \eta_c & \text{otherwise} \end{cases} . \quad (90)$$

We adapt the model by defining the fertilization term $F(t) = I(t)F_N(t)$. As a simplification, we consider the absence of any rainfall ($R(t) = 0$) and assume constant reference evapotranspira-

Table 15 – Crop system: Model constant parameters.

	General parameter	Value	Units
r_G	Canopy growth per unit N uptake	560	$\text{m}^2 \text{kg}^{-1} N$
r_M	Canopy decline due to metabolic limitation	0.2	d^{-1}
γ	Slope of increase of senescence after t_{sen}	0.005	d^{-2}
K_{cb}	Maximum T/ET_0	1.03	dimensionless
K_{ec}	Maximum E/ET_0	1.1	dimensionless
t_{sen}	Days until onset of senescence	110	d
W^*	Normalized daily water productivity	$3.37 \cdot 10^{-2}$	$\text{kg } B \text{ m}^{-2} \text{ d}^{-1}$
h	Maximum harvest index	0.5	$\text{kg } Y \text{ kg}^{-1} B$
η_C	Maximum nitrogen concentration taken up	0.054	$\text{kg } N \text{ m}^{-3} \text{ water}$
D	Nitrogen deposition rate	$5.5 \cdot 10^{-6}$	$\text{kg } \text{m}^{-2} \text{ d}^{-1}$
F_t	Maximum nitrogen uptake	0.0286	$\text{kg } N \text{ m}^{-2}$
	Climate and soil parameter	Value	Units
ET_0	Reference evapotranspiration	$5 \cdot 10^{-3}$	$\text{m } \text{d}^{-1}$
S_h	Hygroscopic point	0.14	dimensionless
S_w	Wilting point	0.17	dimensionless
S^*	Point of incipient stomatal closure	0.35	dimensionless
S_{fc}	Field capacity	0.59	dimensionless
k_{sat}	Saturated hydraulic conductivity	0.33	$\text{m } \text{d}^{-1}$
d	Leakage parameter	13	dimensionless
a	Fraction of nitrogen dissolved	1	dimensionless
ϕ	Soil porosity	0.43	dimensionless
Z	Soil depth	1	m

Source: Prepared by the author.

tion $ET_0(t)$, the water loss due to the impact of climate on evaporation and plant transpiration. Finally, the equations are dependent on the set of constant parameters presented at Table 15

Optimal control formulation

We consider the problem of maximizing crop biomass at the end of a growing season (NETO; HADDON, et al., 2021). This task is formalised by the finite-horizon optimal control problem of

$$\max_{u_C(\cdot)} B(T) \quad (91a)$$

$$\text{s.t.} \quad \dot{x}_C(t) = f_C(x_C(t), u_C(t) | \theta_C), \quad (91b)$$

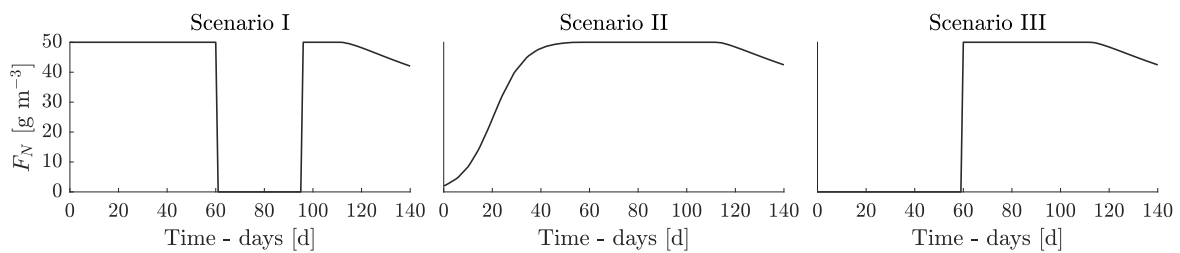
$$\forall t \in [0, T] \quad u_C(t) \in [0, I^{\max}] \times [0, F_N^{\max}], \quad (91c)$$

$$x_C(0) = x_0, \quad (91d)$$

for fixed final time T , initial state x_0 , and input upper bounds I^{\max} and F_N^{\max} . We restrict ourselves to growing seasons lasting $T = 140$ days. In the following, we present the optimal control solutions over several simulated scenarios. Each non-linear optimisation Eq. (91) is solved using a dynamic programming approach. (BONNANS et al., 2017). As the state-space is low-dimensional, values functions for Eq. (91) can be efficiently computed.

The optimal control actions are obtained over three different scenarios corresponding to different initial soil nitrogen content. Specifically, we consider $N(0) = 1 \text{ g m}^{-3}$ for Scenario I, $N(0) = 8.2 \text{ g m}^{-3}$ for Scenario II, and $N(0) = 15 \text{ g m}^{-3}$ for Scenario III. The same initial conditions are considered for the remaining state-variables in all scenarios. The resulting optimal irrigation nitrogen F_N for each scenario are shown in Figure 33. In general, the controller must supply more nitrogen to the crop in Scenario I than in Scenarios II and III. We note, for our experiments, that this does not translate into more biomass as the crop is initially under stress and the controls are unable to drive the soil nitrogen concentrations to the critical level fast enough.

Figure 33 – Crop model: Nitrogen concentrations of irrigation water, F_N , for optimal crop growth.



Source: Prepared by the authors.

Appendix B – Omitted proofs and definitions

In the following we present additional definitions and detailed proofs for the theorems presented in Chapter 2. The theorems are restated in this section.

Observability of LTI systems

This section presents the observability counterpart of all definitions and theorems in Section 2.1.2. Let the observability Gramian of the pair (A, C) be the $N_x \times N_x$ symmetric matrix

$$W_o(t) = \int_0^t e^{A^\top \tau} C^\top C e^{A \tau} d\tau, \quad (92)$$

a sufficient and necessary observability condition is $\det(W_o(t)) \neq 0, \forall t > 0$. The computation of Gramian-based criteria in Eq. (92) is straightforward but unpractical. Equivalent criteria can be defined in terms of the system's observability matrix (KALMAN, R., 1960).

Let $\mathcal{O} = \begin{bmatrix} C^\top & A^\top C^\top & (A^\top)^2 C^\top & \dots & (A^\top)^{N_x-1} C^\top \end{bmatrix}^\top$ be the $(N_y \times N_x) \times N_x$ observability matrix of the system. A sufficient and necessary condition for observability is

$$\text{rank}(\mathcal{O}) = N_x. \quad (93)$$

By verifying that \mathcal{O} is full-rank, the criteria in Eq. (93) is more direct and, for low-dimensional systems, its evaluation only requires a small number of matrix multiplications. However, the computation of matrix \mathcal{O} can still be troublesome when the dimensionality of the state vector is large. This limitation is due to numerical over- and under-flow that may result from computing large powers of A and A^\top .

A scalable alternative that overcomes the limitations of both Gramian-based and Kalman's rank criteria is provided by the Popov-Belevitch-Hautus (PBH) test for observability. Necessary and sufficient conditions are given by the following lemma:

Lemma .1. (HAUTUS, 1970). *The following statements are all equivalent:*

$$\text{I. The pair } (A, C) \text{ is observable} \quad (94a)$$

$$\text{II. } \text{rank}\left(\begin{bmatrix} \lambda I - A^\top & C^\top \end{bmatrix}\right) = N_x, \forall \lambda \in \mathbb{C}; \quad (94b)$$

$$\text{III. } \text{rank}\left(\begin{bmatrix} \lambda_i I - A^\top & C^\top \end{bmatrix}\right) = N_x, \forall \lambda_i \in \sigma(A) \subset \mathbb{C}. \quad (94c)$$

Based on Lemma .1, the pair (A, C) is said to be observable if and only if, for each $\lambda_i \in \sigma(A)$ (that is, when $\text{rank}(\lambda_i I - A^\top) < N_x$), the columns of C have at least one component in the direction $v_i \in \mathbb{R}^{N_x}$, v_i being the associated eigenvector of A associated to λ_i ; The eigenvectors

v_i for which $\text{rank}([\lambda_i I - A^\top C^\top]^\top) < N_x$ indicate directions that are unobservable with the measurements determined by C . Since observability is invariant with respect to similarity transformations represented by nonsingular matrices $P \in \mathbb{R}^{N_x \times N_x}$, the following holds:

- Pair (A, C) is observable if and only if pair $(A', C') = (P^{-1}AP, CP)$ is observable.

Controllability and observability metrics

Full-state controllability and observability are binary properties. Starting from the seminal work by Müller and Weber (1972), various scalar metrics have been proposed to quantify the difficulty of the control and observation task. We overview energy-related metrics recently proposed by Pasqualetti et al. (2014), and Summers et al. (2016) for the observability of LTI systems.

Define the quadratic control and measurement energies

$$E_c(u(t), t | R) = \int_0^t u^\top(\tau) R u(\tau) d\tau = \|u(t)\|_R^2; \quad (95a)$$

$$E_o(y(t), t | Q) = \int_0^t y^\top(\tau) Q y(\tau) d\tau = \|y(t)\|_Q^2. \quad (95b)$$

In optimal quadratic regulation, we search for a controller that minimises the sum of these energies, for some user-defined positive definite weighting matrices R and Q (size $N_x \times N_x$ and $N_y \times N_y$, respectively). When minimised individually with the identity matrix $Q = I_y$, the unweighted measurement energy determine

- $x(0) = W_o^{-1}(t) \int_0^t e^{A^\top \tau} C^\top y(\tau) d\tau$, the initial state from measurement $\tilde{y}(t)$ of minimum L_2 -effort $E_o^*(t | \tilde{y}(t)) = x(0)^\top W_o(t) x(0)$.

Finite- and infinite-horizon observability metrics can be derived from Eq. (92). The eigenvectors $\{v_{nx}(\lambda_{nx}^o)\}_{nx=1}^{N_x}$ associated with the eigenvalues $\lambda_{nx}^o \in \sigma(W_o(t))$ correspond to directions of increasingly larger output energy the smaller λ_{nx}^o . The measurement effort associated with pair (A, C) can thus be quantified by single scalars defined from the spectrum $\sigma(W_o(t)) = \{\lambda_{nx}^o\}_{nx=0}^{N_x}$.

Because infinite-time Gramian, $W_o(\infty)$, always exist for Hurwitz systems, Eq. (17), and their computation can be performed efficiently by solving Lyapunov equations (BENNER et al., 2008), we only overview a number of infinite-time metrics. Their finite-time counterparts are evaluated by integrating Eq. (19) and (92).

Definition .1. (Energy-related observability metrics, (SUMMERS et al., 2016)) Let $W_o(\infty)$ be the solution of $W_o(\infty)A^\top + AW_o(\infty) + C^\top C = 0$. The output effort for the pair (A, C) can be quantified according to the following scalar metrics:

- I. $\text{trace}(W_o(\infty))$: Inversely related to the output effort averaged over all state-space directions;

- II. $\text{trace}(W_o^\dagger(\infty))$: Related to the output effort averaged over all directions in the state-space;
- III. $\log(\det(W_o(\infty)))$: Related to the volume of a N_x -dimensional hyper-ellipsoid whose points are observable with one unit or less of output energy;
- IV. $\lambda_{\min}^o(W_o(\infty))$: Inversely related to the output energy along the least observable eigen-direction.

By duality, the measurement effort associated to attempting to reconstruct the full-state by only measuring one individual state variable $x_{i}nx$ at a time is quantified by

$$C_o(nx) = \text{trace}(W_{o,nx}(\infty)). \quad (96)$$

This non-negative quantity, the average observability centrality (SUMMERS et al., 2016), is computed by assuming a single sensor that measures only the nx -th state variable: That is, when $C = e_{nx}^\top$, a unit vector in the standard basis of \mathbb{R}^{N_x} . The infinite-horizon observability Gramians $W_{o,nx}(\infty) \in \mathbb{R}^{N_x \times N_x}$ are computed independently for all $nx \in \{1, \dots, N_x\}$ by solving $W_{o,nx}(\infty)A^\top + AW_{o,i}(\infty) = -e_{nx}e_{nx}^\top$.

Structural controllability and observability

The structural pair (A, C) can be studied by mapping the state and output equations onto a digraph $\mathcal{G}_o = (\mathcal{V}_o, \mathcal{E}_o)$. The vertex set $\mathcal{V}_o = \mathcal{V}_A \cup \mathcal{V}_C$ consists of the union of vertex set $\mathcal{V}_A = \{x_1, \dots, x_{N_x}\}$ of state components and of vertex set $\mathcal{V}_C = \{y_1, \dots, y_{N_y}\}$ of outputs, while the edge set $\mathcal{E}_o = \mathcal{E}_A \cup \mathcal{E}_C$ is the union of set $\mathcal{E}_A = \{(x_{nx_1}, x_{nx_2}) \mid A_{nx_1, nx_2} \neq 0\}$ of directed edges between state component vertices and set $\mathcal{E}_C = \{(x_{nx}, y_{ny}) \mid C_{ny, nx} \neq 0\}$ of directed edges between state and output components vertices.

The pair (A, C) is said to be structurally observable if the nonzero elements of A and C can be set in such a way that the system is observable in the classical sense. Formally,

Definition .2. (Structural Observability). The pair (A, C) is said to be structurally observable if and only if there exists an observable pair (\bar{A}, \bar{C}) of the same dimension and structure of the pair (A, C) such that $\|\bar{A} - A\| < \varepsilon$ and $\|\bar{C} - C\| < \varepsilon$, for an arbitrarily small $\varepsilon > 0$.

Two pairs (A, C) and (\bar{A}, \bar{C}) have the same structure if they have the same dimensions and each element $A_{nx_1, nx_2} \neq 0$ (respectively, $C_{ny, nx} \neq 0$) whenever $\bar{A}_{nx_1, nx_2} \neq 0$ (respectively, $\bar{C}_{ny, nx} \neq 0$). Because of the duality between controllability and observability, also the necessary and sufficient conditions for structural observability can be derived from (LIN, 1974):

Lemma .2. Let $\mathcal{G}_o = (\mathcal{V}_o, \mathcal{E}_o)$ be the directed network associated to the pair (A, C) . The pair (A, C) is said to be structurally observable if and only if the following conditions hold:

- (Accessibility) For every $x_{nx} \in \mathcal{V}_A$ there exists at least one directed path from x_{nu} to any $y_{ny} \in \mathcal{V}_C$.
- (Dilation-free) For every $\mathcal{S} \subseteq \mathcal{V}_A$, $|T(\mathcal{S})| \geq |\mathcal{S}|$, where $T(\mathcal{S}) = \{v_j \in \mathcal{V}_o \mid x_{nx} \in \mathcal{S} \wedge (x_{nx}, v_j) \in \mathcal{E}_o\}$ denotes a neighbourhood set for \mathcal{S} .

The first condition can be verified by identifying the output vertices that are accessible from each possible origin vertex (a state component) using any graph search algorithm. The second condition can be verified by forming a maximum matching $\mathcal{M} \subseteq \Gamma$ of an equivalent bipartite graph $\mathcal{K} = (\mathcal{V}_A^+ \cup \mathcal{V}_A^-, \Gamma)$ and then checking that all unmatched state vertices $x_{nx} \in \mathcal{V}_A^+$ are directly connected to distinct output vertices in $\mathcal{G}_o = (\mathcal{V}_o, \mathcal{E}_o)$ (LIU et al., 2013). The bipartite graph $\mathcal{K} = (\mathcal{V}_A^+ \cup \mathcal{V}_A^-, \Gamma)$ is defined by the disjoint and independent vertex sets $\mathcal{V}_A^+ = \{x_1^+, \dots, x_{N_x}^+\}$ and $\mathcal{V}_A^- = \{x_1^-, \dots, x_{N_x}^-\}$, and by the undirected edge set $\Gamma = \{(x_i^+, x_j^-) \mid (x_i, x_j) \in \mathcal{E}_o\}$. Unmatched state vertices linked to distinct output vertices form a \mathcal{V}_A^+ -perfect matching.

Stabilizability and detectability

A system is said detectable if it is possible to asymptotically approximate its state-vector from a sequence of measurements. This condition is often perceived as a weaker alternative to full-state observability. Formally,

Definition .3. (Detectability). The pair (A, C) is said to be detectable if, giving any initial state $x(0)$, it is possible to compute a state estimate $\hat{x}(t)$ from the force-free evolution of $y(t)$, so that $(x(t) - \hat{x}(t)) \rightarrow 0$ as $t \rightarrow \infty$.

By duality, sufficient and necessary conditions for detectability can be also derived from the Kalman canonical decomposition of the system. Let $\mathcal{O} = [C^T \ A^T C^T \ (A^T)^2 C^T \ \dots \ (A^T)^{N_x-1} C^T]^T$ be the $\mathbb{R}^{N_y N_x \times N_x}$ observability matrix of a system (A, C) , with $\text{rank}(\mathcal{O}) = N_1 \leq N_x$. There exists a nonsingular matrix $P_o \in \mathbb{R}^{N_x \times N_x}$, whose first N_1 rows are the linearly independent rows of \mathcal{O} , such that the transformation $\tilde{x} = P_o^{-1} x$ results in a model in the form

$$\begin{aligned} \begin{bmatrix} \dot{\tilde{x}}_o(t) \\ \dot{\tilde{x}}_{\bar{o}}(t) \end{bmatrix} &= \begin{bmatrix} \tilde{A}_o & 0 \\ \tilde{A}_{21} & \tilde{A}_{\bar{o}} \end{bmatrix} \begin{bmatrix} \tilde{x}_o(t) \\ \tilde{x}_{\bar{o}}(t) \end{bmatrix} \\ y(t) &= \begin{bmatrix} \tilde{C}_o & 0 \end{bmatrix} \begin{bmatrix} \tilde{x}_o(t) \\ \tilde{x}_{\bar{o}}(t) \end{bmatrix}, \end{aligned}$$

with $\tilde{x}_o(t) \in \mathbb{R}^{N_1}$ and $\tilde{x}_{\bar{o}}(t) \in \mathbb{R}^{(N_x - N_1)}$. A sufficient and necessary condition for detectability is that $\text{Re}(\lambda_j) < 0$ for all $\lambda_j \in \sigma(\tilde{A}_{\bar{o}}) \subset \sigma(A)$ (CHEN, 1998). Although straightforward, this criterion is unpractical for high-dimensional systems as the design of P_o requires the computation of the observability matrix $\mathcal{O} = [C^T \ A^T C^T \ (A^T)^2 C^T \ \dots \ (A^T)^{N_x-1} C^T]^T$.

A scalable alternative is given by the Popov-Belevitch-Hautus (PBH) detectability test, based

on the Hautus lemma:

Lemma .3. (HAUTUS, 1970). Let $\sigma(A) = \{\lambda_i\}_{i=1}^{N_x}$ be the spectrum of A . Now, let $\tilde{\sigma}(A) = \{\lambda_i \mid \lambda_i \in \sigma(A) \wedge \text{Re}(\lambda_i) \geq 0\}$ be the set of eigenvalues with positive real part. The statement ‘the pair (A, C) is detectable’ is equivalent to the following statements:

$$\text{I. } \text{rank}\left(\begin{bmatrix} \lambda I - A^\top & C^\top \end{bmatrix}^\top\right) = N_x, \forall \lambda \in \mathbb{C}_{\geq 0}; \quad (97a)$$

$$\text{II. } \text{rank}\left(\begin{bmatrix} \lambda_i I - A^\top & C^\top \end{bmatrix}^\top\right) = N_x, \forall \lambda_i \in \tilde{\sigma}(A) \subset \mathbb{C}_{\geq 0}. \quad (97b)$$

Thus, the pair (A, C) is detectable if and only if, for each unstable eigenvalue λ_i of A (that is, when $\text{Re}(\lambda_i) \geq 0$ and $\text{rank}(\lambda_i I - A^\top) < N_x$), the rows of C have at least one component in the state-space direction associated to the eigenvector of A corresponding to λ_i , $v_i \in \mathbb{R}^{N_x}$. Notice that every system (A, C) with a stable matrix A is consequently detectable, since $\tilde{\sigma}(A) = \emptyset$.

Optimal control and estimation

In the following, the detailed proof of theorem and prepositions of Chapters 2.2 and 2.3 are presented.

Lemma .4. (Affine state-space discretisation) Consider a continuous-time affine state-space,

$$\dot{x}(t) = z + Ax(t) + Bu(t) + Gw(t); \quad (98a)$$

$$y(t) = Cx(t). \quad (98b)$$

Considering piecewise constant inputs $u(t) = u(t_k)$ and $w(t) = w(t_k)$ for every $t = [t_k, t_{k+1})$, with $t_k \in k\Delta t$ given sampling period $\Delta t > 0$, the discrete-time realisation of Eq. (98) is

$$x_{k+1} = z_{\Delta t} + A_{\Delta t}x_k + B_{\Delta t}u_k + G_{\Delta t}w_k; \quad (99a)$$

$$y_k = Cx_k, \quad (99b)$$

with matrices $A_{\Delta t} = e^{A\Delta t}$, $B_{\Delta t} = S_{\Delta t}B$, $G_{\Delta t} = S_{\Delta t}G$, and vector $z_{\Delta t} = S_{\Delta t}z$, given auxiliary $S_{\Delta t} = A^{-1}(e^{A\Delta t} - I)$. The discrete variables are $x_k = x(k\Delta t)$, $u_k = u(k\Delta t)$ and $w_k = w(k\Delta t)$.

Proof. Consider the state equation in Eq. (98a). Multiplying both sides by e^{-At} leads to

$$\begin{aligned} e^{-At}\dot{x}(t) &= e^{-At}(z + Ax(t) + Bu(t) + Gw(t)); \\ e^{-At}\dot{x}(t) - e^{-At}Ax(t) &= e^{-At}(z + Bu(t) + Gw(t)); \\ d(e^{-At}x(t))/dt &= e^{-At}(z + Bu(t) + Gw(t)), \end{aligned}$$

in which the last step we use the property $d(e^{-At}x(t))/dt = e^{-At}\dot{x}(t) - e^{-At}Ax(t)$. Integrating

both sides from initial instant $t_k = k\Delta t$ to instant $t_{k+1} = (k+1)\Delta t$ yields

$$\begin{aligned} (e^{-At}x(t))\Big|_{t_k}^{t_{k+1}} &= \int_{t_k}^{t_{k+1}} e^{-A\tau}(z + Bu(\tau) + Gw(\tau))d\tau; \\ e^{-At_{k+1}}x(t_{k+1}) - e^{-At_k}x(t_k) &= \int_{t_k}^{t_{k+1}} e^{-A\tau}(z + Bu(\tau) + Gw(\tau))d\tau; \\ e^{-At_{k+1}}x(t_{k+1}) &= e^{-At_k}x(t_k) + \int_{t_k}^{t_{k+1}} e^{-A\tau}(z + Bu(\tau) + Gw(\tau))d\tau. \end{aligned}$$

Finally, multiplying both sides by the matrix exponential $e^{At_{k+1}}$ results in the state transition

$$x_{k+1} = A_{\Delta t}x_k + \int_{t_k}^{t_{k+1}} e^{A(t_{k+1}-\tau)}(z + Bu(\tau) + Gw(\tau))d\tau,$$

with $A_{\Delta t} = e^{A(t_{k+1}-t_k)} = e^{A\Delta t}$. Letting $u(\tau) = u_k$ and $w(\tau) = w_k$ for the interval $\tau \in [t_k, t_{k+1})$,

$$x_{k+1} = A_{\Delta t}x_k + \int_{t_k}^{t_{k+1}} e^{A(t_{k+1}-\tau)}d\tau z + \int_{t_k}^{t_{k+1}} e^{A(t_{k+1}-\tau)}d\tau Bu_k + \int_{t_k}^{t_{k+1}} e^{A(t_{k+1}-\tau)}d\tau Gw_k,$$

from which we define $S_{\Delta t} = \int_{t_k}^{t_{k+1}} e^{A(t_{k+1}-\tau)}d\tau$. Defining $\lambda = t_{k+1} - \tau$ and using the property $Ae^{A\lambda} = d(e^{A\lambda})/d\lambda$, the matrix $S_{\Delta t}$ can be written as

$$S_{\Delta t} = - \int_{\Delta t}^0 e^{A\lambda} d\lambda = \int_0^{\Delta t} (A^{-1}A)e^{A\lambda} d\lambda = A^{-1} \int_{\Delta t}^0 Ae^{A\lambda} d\lambda = A^{-1}(e^{A\lambda})\Big|_0^{\Delta t} = A^{-1}(e^{A\Delta t} - I)$$

The corresponding discrete-time affine state-space is thus given by

$$\begin{aligned} x_{k+1} &= z_{\Delta t} + A_{\Delta t}x_k + B_{\Delta t}u_k + G_{\Delta t}w_k; \\ y_k &= Cx_k, \end{aligned}$$

with matrices $B_{\Delta t} = S_{\Delta t}B$, $G_{\Delta t} = S_{\Delta t}G$, and constant vector $z_{\Delta t} = S_{\Delta t}z$. □

Theorem .5. (*c-AQR Transcription*) Consider the optimal control problem in Definition. 2.6. The described optimization can be converted into a quadratic program

$$\min_U U^T H U + g^T U + r \tag{100a}$$

$$s.t. \quad E_u U \leq e_u \tag{100b}$$

with decision vector $U = (x_k, \dots, x_{k+N}, u_k, \dots, u_{k+N-1}) \in \mathbb{R}^{(N)N_x + (N-1)N_u}$ and symmetric matrix $H = H^T \succeq 0$. Assuming the sequential approach, the problem reduces to decision vector $U = (u_k, \dots, u_{k+N-1}) \in \mathbb{R}^{(N-1)N_u}$ and positive definite matrix $H = H^T \succ 0$.

Proof. In the first part of this proof, we assume the simultaneous approach. Considering the

terms in Eq. (35a) regarding the controls u_n ($n = k, \dots, k+N-1$),

$$\begin{aligned}
\sum_{n=k}^{k+N-1} \|u_n - u_n^{sp}\|_R^2 &= \sum_{n=k}^{k+N-1} (u_n - u_n^{sp})^\top R (u_n - u_n^{sp}) \\
&= \begin{bmatrix} u_k \\ \vdots \\ u_{k+N-1} \end{bmatrix}^\top \begin{bmatrix} R & \cdots & 0 \\ \vdots & \ddots & \vdots \\ 0 & \cdots & R \end{bmatrix} \begin{bmatrix} u_k \\ \vdots \\ u_{k+N-1} \end{bmatrix} - 2 \begin{bmatrix} u_k^{sp} \\ \vdots \\ u_{k+N-1}^{sp} \end{bmatrix}^\top \begin{bmatrix} R & \cdots & 0 \\ \vdots & \ddots & \vdots \\ 0 & \cdots & R \end{bmatrix} \begin{bmatrix} u_k \\ \vdots \\ u_{k+N-1} \end{bmatrix} \\
&\quad + \begin{bmatrix} u_k^{sp} \\ \vdots \\ u_{k+N-1}^{sp} \end{bmatrix}^\top \begin{bmatrix} R & \cdots & 0 \\ \vdots & \ddots & \vdots \\ 0 & \cdots & R \end{bmatrix} \begin{bmatrix} u_k^{sp} \\ \vdots \\ u_{k+N-1}^{sp} \end{bmatrix} \\
&= \tilde{U}^\top \tilde{R} \tilde{U} - 2 \tilde{U}^{sp\top} \tilde{R} \tilde{U} + \tilde{U}^{sp\top} \tilde{R} \tilde{U}^{sp}.
\end{aligned}$$

Assuming $Q_f = Q$, without loss of generality, the terms regarding x_n ($n = k, \dots, k+N$) are

$$\begin{aligned}
\sum_{n=k}^{k+N} \|x_n - x_n^{sp}\|_Q^2 &= \sum_{n=k}^{k+N} (x_n - x_n^{sp})^\top Q (x_n - x_n^{sp}) \\
&= \begin{bmatrix} x_k \\ \vdots \\ x_{k+N} \end{bmatrix}^\top \begin{bmatrix} Q & \cdots & 0 \\ \vdots & \ddots & \vdots \\ 0 & \cdots & Q \end{bmatrix} \begin{bmatrix} x_k \\ \vdots \\ x_{k+N} \end{bmatrix} - 2 \begin{bmatrix} x_k^{sp} \\ \vdots \\ x_{k+N}^{sp} \end{bmatrix}^\top \begin{bmatrix} Q & \cdots & 0 \\ \vdots & \ddots & \vdots \\ 0 & \cdots & Q \end{bmatrix} \begin{bmatrix} x_k \\ \vdots \\ x_{k+N} \end{bmatrix} \\
&\quad + \begin{bmatrix} x_k^{sp} \\ \vdots \\ x_{k+N}^{sp} \end{bmatrix}^\top \begin{bmatrix} Q & \cdots & 0 \\ \vdots & \ddots & \vdots \\ 0 & \cdots & Q \end{bmatrix} \begin{bmatrix} x_k^{sp} \\ \vdots \\ x_{k+N}^{sp} \end{bmatrix} \\
&= X^\top \tilde{Q} X - 2 X^{sp\top} \tilde{Q} X + X^{sp\top} \tilde{Q} X^{sp}.
\end{aligned}$$

Letting $U = (x_k, \dots, x_{k+N}, u_k, \dots, u_{k+N-1}) = [X \tilde{U}]^\top$, the cost function is transcribed as

$$\begin{aligned}
J_{\Delta t}(x, u) &= \begin{bmatrix} X \\ \tilde{U} \end{bmatrix}^\top \begin{bmatrix} \tilde{Q} & 0 \\ 0 & \tilde{R} \end{bmatrix} \begin{bmatrix} X \\ \tilde{U} \end{bmatrix} + \left(2 \begin{bmatrix} \tilde{Q} & 0 \\ 0 & \tilde{R} \end{bmatrix} \begin{bmatrix} X^{sp} \\ \tilde{U}^{sp} \end{bmatrix} \right)^\top \begin{bmatrix} X \\ \tilde{U} \end{bmatrix} + \begin{bmatrix} X^{sp} \\ \tilde{U}^{sp} \end{bmatrix}^\top \begin{bmatrix} \tilde{Q} & 0 \\ 0 & \tilde{R} \end{bmatrix} \begin{bmatrix} X^{sp} \\ \tilde{U}^{sp} \end{bmatrix}; \\
&= U^\top H U + g^\top U + r,
\end{aligned}$$

which is in the form of Eq. (100a). The dynamic constraints are converted into the inequality

$$0 \leq \begin{bmatrix} -I & 0 & \cdots & 0 & 0 \\ A_{\Delta t} & -I & \cdots & 0 & 0 \\ \vdots & \vdots & \ddots & \vdots & \vdots \\ 0 & 0 & \cdots & -I & 0 \\ 0 & 0 & \cdots & A_{\Delta t} & -I \end{bmatrix} X + \begin{bmatrix} 0 & 0 & \cdots & 0 \\ B_{\Delta t} & 0 & \cdots & 0 \\ \vdots & \vdots & \ddots & \vdots \\ 0 & 0 & \cdots & 0 \\ 0 & 0 & \cdots & B_{\Delta t} \end{bmatrix} \tilde{U} + \begin{bmatrix} \hat{x}_k \\ z_{\Delta t} + G_{\Delta t} w_0 \\ \vdots \\ z_{\Delta t} + G_{\Delta t} w_{k+N-2} \\ z_{\Delta t} + G_{\Delta t} w_{k+N-1} \end{bmatrix} \leq 0,$$

which is in the form $0 \leq \tilde{E}_x X + \tilde{E}_u \tilde{U} + \tilde{e}_u \leq 0$. This expression can also be written as

$$\begin{bmatrix} \tilde{E}_x & \tilde{E}_u \\ -\tilde{E}_x & -\tilde{E}_u \end{bmatrix} U \leq \begin{bmatrix} \tilde{e}_u \\ -\tilde{e}_u \end{bmatrix}.$$

Moreover, the inequalities $H_x x_n \leq h_x$ and $H_u u_n \leq h_u$ (for $n = 0, \dots, N-1$) are written as

$$\begin{bmatrix} H_x & \cdots & 0 & 0 & \cdots & 0 \\ \vdots & \ddots & \vdots & \vdots & \ddots & 0 \\ 0 & \cdots & H_x & 0 & \cdots & 0 \\ 0 & \cdots & 0 & H_u & \cdots & 0 \\ \vdots & \ddots & \vdots & \vdots & \ddots & 0 \\ 0 & \cdots & 0 & 0 & \cdots & H_u \end{bmatrix} U \leq \begin{bmatrix} h_x \\ \vdots \\ h_x \\ h_u \\ \vdots \\ h_u \end{bmatrix},$$

which is in the form $\text{diag}[H_X H_{\tilde{U}}]U \leq [h_X h_{\tilde{U}}]^\top$. Finally, all constraints are compiled as

$$\begin{bmatrix} \tilde{E}_x & \tilde{E}_u \\ -\tilde{E}_x & -\tilde{E}_u \\ H_X & 0 \\ 0 & H_{\tilde{U}} \end{bmatrix} U \leq \begin{bmatrix} \tilde{e}_u \\ -\tilde{e}_u \\ h_X \\ h_{\tilde{U}} \end{bmatrix},$$

which is in the form of Eq. (100b), $E_u U + E_x X \leq e_u$, with $E_x = 0$.

In the second part of this proof, we assume the sequential approach with $U = (u_k, \dots, u_{k+N-1})$. Considering the formula, $x_{n+1} = A_{\Delta t}^{n+1} x_0 + \sum_{k=0}^n A_{\Delta t}^k B_{\Delta t} u_{n-k+1} + \sum_{k=0}^n A_{\Delta t}^k (G_{\Delta t} w_{n-k+1} + z_{\Delta t})$, the vector $X = (x_k, \dots, x_{k+N})$ is expanded as

$$X = \begin{bmatrix} A_{\Delta t}^0 \\ A_{\Delta t}^1 \\ \vdots \\ A_{\Delta t}^N \end{bmatrix} x_k + \begin{bmatrix} 0 & 0 & \cdots & 0 \\ B_{\Delta t} & 0 & \cdots & 0 \\ \vdots & \vdots & \ddots & \vdots \\ A_{\Delta t}^{N-1} B_{\Delta t} & A_{\Delta t}^{N-2} B_{\Delta t} & \cdots & B_{\Delta t} \end{bmatrix} U + Z = \tilde{A} x_k + \tilde{B} U + Z,$$

with constant term $Z = \sum_{k=0}^n A_{\Delta t}^k (G_{\Delta t} w_{n-k+1} + z_{\Delta t})$. Using this representation, the terms of the cost function regarding x_n ($n = k, \dots, k+N$) yield

$$\begin{aligned} \sum_{n=k}^{k+N} \|x_n - x_n^{sp}\|_Q^2 &= X^\top \tilde{Q} X - 2(X^{sp})^\top \tilde{Q} X + (X^{sp})^\top \tilde{Q} X^{sp}; \\ &= U^\top \tilde{B}^\top \tilde{Q} \tilde{B} U + 2(\tilde{A} x_k + z + X^{sp})^\top \tilde{Q} \tilde{B} U + \text{const.} \end{aligned}$$

Using the previous result of $\sum_{n=k}^{k+N-1} \|u_n - u_n^{sp}\|_R^2 = U^\top \tilde{R} U - 2(U^{sp})^\top \tilde{R} U + (U^{sp})^\top \tilde{R} U^{sp}$, the cost

function can thus be transcribed as

$$J_{\Delta t}(x_k, u) = U^\top (\tilde{B}^\top \tilde{Q} \tilde{B} + \tilde{R}) U + 2(\tilde{B}^\top \tilde{Q} \tilde{A} x_k + \tilde{B}^\top \tilde{Q} z + \tilde{B}^\top \tilde{Q} X^{sp} + \tilde{R} U^{sp})^\top U + r$$

with all constant terms accumulated in $r = (\tilde{A} x_k + Z)^\top \tilde{Q} (\tilde{A} x_k + Z) + 2(X^{sp})^\top \tilde{Q} (\tilde{A} x_k + Z) + (X^{sp})^\top \tilde{Q} X^{sp} + (U^{sp})^\top \tilde{R} U^{sp}$. This equation is in form Eq. (100a), with $H = (\tilde{B}^\top \tilde{Q} \tilde{B} + \tilde{R}) \succ 0$. Similarly to the previous part, the inequality constraints are represented as

$$\begin{bmatrix} H_x A_{\Delta t}^0 \\ \vdots \\ H_x A_{\Delta t}^N \\ 0 \\ \vdots \\ 0 \end{bmatrix} x_k + \begin{bmatrix} 0 & \cdots & 0 \\ \vdots & \ddots & \vdots \\ H_x A_{\Delta t}^{N-1} B_{\Delta t} & \cdots & H_x B_{\Delta t} \\ H_u & \cdots & 0 \\ \vdots & \ddots & 0 \\ 0 & \cdots & H_u \end{bmatrix} U \leq \begin{bmatrix} h_x \\ \vdots \\ h_x \\ h_u \\ \vdots \\ h_u \end{bmatrix},$$

which is the form $h_{x_k} + E_u U \leq \tilde{e}_u$. Finally, this inequality can be represented in the form of Eq. (100b) by defining the vector $e_u = \tilde{e}_u - h_{x_k}$. \square

Lemma .6. (*Maximum a posteriori estimate, MAP*) Let $x_0 \sim p_{x_0}(x_0 | \theta_{x_0})$, $v_k \sim p_v(v_k | \theta_v)$ and $w_k \sim p_w(w_k | \theta_w)$, and consider the HMM described in Eq. (45). The maximum a posteriori (MAP) estimate from the posterior probability $P(x, w | y)$ is the solution of

$$\max_{\substack{x_0, \dots, x_{k+1}, \\ w_0, \dots, w_k}} \tilde{P}(x, w | y) = p_{x_0}(x_0) \prod_{n=0}^k p_v(v_n | \theta_v) p_w(w_n | \theta_w) \quad (101a)$$

$$\text{s.t.} \quad x_{n+1} = f_{\Delta t}(x_n, u_n, w_n | \theta_x), \quad (101b)$$

$$\forall n \in [0, k] \quad x_n \in \mathcal{X}, \quad w_n \in \mathcal{W}, \quad (101c)$$

Proof. Consider the maximum a posteriori estimate of the probability $P(x, w | y)$,

$$\max_{\substack{x_0, \dots, x_{k+1}, \\ w_0, \dots, w_k}} \tilde{P}(x, w | y) = p(y_0, \dots, y_k | x_0, \dots, x_{k+1}, w_0, \dots, w_k) p(x_0, \dots, x_{k+1}, w_0, \dots, w_k).$$

Using the Markov property and the fact that the measurements are independent, the likelihood probability $P(y | x, w) = p(y_0, \dots, y_k | x_0, \dots, x_{k+1}, w_0, \dots, w_k)$ can be factorized as

$$P(y | x, w) = \prod_{n=0}^k p(y_n | y_0, \dots, y_{n-1}, x_0, \dots, x_{k+1}, w_0, \dots, w_k) = \prod_{n=0}^k p(y_n | x_n).$$

Considering the change of variable $y_n = g(x_n, u_n) + v_n$,

$$P(y|x, w) = \prod_{n=0}^k p(g(x_n, u_n) + v_n|x_n) = \prod_{n=0}^k p_{v_n}(v_n|\theta_v)$$

Using the Markov property and the fact that the process noise is independent, the prior probability $P(x, w) = p(x_0, \dots, x_{k+1}, w_0, \dots, w_k)$ can also be factorized as

$$\begin{aligned} P(x, w) &= p_{x_0}(x_0|w_0, \dots, w_k) \prod_{n=0}^k p(x_{n+1}|x_0, \dots, x_n, w_0, \dots, w_k) p(w_n|w_0, \dots, w_{n-1}) \\ &= p_{x_0}(x_0|\theta_{x_0}) \prod_{n=0}^k p(x_{n+1}|x_n, w_n) p_{w_n}(w_n). \end{aligned}$$

Restricting the support of x_{n+1} to the set $\Omega = \{x_{k+1} = f_{\Delta t}(x_n, u_n, w_n|\theta_x) : \forall x_n \in \mathcal{X}, \forall w_n \in \mathcal{W}\}$,

$$P(x, w) = p_{x_0}(x_0|\theta_{x_0}) \prod_{n=0}^k p_{w_n}(w_n|\theta_w).$$

Therefore, the MAP estimate can be expressed through the optimisation

$$\max_{\substack{x_0, \dots, x_{k+1}, \\ w_0, \dots, w_k}} \tilde{P}(x, w|y) = p_{x_0}(x_0) \prod_{n=0}^k p_v(v_n|\theta_v) p_w(w_n|\theta_w) \quad (102a)$$

$$\text{s.t.} \quad x_{n+1} = f_{\Delta t}(x_n, u_n, w_n|\theta_x), \quad (102b)$$

$$\forall n \in [0, k] \quad x_n \in \mathcal{X}, \quad w_n \in \mathcal{W}. \quad (102c)$$

□

Theorem .7. (*c-AGM Transcription*) Consider the optimal estimation problem in Definition. 2.11. The described optimization can be converted into a quadratic program

$$\min_W \quad W^\top H W + g^\top W + r \quad (103a)$$

$$\text{s.t.} \quad E_w W \leq e_w \quad (103b)$$

with decision vector $W = (x_{k-N+1}, \dots, x_{k+1}, w_{k-N+1}, \dots, w_k) \in \mathbb{R}^{(N)N_x + (N-1)N_w}$ and symmetric matrix $H = H^\top \succeq 0$. Assuming the sequential approach, the problem reduces to decision vector $W = (x_{k-N+1}, w_{k-N+1}, \dots, w_k) \in \mathbb{R}^{N_x + (N-1)N_w}$ and positive definite matrix $H = H^\top \succ 0$.

Proof. Identical to the proof of Theorem .5. □